Use Authorization

In presenting this dissertation in partial fulfillment of the requirements for an advanced degree at Idaho State University, I agree that the Library shall make it freely available for inspection. I further state that permission to download and/or print my dissertation for scholarly purposes may be granted by the Dean of the Graduate School, Dean of my academic division, or by the University Librarian. It is understood that any copying or publication of this dissertation for financial gain shall not be allowed without my written permission.

Signature ___________________________________

Date ____

EVALUATION OF NEAR FIELD ATMOSPHERIC DISPERSION AROUND NUCLEAR FACILITIES USING A LORENTZIAN DISTRIBUTION METHODOLOGY

by

Gavin C. Hawkley

A dissertation

submitted in partial fulfillment

of the requirements for the degree of

Doctor of Philosophy in the Department of Physics

Idaho State University

Fall 2014

Committee Approval

To the Graduate Faculty:

The members of the committee appointed to examine the dissertation of GAVIN C. HAWKLEY find it satisfactory and recommend that it be accepted.

____

Dr. Jason Harris,
Major Advisor

____

Dr. Thomas Gesell,
Committee Member

____

Dr. Richard Brey,
Committee Member

____

Dr. Jeffrey Whicker,
Committee Member

____

Dr. Erdinch Tatar,
Graduate Faculty Representative

TABLE OF CONTENTS

LIST OF ACRONYMS

ABL	Atmospheric Boundary Layer
AED	Aerodynamic Equivalent Diameter
AERMAP	American Meteorological Society/Environmental protection Agency Regulatory MAP
AERMET	American Meteorological Society/Environmental protection Agency Regulatory Meteorology
AERMOD	American Meteorological Society/Environmental protection Agency Regulatory Model
AIRNET	Air Monitoring Network
ARCON	Atmospheric Relative Concentration
ARF	Airborne Release Fraction
CAP	Clean Air Act Assessment Package
CED	Committed Effective Dose
CFR	Code of Federal Regulations
DCF	Dose Conversion Factor
DOE	Department of Energy
DP	Delta Prime
DR	Damage Ratio
EPA	Environmental Protection Area
FBA	Fractional Bias Average
HEPA	High Efficiency Particulate Air
ICRP	International Commission on Radiation Protection
LANL	Los Alamos National Laboratory
LPF	Leak Path Factor
MACCS	MELCOR Accident Consequence Code System
MAR	Material at Risk
MDA	Material Disposal Area
MEI	Maximum Exposed Individual
NCRP	National Commission on Radiation Protection
NRC	Nuclear Regulatory Commission
PRIME	Plume Rise Model Enhancements
RF	Respirable Fraction
RMS	Root-mean-square
RSAC	Radiological Safety Analysis Computer
SSC	Structures, Systems, and Components
ST	Source Term
TED	Total Effective Dose

ABSTRACT

Atmospheric dispersion modeling within the near field of a nuclear facility typically employs application of a building wake correction to the Gaussian plume model, whereby a point source is modeled as a plane source. The plane source results in greater near field dilution and reduces the far field effluent concentration. However, the correction does not account for the concentration profile within the near field. Receptors of interest, such as the maximum exposed individual may exist within the near field and thus in the realm of building wake effects. Furthermore, release parameters and displacement characteristics may be unknown, particularly during upset conditions. There is, therefore, a need to analyze and estimate an enveloping concentration profile within the near field of a release. This investigation included the analysis of 64-air samples collected over 128 weeks at the Los Alamos National Laboratory. Variables of importance were then derived from the measurement data, and a new methodology was introduced. The new methodology developed and employed the first use of Lorentzian based dispersion coefficients, and allowed for: the calculation of dispersion coefficients along the lateral axis of the near field recirculation cavity; the development of recirculation cavity boundaries; an enveloping evaluation of the associated concentration profile. The results evaluated the effectiveness of the Lorentzian distribution methodology for estimating near field releases, and emphasized the need to adequately place air monitoring stations for complete concentration characterization. Additionally, the importance of the sampling period and operational conditions are discussed to balance operational feedback and the reporting of public dose.

1.0 INTRODUCTION

Radionuclides can be released to the atmosphere from radiological and nuclear facilities during routine operations and as a result of unintentional events. It is expected that releases to the atmosphere will dominate the dose received by people when compared to other exposure mechanisms within the environmental media (Little 1984, DOE 1994b). As a result, facility workers and the surrounding public could be exposed to radiation from the inhalation of radionuclides in the air or the ingestion of matter that has been contaminated by radioactive materials. For some non-reactor nuclear facilities, such as those processes involving the storage of nuclear waste, the surface and groundwater pathways may be more important. However, such scenarios are expected to propagate more slowly than those involved with an atmospheric release. (Crawford et al. 2008)

For facilities which have forced flow filtered ventilation systems, the flow paths are dominated by the ventilation. The fraction of airborne particles released to the outside environment is thus a function of system efficiency. When the fans are not operating, the accident flow paths to the environment consist of penetrations such as exhaust lines and doors. The air exchange rates under such conditions are driven by wind and heat induced pressure gradients. (Jordan and Leonard 2003)

The airborne particles of interest consist of aerosols, which are solid or liquid particles suspended in air. Smaller particles have higher diffusivities than larger ones and traverse streamlines by Brownian motion, whereby larger particles have higher inertia and tend to traverse streamlines as a result of their inertial lag. Furthermore, the fraction of material released which is of interest for the inhalation pathway is termed the respirable size range consisting of 10 µm or less aerodynamic equivalent diameter (AED) particles that are made airborne in response to the accident initiating event. The AED is the parameter of interest for respirable particles as it normalizes materials of different density. The AED is proportional to the product of the (spherical equivalent diameter) and the ((material density of an aerosol particle) $^{0.5}$). (DOE 1994a)

The magnitude of radiological exposure resulting from atmospheric releases depends on atmospheric transport, diffusion, and deposition processes. As such, the determination of where the airborne particles are traveling, when they will arrive at a specified receptor and the concentration of radionuclides at the receptor are all crucial parameters. Within most paths of propagation, i.e., leak paths, flow is adequately turbulent to keep the respirable particles in suspension as long as they do not enter the stagnant boundary layer existing within the proximity of surfaces, and can be assumed to be completely mixed in the cross-flow directions (Hinds 1999). In a perfect world, dose assessments would be empirically based on air concentration and external exposure rate measurements made at the receptor location. However, this is not always possible, or applicable to the scope of the assessment. For example, if one is conducting a radiological dose consequence analysis for the evaluation of the maximum exposed individual (MEI), the goal would be to conservatively envelope the potential radiological release and transport. However, measurement data may not be available. Therefore, mathematical models must be employed to provide a realistically conservative estimate of the radiological consequence resulting from atmospheric releases. Large differences in estimated radiological consequences can exist as a result of specific model assumptions and the data utilized in the development and testing of the model algorithms. As such, models should be selected and applied that provide a best fit to the situation being evaluated.

The standard model applied to atmospheric dispersion calculations is the Gaussian plume model. However, a problem arises when one attempts to apply this model within the near field of a radiological release. Within the near field of a nuclear or radiological facility of interest, building wake effects are induced by the pressure differentials associated with the turbulence created by an obstruction to the flow of wind. However, building wake correction factors typically neglect turbulence profiles and simply treat the release as a plane source to increase dilution within the near field, rather than using the point source typical of the Gaussian plume model.

Therefore, a methodology which would allow for a bounding, estimate of the downwind concentration profiles, based upon realistically conservative parameters, would further increase our ability to estimate the respective dose consequence to the MEI. Additionally, an understanding of the building wake effects is essential for the placement of air samplers with respect to the contaminant release locations and facility specifications. If the measurement devices do not adequately sample the MEI due to poor placement, or are spaced too far apart to measure potential peaks within the concentration profile, the potential radiological consequence and resulting risks may be underestimated. The development of an atmospheric modeling methodology that accounts for building wake effects within the near field of a facility requires an understanding of the mechanisms that effect atmospheric dispersion and the concentration distribution within the near field of the facility.

1.1 Gaussian Plume Model

The typical system employed for dispersion estimates was suggested by Pasquill (1961) and modified by Gifford (1961). The system considers a point of origin beneath the point of release with the mean wind direction aligned horizontally with the x axis, the y axis aligned perpendicular to the x axis, and the z axis extending vertically. The plume travels along the mean wind direction and thus parallel to the x axis, as shown in Fig. 1. (Turner 1970)

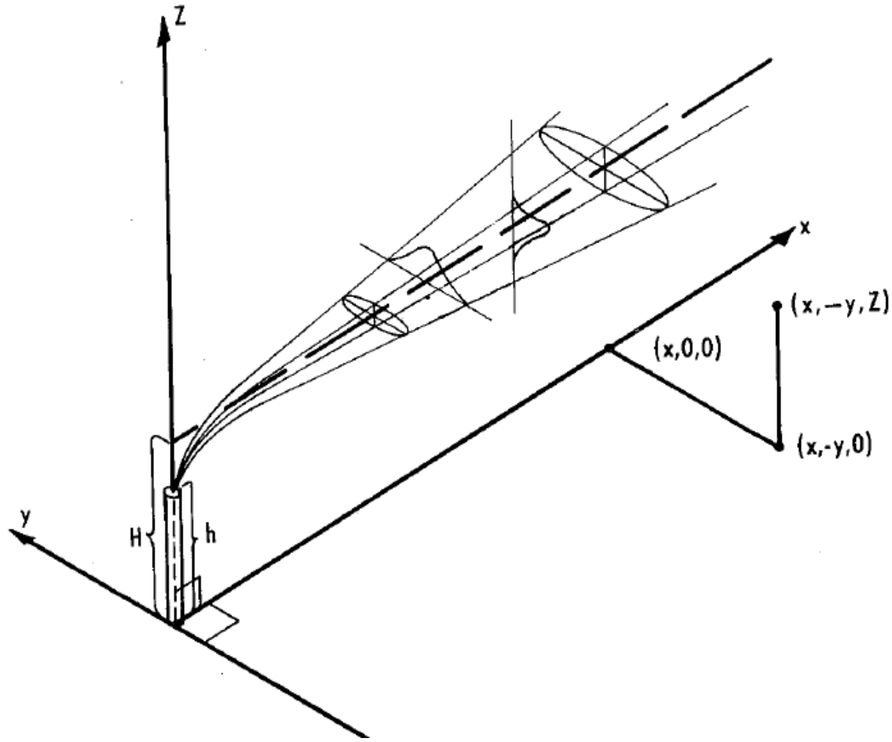

Fig. 1. Coordinate system showing Gaussian distribution. (Figure from Turner 1970)

A typical atmospheric release will emanate from a point source that emits effluents at a rate equal to Q (Bq s^{-1}). The effluent enters the atmospheric volume at the release point where mixing is initialized by the wind velocity μ (m s^{-1}) and turbulence profile within the volume. Depending on the atmospheric turbulence at the time of release the plume may mix uniformly within the x, y, or z directions, and be pushed downwind as a function of μ. The concentration at a point downwind is thus directly proportional to the rate of release and inversely proportional to the wind speed (Martin 2006). Further, Gaussian-distributed plumes represent the dispersion of a release from a point source under some degree of atmospheric instability. Thus, the concentration will decrease as a function of lateral and vertical expansion at a downwind point x;

diffusion coefficients σ_y and σ_z are used to describe diffusion of the plume within the lateral and vertical dimensions, respectively.

The key parameter to the quantification of Gaussian atmospheric dilution and dispersion is expressed as the ratio χ/Q which is the integral of the concentration over a specified time period in units of s m^{-3}, where χ is the concentration of the pollutant in air at a downwind location, and Q is the release rate of the radiological release, or the total activity of the release of an effluent at a dimension x,y,z (positions within a Cartesian coordinate system oriented with the x-axis in the direction of the mean horizontal wind vector, the y axis within the lateral crosswind direction, and the z axis representing the vertical dimension) from a release height, H, plus any postulated plume rise, as provided by Equation No.1. (Turner 1970, MACCS2 2004)

Eqn. 1 $$\frac{\chi}{Q}\ (x,y,z;H) = \frac{1}{2\pi\ \sigma_z\ \sigma_y\ \mu} \exp\left[-\frac{1}{2}\left(\frac{y}{\sigma_y}\right)^2\right]$$

$$x\left\{\exp\left[-\frac{1}{2}\left(\frac{z-H}{\sigma_z}\right)^2\right] + \exp\left[-\frac{1}{2}\left(\frac{z+H}{\sigma_z}\right)^2\right]\right\}$$

For the calculation of concentration at ground level, z = 0, as used for dose assessments, Equation No. 1 simplifies to a bivariate normal distribution (Slade 1968):

Eqn. 2 $$\frac{\chi}{Q}\ (x,y,0;H) = \frac{1}{\pi\ \sigma_z\ \sigma_y\ \mu} \exp\left[-\frac{1}{2}\ (\frac{y}{\sigma_y})^2\right] \exp\left[-\frac{1}{2}\left(\frac{H}{\sigma_z}\right)^2\right]$$

For the calculation of the highest concentrations that occur along the plume centerline, where y = 0, Equation No. 2 further simplifies to:

Eqn. 3 $$\frac{\chi}{Q}\ (x,y,0;H) = \frac{1}{\pi\ \sigma_z\ \sigma_y\ \mu} \exp\left[-\frac{1}{2}\ (\frac{H}{\sigma_z})^2\right]$$

Additionally, the manner with which radionuclides are released into the atmosphere, whether an instantaneous puff release or a continuous release, may affect the downwind concentration and may be accounted for within the model, e.g., step progression release fractions. Three dominant time dependent mechanisms influence the effluent concentration: an instantaneous release in which dilution occurs by turbulent diffusion as the effluent travels downwind; a short-term release period in which the average concentration downwind is affected by both turbulent dilution and dispersion via large eddies that are too big to affect the turbulent mixing within the plume, i.e., wind meander; a longer release period in which changes in wind direction and wind speed influence the effective concentration at any point as a function of the first two mechanisms, as well as the fraction of time that the point is within the plume pattern.(Slade 1968)

1.2 Building Wake Effects

The prevailing wind speed and direction are key elements in plume dispersion and transport analysis. Additionally, mechanical turbulence is generated when air flows around fixed objects, or roughness elements, on the earth's surface and when adjacent parcels of air move at different speeds or in different directions, and this mechanical turbulence is also an important dispersion mechanism. Surface roughness affects the microscale flows and the turbulence of the air within the atmospheric boundary layer (ABL), which is approximated as the layer between the ground and the mixing height. Essentially, a greater surface roughness transitions into a greater degree of mechanical turbulence. A greater degree of mechanical turbulence transitions into a greater rate of diffusion. (MACCS2 2004)

Mechanical turbulence is also generated when air interacts with some fixed obstacle, such as the ground, vegetation and structures. Turbulence generated by airflow around a building, results in two aerodynamic structures, the wake and cavity (MACCS2 2004). The interaction of the initially stagnant wake surrounding the facility with the incoming wind causes the wake fluid to move downwind, thereby inducing a circulatory return flow along the ground to replace the lost fluid. This circulation causes a streamline that divides the wake into two zones. Fluid above and to the side of this streamline continues to move downwind and is termed the wake zone. Fluid enclosed within this region continues to recirculate and is termed the cavity zone, as it essentially represents a low pressure cavity within the wake. Diffusion allows the entrapped effluent to eventually transverse the streamlines. Even with diffusion, the concentration reached in many cases is high. (Slade 1968)

Wake and cavity effects are assumed to be applicable at a distance of approximately 100 m and less, the total distance depending on the height and width of the object. As such, building structures, vegetation, and the placement of wind/air measurement instrumentation with respect to air flow obstructions all become important (MACCS2 2004). Downwind and upwind receptors of interest may exist within the building wake, specifically within the recirculation (cavity) zones. Experimental data shows that such effects may reach up to 600 m downwind from a given facility (Halitsky 1976).

Such effects may be characterized by a variation within the μ or pressure fields created by physical obstructions. For example, say we have a μ of 5 m s^{-1} at 600 m upwind from the obstruction. This value will be taken as our base μ. Now we characterize the wind velocities at various downwind distances from the obstruction and we notice that the velocity varies from approximately 1.5 m s^{-1} at 100 m downwind from the facility, to 3.0 m s^{-1} at 300 m, to the background μ of 5 m s^{-1} at 600 m downwind from the facility, thus representing exit from the wake effects caused by the obstruction (Halitsky 1976).

Average winds and turbulence values used within transport and diffusion calculations utilize varying scales depending on the size of the plume within the atmosphere, and the level of resolution of the input data. For instance, an entire plume typically moves according to the average wind flow, but the radiological contamination is most efficiently diffused by turbulent eddies within the atmosphere which are approximately the same size of the plume. Eddies that are much smaller than the plume tend to fuzz the cloud edges, while much larger eddies tend to direct the entire plume. (Hanna et al. 1982)

Eddies are formulated within the vicinity of buildings and other obstructions which disturb the flow of air within the environmental atmosphere**.**

The three main zones of flow around a building are as follows (Pasquill and Smith 1983):

- The upwind displacement zone, where the approaching air is deflected around the building. Beneath the upwind displacement zone exists a recirculation cavity as shown in Fig. 2. The representation of the upwind recirculation zone is not drawn to scale as the size of such a zone will depend upon the site specific meteorological conditions.
- The relatively isolated cavity zone immediately on the leeward side of the building
- The highly disturbed wake zone farther downwind from the building.

Furthermore, Fig.2 displays a two-dimensional representation of the mean velocity profile. Whereby the letters: (a, b) represent the beginning of the upwind side of the displacement zone; (m, n, o, p) and (q, r, s, t) represent the streamlines around the building, i.e., the wake zone and displacement zone boundaries, respectively; (c, d, e, f) represent the corners of the building; (g, h, i, k) represent the cavity zone boundary. Additionally, the numbers represent the progression of the mean velocity profile. Notice how the μ decreases within the upwind and downwind recirculation cavities, this characteristic is known as the velocity deficit and represents a departure from the mean wind velocity as displayed at the far right and left of the figure.

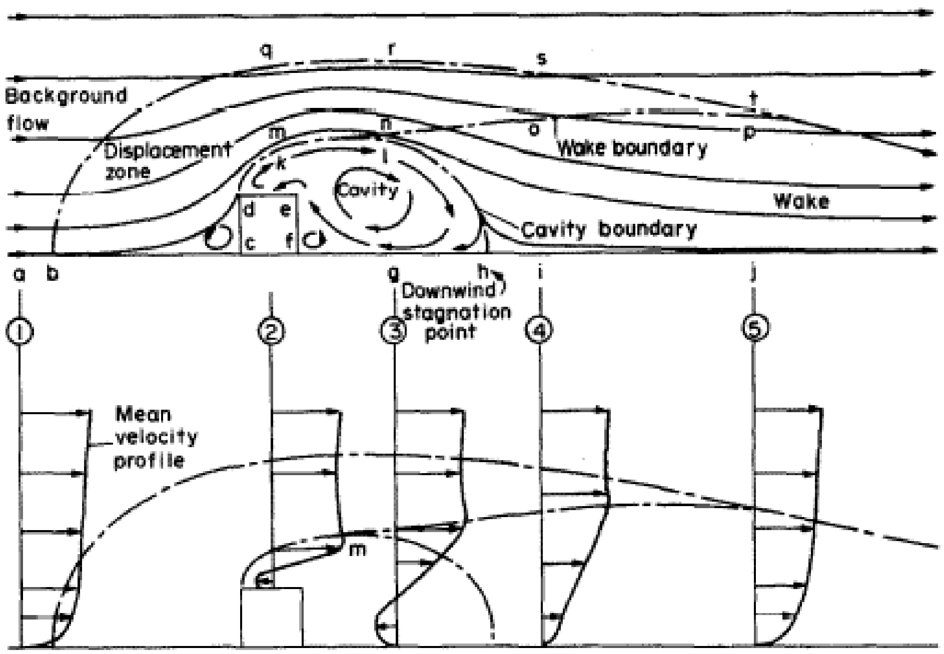

Fig. 2. Sketch of flow zones around a cube on the ground. (Halitsky 1976)

In regards to plume dispersion, if the radiological effluent from a stack penetrates into the displacement zone, the effects of the building on the plume are negligible and the release is equivalent to one coming from an elevated point source. However, if the plume fails to penetrate the displacement zone, it is drawn into the wake or cavity zone and should be treated as coming from a ground-level volume source (Thuillier and Mancuso 1980). Additionally, plumes that fail to penetrate into the displacement zone and are entrapped in the cavity zone, increase the risk for exposure to people on the ground attempting to evacuate the building, and those within the building itself, as the effluent may enter intake vents and the building ventilation system (Schulman et al. 2000, Briggs 1974).

Building wake effects are typically associated with the building from which the release occurs. However, this is not always the case, if the release originates from a building within the vicinity of a much larger building, the larger building may exert more influence on the dispersion of the plume than the building from which the release initializes (NCRP 1993).

Thermal turbulence is contained within the ABL, and the top of the ABL is the boundary of the inversion layer. The plume is effectively unable to penetrate this layer, resulting in the effluents being trapped between the ground surface and the top of the ABL layer. Because turbulent diffusion and thus mixing of air with the effluent plume are restricted to the ABL, the distance from the surface to the top of the ABL may be called the mixing height. Mixing heights vary greatly. In fact, under unstable conditions the mixing height may reach 2,000 m or more, and under stable conditions the mixing height may be 100 m or less and extremely difficult to define. (Garratt 1994)

Atmospheric dispersion models play a key role in evaluating the actual or hypothetical transport and impact of radionuclides released into the atmosphere. The fundamental goal of any dispersion model is to account for all of the material released into the atmosphere from a specific source. The model must address three fundamental questions (Barr and Clements 1984):

- Where does the released material go and when does it arrive at a particular location?
- How fast is the material diluted as it travels
- How fast and by what mechanism the material is ultimately removed from the atmosphere?

2.0 REVIEW OF NEAR FIELD LITERATURE

2.1 Gaussian Model Limitations and Approximations

In regards to turbulent flow, the concept of eddy diffusion coefficients arises from an analogy to the molecular transfer of momentum and heat for gases. The concept speaks to the formation of a control volume, the time change of concentration of effluents within the volume is the result of convergence or divergence of the effluent fluxes in each of the three directions (x, y, and z), and is represented by the following equation (Crawford et al. 2008):

Eqn. 4
$$F_x = K_x \frac{\partial \chi}{\partial x}$$

Where:

F_x = flux of pollutant in the x direction (g m^{-2} s^{-1})

K_x = eddy diffusivity in the x direction (m^2 s^{-1})

χ = concentration of the pollutant (g m^{-3})

Atmospheric dispersion/diffusion parameters within Gaussian diffusion models arise from the analytical solution to the three-dimensional diffusion equation shown in Equation No. 5. The theoretical basis for atmospheric diffusion was based upon the application of macroscale analogies to the microscale molecular processes of heat and momentum transfer. Whereby, diffusion is described as the product of gradient of the concentration in space and the coefficient of diffusivity, with transport occurring from an area of high content to low content.

Eqn. 5
$$\frac{\partial \chi}{\partial t} = \frac{\partial}{\partial x}\left[K_x\left(\frac{\partial \chi}{\partial x}\right)\right] + \frac{\partial}{\partial y}\left[K_y\left(\frac{\partial \chi}{\partial y}\right)\right] + \frac{\partial}{\partial z}\left[K_z\left(\frac{\partial \chi}{\partial z}\right)\right]$$

Where:

x, y, and z = the downwind, crosswind, and vertical directions, respectively

K_x, K_y, and K_z = the eddy diffusivities in the x, y, and z directions, respectively

The estimation of diffusion thus depends upon determining applicable values of the coefficient of diffusivity and the solutions to differential equations which describe the concentration gradient in space and time (Slade 1968). As such, the difference in fluxes in to and out of a defined volume is equal to the change in the content of the volume with time. As described in chapter one of this dissertation, solutions to the Gaussian model represent the transport and dispersion of effluent concentrations into the atmosphere and are described by the Gaussian distribution within all three directions (x, y, and z). Application of this concept works well for microscale molecular processes; however, is limited in its application at the macroscale to atmospheric diffusion because turbulent transfer processes are much larger than molecular processes (Crawford et al. 2008). Despite these restrictions diffusion via the gradient approach became a cornerstone for diffusion modeling. Still, the inability of the standard Gaussian model to estimate dispersion within the proximity of turbulent flow is a major limitation, and will be discussed later in this section.

Additional contributions to the concept of diffusion were made with the introduction of diffusion by continuous motion, which stated that the final position of particulate within an turbulent medium could be determined through a knowledge of the turbulent velocities acting upon the particulate throughout its progression from release to destination. If we designate the summation of particulates, as a plume, and follow that plume, the concentration of effluent particulate within the plume could be estimated from knowledge of the spectrum of the existing atmospheric turbulence (Slade 1968). In respect to the molecular kinematic scenario, molecular exchanges occur over the mean free mixing length of the gas molecules. Within turbulent flow, the mixing occurs over the mean distance between turbulent eddies**.** Because the molecular transfer rates for particles and gases are much smaller [e.g., in one second, the rms travel distances are 0.6, 5.9 x 10^{-4}, and 1.7 x 10^{-4} cm for an air molecule, 1 μm, and 10 μm particles, respectively (Hinds 1982)] compared to turbulent atmospheric flow (e.g., scale of meters per second), the molecular transfer is ignored. Also, within molecular problems kinematic viscosity is important. However, the viscosity is neglected within turbulent flow.

Furthermore, the eddy diffusion coefficients are assumed to be constant in space and time, which is true for the molecular scenario, but not turbulent flow within the atmosphere. Therefore, if possible, an empirical approach should be used for obtaining σ as function of distance and stability conditions within the atmosphere. (Slade 1968)

Within the vertical direction, K_z is approximated as a function of height above the ground, which yields the maximum vertical eddy dimension. Within the horizontal direction, the K values are related to the size of the turbulent eddies which most efficiently diffuse the pollutant. Richardson (1926) studied the relative diffusion of particles on Loch Long, Scotland, and found that:

Eqn. 6 $$K \cong 0.07l^{1.4}$$

For the atmosphere and using relatively crude data, Richardson (1926) found that:

Eqn. 7 $$K \cong 0.2l^{4/3}$$

Where *l* is anyone of the following, based upon the application:

- Horizontal mixing length
- Mean distance between two particles
- Standard deviation of particles around a center point (i.e., the standard deviation of a Gaussian distribution)
- Characteristic dimension of the eddies most responsible for the diffusion

Further development of the eddy diffusion concept was provided by Kolmogorov in 1941 from his work on similarity theory, and from Obukhov within the same year, who evaluated energy balance within the turbulent spectrum (Crawford et al. 2008). Taylor (1959) expanded the similarity theory assumption that turbulent energy progressed unchanged from larger eddies to small eddies by incorporating dimensional analysis and showed that the turbulent diffusion rate is the crucial parameter to consider within atmospheric diffusion. Batchelor (1950) applied these concepts to the spread of a plume of particles about its center point as a function of time, and highlighted that σ is the separation of particles as approximated by the standard distribution for a Gaussian distribution. Also, the approximations from similarity theory should apply only within the near field of the atmosphere where all turbulence is isotropic, i.e., within the cavity zone. Beyond which, i.e., the wake zone, the cloud of pollutants becomes larger than the largest horizontal eddies, where turbulent dispersion becomes the dominant mechanism as opposed to molecular diffusion. (Slade 1968)

As the previous discussion alludes to, with adequate time averaging, the analytical solutions to the three dimensional diffusion equations do approximate a Gaussian shaped solution in which mass is conserved. Additionally, Gaussian models for atmospheric diffusion typically agree well with measured data and their results are generated quickly. (Crawford et al. 2008)

However, a model user must exercise care over the downwind distance for which the Gaussian model is applied. The American Meteorological Society published a paper which indicated that the Gaussian dispersion model is estimated to be within an accuracy of a factor of two, within distances of 100 m to 10–20 km. This accuracy is applicable when onsite meteorological tower data is available, and conditions are reasonably steady with relatively homogenous horizontal diffusion (Briggs et al. 1977). At distances greater than 20 km or closer than 100 m, the accuracy should be considered to be an order of magnitude at best. Also, variables such as rough or urban terrain, building wakes, and plume meandering introduce more uncertainty into the Gaussian model predictions.

Additionally the standard Gaussian plume model may not directly apply to flow around buildings, or within the vicinity of buildings, i.e., building wake effects. A typical method of addressing these effects is to assume that the plume is released from ground level and then to modify the standard diffusion parameters σ_y and σ_z utilized within the model. One such modification was proposed in NRC Regulatory Guide 1.111 (NRC 1977). Furthermore, to accurately address wake effects empirical measurements and/or physical modeling may be required for an accurate evaluation of the airflow and resulting dispersion surrounding the facility of interest. (Widner et al. 1991)

As discussed earlier, ground level releases and releases from small stacks may be entrained in the downwind or upwind recirculation cavities of a building due to the aerodynamic effect of the facility on the air flow within which the release occurs. The illustration within Fig. 3 displays the wake and cavity zones downwind of a nuclear facility. The downwind direction is x, the facility height is H_B, and A_B is the cross-sectional area of the building most perpendicular to the flow of the plume, i.e., the surface area of the largest wall of the building nearest the receptor. The extent of the cavity zone may have been shown to be approximately a downwind distance of 2.5 $AB^{0.5}$. (MACCS2 2004)

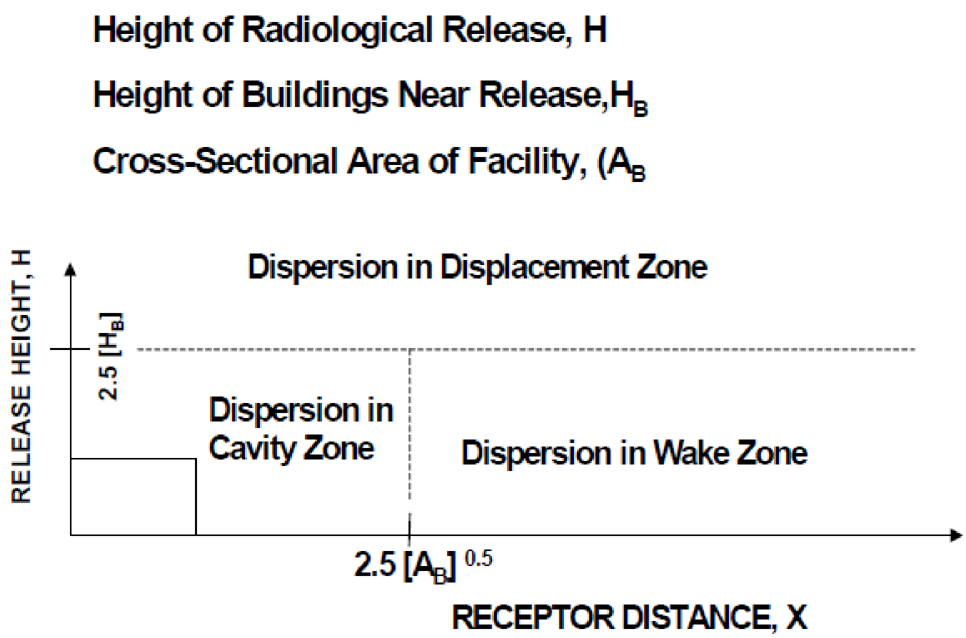

Fig. 3. Cavity and wake zones downwind of a building structure (MACCS2 2004).

A traditional approach for accounting for building wake effects, the ground level dilution factor equation is modified to (MACCS2 2004):

Eqn. 8
$$\frac{\chi}{Q} = (\mu\,[\pi\sigma_y\sigma_Z + cA])^{-1}$$

Where:

c is the building shape factor, usually taken to be 0.5

A is the smallest cross-sectional area of the building

μ is the 10-meter height wind speed

σ_z is corrected for the wake effect

However, a correction to the vertical diffusion coefficient is essentially a best guess approximation, unless the correction can be based on empirical data.

This methodology is to be applied within the context of NRC Regulatory Guide 1.145 for non-stack releases, e.g., building penetrations. (NRC 1983)

Once a radioactive plume enters the atmosphere, it is assumed to travel according to one wind direction throughout the entirety of an assessment process and is an implicit parameter within the Gaussian model. One of the major limitations in the Gaussian plume model is that spatial and temporal variations in wind direction are not considered.

Traditionally, atmospheric stability is categorized into stability classes, which are used in the Gaussian plume model and the selection of class is crucial to the calculation of the downwind concentration. For example, Pasquill-Gifford stability classes range from A, most unstable, to F or G, most stable. The Gaussian diffusion parameters σ_y and σ_z (Eqn. 1) are chosen on the basis of stability class. Limitations associated with the Gaussian model can be compensated for by selecting diffusion parameters which are based on empirical observations. Therefore, one should select a set of diffusion parameters that are based on measurements and theoretical assumptions which most closely coincide with the conditions expected within the model application. Also, selecting diffusion parameters relative to the desired sampling time is recommended. (Crawford et al. 2008)

In addition to a model represented by one compartment volume, multibox models have also been used in pollution studies which consist of a defined bottom (ground) and top (ABL) of the relative box. The equation governing these models is based on the mass conservation equation and accounts for advective fluxes and diffusion into and out of the compartmental volume. However, the equation is nonlinear and cannot be solved analytically. Therefore, a simplification is applied which eliminates the vertical flux and diffusion parameters and assumes uniform mixing between the ground and ABL layer. However, specification of the wind data input, and turbulent eddy diffusivities within the horizontal plane are still pertinent. (Knox and Walton 1984).

Another type of model which is finding increased applicability is the screening model. An application of which is in the quantification and prioritization of contaminated sites for possible cleanup activities (Hoffman et al. 1993). The National Council on Radiation Protection and Measurements (NCRP) has published a summary of screening models designed for evaluating the impact of the atmospheric emission of radionuclides, including several empirical formulas for the calculation of cavity and wake zone concentrations. (NCRP 1996) However, screening models typically provide bounding concentrations with limited applicability beyond simple screening, i.e., the concentrations are diluted according to the surface area on the lee side of the building and do not provide a lateral concentration profile.

While atmospheric dispersion processes dilute downwind plume concentrations, others mechanisms exist that remove effluents from the plume. The removal processes consist of dry deposition: which results from gravitational settling of material from the plume, and impaction due to potentially large downwash; and wet deposition, also known as precipitation scavenging. (MACCS2 2004)

Two common dry deposition models are the source depletion model and the surface depletion model. The source depletion model computes the rate at which effluents within the plume deposit upon the ground according to the product of the ground level concentration of the effluents, and the dry deposition velocity of the effluent (Chamberlain 1953). This approach uniformly depletes the cloud, however, does not disturb the normal distribution of the concentration throughout the height of the plume, an assumption which is valid during neutral or unstable atmospheric conditions (MACCS2 2004). The surface depletion method is computationally more complex than the source depletion model, as it depletes the source at the plume/earth interface. Application of the surface model thus changes the source material distribution within the plume. As mentioned previously, parameterization of dry deposition processes are usually accomplished by the utilization of a dry deposition velocity.

According to MACCS2 (2004), the deposition velocity is defined as a deposition flux (F_d) divided by the airborne concentration of radioactive material (χ):

Eqn. 9
$$v_d = \frac{F_d}{\chi}$$

The deposition flux is a function of the particle size, wind speed, atmospheric instability, and surface roughness (Sehmel and Sutter 1974). Various field experiments performed over the years resulted in dry deposition velocities over a range of 0.001 to 180 cm s^{-1} for particulates, and 0.002 to 26 cm s^{-1} for gases. (MACCS2 2004)

Furthermore, surface roughness typically affects the magnitude of vertical turbulence, and hence, vertical atmospheric diffusion. The rougher the surface below the region of atmospheric transport, the larger the turbulent eddies that are formed when the plume interfaces with the earth's surface. A non-smooth terrain may necessitate the application of a linear scaling to increase the effective value of σ_z (MACCS2 2004). However, within the cavity zone vertical turbulence is dominated by the recirculatory volumes generated by the flow of wind atop the building of interest.

As particles are depleted from a plume due to the air/earth interactions, they are also returned to the plume via resuspension. Resuspension is the process of lifting small particles, typically less than 50 μm, from the ground surface back into air by wind force (Whicker and Rood 2008). A major cause of resuspension is mechanical disturbance. Parameters which affect the rate of resuspension include wind speed, turbulence, and density. According to Sehmel (1980), measured rates of resuspension have varied over 10 orders of magnitude through time and space, thus making the selection of a resuspension value difficult.

2.2 Regulatory Models: Guidance Pertaining to Capabilities and Limitations

Continuing research is still needed before atmospheric turbulence and dispersion is completely described. However, multiple dispersion theories have been proposed which serve as the basis for practical models of atmospheric dispersion. However, all models, no matter how simple or complex, are approximation of reality with some level of uncertainty. Thus, models must be used carefully, with some indication or explanation of their inherent uncertainties known to the analyst (Kirchner 2008). Understanding the limitations and proper application of atmospheric dispersion models necessitates an understanding of the current models and how they are used. A discussion on commonly used atmospheric dispersion codes are provided next. The basic structure, assumptions and limitations of the models are discussed.

2.2.1 MACCS2

MACCS2 - MELCOR Accident Consequence Code System for the Calculation of the Health and Economic Consequences of Accidental Atmospheric Radiological Releases is a Gaussian plume model used in analyzing atmospheric dispersion and the subsequent radiological consequence of accidental releases of radioactive material from postulated accident conditions. MACCS2 predicts dispersion of radionuclides via the use of straight-line Gaussian plumes. Input variables such as direction, duration, sensible heat, and initial radionuclide concentration may be varied per plume. MACCS2 modeling consists of three modules: ATMOS handles the atmospheric transport and dispersion of material via a Gaussian plume model with Pasquill-Gifford dispersion parameters; EARLY models consequences of the accident to the surrounding area within an emergency action period; and CHRONC considers the long term impact to the surround area during the period following the emergency action period. (MACCS2 2004)

The use of these codes is best suited for relatively short release times, ranging from instant to several days, and more than one weather spatial location cannot be input into the model. Also, Gaussian models are inherently flat-earth models, and perform best over regions of transport where there is negligible variation in terrain. As such, neglecting terrain variations such as nearby buildings, tall vegetation, or grade variations are simplistic conservatisms when not taken into account within dispersion parameterization**.** As with all Gaussian models, MACCS2 is not well suited for dispersion modeling within the near field, or long-range dispersion. (MACCS2 2004)

For distances beyond the near field, typically assumed to be beyond a downwind distance of 100 m and extending to a long-range distance of approximately 10,000 m, many methods have been proposed for establishing the magnitudes of diffusion coefficients σ_y and σ_z. Most of which are based on empirical fitting curves of data that were taken during experiments over flat grassland as documented by Haugen in 1959. One commonly used curve-fitting method is that of Tadmor and Gur, in which each σ is expressed as: $\sigma = a\ x\ b + c$ where *a*, *b*, and *c* are empirical constants (MACCS2 2004). Long-range dispersions are likely to vary depending on the variance of meteorological conditions at locations far from those at the source of the release. Long-range dose projections are better calculated with regional models which are able to account for multiple meteorological conditions.

For distances within the near field or less than about 100 m, these coefficients generally do not provide a good fit to the measured data points and the models are generally considered rough approximations. Such approximations acknowledge the large degree of modeling uncertainty within the near field and the range of applicable dispersion parameterization. This is because Gaussian models, with the underlying steady-state assumptions, do not consistently perform well for atmospheric releases within the near-field. As discussed previously, the concentrations at close-in distances are influenced by the physical presence of neighboring structures, i.e., building wake effects. Thus the application of a standard set of diffusion coefficients is inadequate as they ignore increased vertical turbulence from wake effects, down washing into the cavity within the lee of the building, as well as recirculation (MACCS2 2004). Chanin and Young (1998) discourage the application of MACCS2 for distances within a near field of 500 m for laboratory or industrial scale facilities, based on reference to the field measurements and Gaussian model applicability in the wake of large facilities. As a default, Tadmor-Gur, Briggs, or Pasquill-Gifford standard deviation sets are often adjusted to account for site-specific and surface roughness characteristics (MACCS2 2004). The limitations of the MACCS2 model, as they pertain to the Gaussian plume model, are displayed below in Table 1.

Table 1. MACCS 2 limitations. (MACCS2 2004)

Topic	Applicable Regime	Basis	Source or Reference
Distance from Source	100 m < x < 10 km – 20 km	Dispersion parameterization	(Haugen, 1959); Other accounts of Prairie Grass experiments;
Sensible Energy	Well-defined (e.g., sensible heat, timing, certainty of radiological release with combustibles) releases	Point-wise (stack) or pool-type (area) release	Briggs (1975); Mills (1987)
Release Duration	Approximately three minutes to ten hours	Dependent on basis dispersion parameters	NUREG/CR-4551; Tadmor (1969); Gifford (1975)
Terrain Sensitivity	Flat-earth to "gently rolling"	Adjust dispersion parameter set to region of interest with AMS model; Complicated terrain over the region of transport may require Lagrangian particle or other models	AMS (1977); (Hanna, 1982); Hanna (2002); Others
Building wake effects	Within approximately ten x characteristic building dimension lengths	See discussion beginning page A-29 of this report.	Turner (1970)

2.2.2 AERMOD

The EPA developed a steady-state model termed AERMOD. The model includes the many recent advances in boundary layer physics, and calculates the concentration statistics at various points in the region of interest from long-term release data from a single meteorological station. AERMOD comprises two preprocessors and a dispersion module. The first preprocessor is called AERMET and provides AERMOD with meteorological boundaries, specifically physical parameters to characterize the vertical structure of the planetary boundary layer. The second preprocessor is called AERMAP and provides terrain characterization and generates receptor grids for AERMOD. (Crawford et al. 2008)

AERMOD uses the Plume Rise Model Enhancements (PRIME) procedures developed by Schulman et al. (2000). PRIME is a Gaussian dispersion algorithm that employs two dominant features associated with building downwash: (1) reduced plume rise caused by the descending streamlines lee of the building and increasing entrainment within the wake, and (2) enhanced diffusion coefficients due to tumultuous mixing within the building wake (Canepa 2004). The dimensions of the cavity zone are estimated based on building geometry (Wilson and Britter 1982, Fackrell 1984) and a cavity model within PRIME calculates the plume mass fraction trapped within the recirculation region. The captured plume is later emitted into the far wake as a volume source and added to the primary plume contribution entrained within the wake, to obtain far wake concentration estimates (Schulman et al. 2000). This process is considered adequate for non-buoyant and low momentum releases where pollutants are expected to rapidly be entrained into and vigorously mix within the cavity region generated by the presence of the building. However, uncertainties arise when releases are associated with plume buoyancy and momentum such as from a fire, and or explosion, as such characteristics may change the shape and size of the cavity region, alter the turbulence structure, and vary the amount of trapped pollutants. (Olvera et al. 2007)

Depending upon the fraction of plume mass that is estimated to intercept the cavity boundaries, PRIME will divide plume mass between the re-circulating cavity region and the wake region. The zone boundaries are established from estimates of the locations of the lateral and vertical streamlines separating the cavity zone from the wake zone. Lateral diffusion of the recirculated cavity mass is based on building geometry, and diffusion is assumed to be uniformly mixed along the vertical axis. The turbulence within the wake region decays gradually with distance, and transitions to ambient levels of turbulence within the far-field. Essentially, the induced building wake effects are employed to restrict the plume rise expected in absence of the building.

Within the wake zone, PRIME algorithms are used to calculate effluent concentration with AERMOD-derived ambient turbulent intensities as input. To insure a smooth transition between the near field concentrations estimated by PRIME, and the far field concentrations estimated by AERMOD, concentrations beyond the wake are estimated as the weighted sum of the two calculations. According to EPA-454/R-03-004, the total concentration is calculated using the PRIME algorithms with AERMOD-derived meteorological inputs. C_{AERMOD} is the concentration estimated using AERMOD without considering building wake effects or the weighting parameter.

The structure of the cavity and wake is controlled by the building dimensions, as projected along-wind and crosswind. These dimensions are the building height (H), the projected building width across the flow (W), and the projected length along the flow (L). Within the PRIME model, the length scale for diffusion near a building is defined as (Schulman et al. 2000):

Eqn. 10 $$R = B_S^{2/3} B_L^{1/3}$$

Where B_S is the smaller and B_L is the larger of H and W

According to Schulman et al. (2000), the maximum height of the downwind cavity is equal to:

Eqn. 11 $$H_R = H + 0.22R \text{ at } x = 0.5R$$

Where x is the along-wind distance measured from the upwind face of the building

The length of the downwind recirculation cavity, as measured from the upwind face of the building, is estimated according to:

Eqn. 12 $$L = \frac{1.8W}{[\left(\frac{L}{H}\right)^{0.3}(1.0+\frac{0.24W}{H})} \quad (0.3 \le L/H \le 3.0)$$

If the L/H ratio lies outside the indicated range, L_R is calculated with the nearest limit. The length values yielded by Equation No.12 are much lower than those proposed by Turner (1970), and utilized within the MACCS2 model as displayed in Fig. 12.

Schulman et al. (2000) goes on to further discuss cavity and wake zone dimension calculations as a function of very specific streamline phenomena. These dimensions are then used to calculate a mean streamline slope, and descent downwind from the facility within the x dimension. Plume rise, and dispersion coefficients are also discussed. Specifically, enhanced turbulence intensity and velocity deficit values are calculated within the cavity region and reach a maximum at the lee of the building. The values then decay with two-thirds power downwind. At the distance which the plume centerline intersects the wake region, an eddy diffusivity model for plume growth is used. The key assumption stated within the probability density function model, is that particles released by the source remember their initial velocity. These approximations may be useful for the estimation of the cavity and wake zone interface interactions. However, aside from calculating the centerline concentration, the model is limited in its ability to identify the concentration profile within the L dimension. (Schulman et al. 2000)

2.2.3 ARCON96

U.S NRC Regulatory Guide 1.194 (NRC 2003) provides guidance for the estimation of atmospheric relative concentration (χ/Q) values in support of design basis control room radiological habitability assessments at nuclear power plants. The guide describes methodologies deemed acceptable for use by Nuclear Regulatory Commission (NRC) staff in determining χ/Q values that will be used in the evaluation of potential radiological consequences to the inhabitants of the control room over a range of postulated accident scenarios resulting in the release of radioactive material to the environment. Such evaluations are performed in support of applications for license, and license amendment requests. Additionally, Title 10 of the Code of Federal Regulations (CFR) Part 50 requires that each potential licensee provide an evaluation of the design and performance of structures, systems, and components (SSC) of the facility, with the objective of assessing the mitigation capabilities of the SSCs and the overall risk/consequence to public health and safety as a result of the operation of the facility.

Within 10 CFR Part 50, Appendix A, minimum requirements are established for the principal design criteria for Light-water cooled nuclear power plants. Specifically, General Design Criterion 19 establishes the minimum requirements for the design of the facility control room. Included within this requirement is that adequate protection be provided by the control room to reduce the radiological consequence associated with the progression of a postulated accident condition, thus permitting access to, and occupancy within the control room.

According to NRC (2003), existing dispersion models did not reliably predict, and typically overestimated the radiological concentrations within the wake zone of buildings. The statistical model documented within Ramsdell (1988) made significantly more reliable predictions within building wakes. Developmental work continued by the NRC, and in 1994, the earlier model was revised and included within the ARCON95 code. Slight modifications were made to the code and it was re-issued as ARCON96 and documented in Revision 1 of NUREG/CR-6331(Ramsdell 1995). ARCON96 implemented an improved building wake dispersion algorithm; assessment of ground level, building vent, elevated, and diffuse source release modes; use of hour-by-hour meteorological observations; sector averaging; and directional dependence of dispersion conditions.

The May 9, 1997, version of the ARCON96 code as described in Ramsdell (1995) was deemed an acceptable methodology for the assessment of control room χ/Q values for use in radiological consequence analyses. ARCON96 is a Gaussian based model and utilizes Pasquill-Gifford stability classes for the derivation of σ_y and σ_x. The meteorological inputs needed for χ/Q calculations include wind speed, wind direction, and a measure of atmospheric stability. Such data should be obtained from an onsite meteorological measurement program. The meteorological data set used in these evaluations should represent hourly averages and be representative of the overall site conditions, and be free from near field effects such as building and cooling tower wake effects, and vegetation and terrain effects. Additionally, the analysis may be inappropriate in cases of unusual siting, building arrangement, release characterization, source-receptor configuration, and meteorological specifications. Such situations, specifically those involving extremely short duration releases, receptor distances shorter than about 10 m, and control room air intakes located close to the base of tall elevated stacks, need to be addressed on a case-by-case basis. (NRC 2003)

The code provides options that allow an analyst to model ground-level, elevated stack, and vent-point source releases. The analyst can also model diffuse area sources within the ground-level release mode. The ground-level release mode is utilized for the majority of control room χ/Q assessments. The ground level mode prompts ARCON96 to ignore all user inputs related to plume rise. (NRC 2003)

The cross section of the area source (e.g., maximum building surface dimensions) is computed as the maximum vertical and horizontal dimensions of the above-grade building cross-sectional area, which is sited perpendicular to the line of sight from the center of the building of interest to the control room intake. The release height is set at the vertical center of the perpendicular plane, and in conjunction with the line of sight, is used to establish the plume slant path. The slant path, or source-to-receptor distance is measured from this point to the control room intake.

The 0 to 8 hour 95th-percentile χ/Q value for a single point source to single point receptor geometry, with a difference in elevation less than 30% of the building height may be estimated using Equation No. 13. (NRC 2003)

Eqn. 13
$$\frac{\chi}{Q} = \frac{1}{3\pi\mu\sigma_z\,\sigma_y}$$

Where:

χ/Q = Relative concentration at plume centerline for time interval 0-8 hours in s m^{-3}

3 = Wake factor

μ = Wind speed at 10 meters, m s^{-1}

σ_y,σ_z = Standard deviation, in meters, of the gas concentration in the horizontal and vertical cross wind direction evalated at distance x and by stability class.

When the radioactive material is assumed to leak from many points on the surface of a building, i.e., a diffuse source, in conjunction with a single point receptor, i.e., diffuse source-point receptor geometry, Equation No. 14 is appropriate. This equation is also appropriate for point source-point receptors where the difference in elevation between the source and the receptor is greater than 30% of the height of the upwind building of interest, i.e., the building which creates the most significant building wake impact. The equation has also been deemed applicable for point source- volume receptor geometry e.g., an isolated control room with infiltration occurring at many locations. (NRC 2003)

Eqn. 14 $$\frac{\chi}{Q} = [\mu\left(\pi\sigma_z\sigma_y + \frac{A}{K+2}\right)]^{-1}$$

Where:

χ/Q = Relative concentration at plume centerline for time interval 0-8 hours in s m^{-3}

μ = Wind speed at 10 meters, m s^{-1}

σ_y,σ_z = Standard deviation, in meters, of the gas concentration in the horizontal and vertical cross wind direction evalated at distance x and by stability class.

$K = \frac{3}{(\frac{S}{d})^{1.4}}$

S = Shortest distance between building wake surface and receptor locations, m

d = Diameter or width of building, m

A = Cross section area of building, m^2

2.2.4 CAP88-PC

The CAP88-PC code uses a modified Gaussian plume equation to estimate the average dispersion of radionuclides released from a combined source of up to six emitting sources. That is, all the sources are modeled as if originating from the same point, e.g., stacks cannot be located in different areas of a facility. The emitting sources may be elevated, such as a stack, or uniform area sources, such as a pile of uranium mill tailings. Plume rise may be accounted for via momentum or buoyancy driven plumes. However, the plume rise mechanism is consistent for each source. Uniform area sources are modeled by segmenting the area source into annular segments with the same area. The segmentation is dependent upon the distance between the center of the area source and the receptor, for a radius up to 80 km. Concentrations are calculated at sector midpoints. The midpoint distances are input by the user. At larger distances where the ratio of distance to diameter is greater than 2.5, the area source is modeled as a point source. At close distances the area source becomes a circular source centered at the receptor of interest. Additionally, a point source model is also employed if the area source is 10 m in diameter or less. (Rosnick 2007)

Furthermore, all releases are assumed to be uniform in time and concentration, and impacts of complex terrain variation or building wake effects are not possible. Errors resulting from these assumptions are assumed to have a negligible effect for dose receptors located at a distance, which for most public receptor locations is large compared to the stack height, release area or facility size. Furthermore, dose and risk estimate outputs from CAP88-PC are applicable for low-level chronic exposures only, and cannot be used to model either acute or high level radionuclide intakes, as the dose consequence and resulting health effects data are based on low-level chronic intake dose conversion factors (DCF). (Rosnick 2007)

Plume dispersion is modeled within in the subroutine CONCEN via the straight line Gaussian plume equation displayed by Equation No. 1, and is simplified to the ground level concentration at the plume centerline according to Equation No. 3.An effective χ/Q can be calculated according to the principle of reciprocity. The mean χ/Q from a point source to one or more downwind sector segments is calculated according to the width of the segment or segments. The χ/Q for the entire segmented source is the sum of the χ/Q values for each sector weighted by the portion of the total annular source contained in that sector. (Rosnick 2007)

3.0 METHODS

3.1 Data Collection

It has been recognized throughout the development of classical diffusion theory that semi-empirical and statistical representations of turbulence would eventually give way to more direct empirical approaches, especially in highly complex flow fields (Hanna et al. 1982). For this study, empirical plutonium air concentration data was collected via eight air monitoring network (AIRNET) stations labeled 326, 327, 328, 317, 329, 330, 331, and 169 along the northern boundary of Material Disposal Area (MDA) B within site area TA-21, at the Los Alamos National laboratory (LANL) as shown in Figs. 4 and 5. (LANL 2010a, LANL 2011)

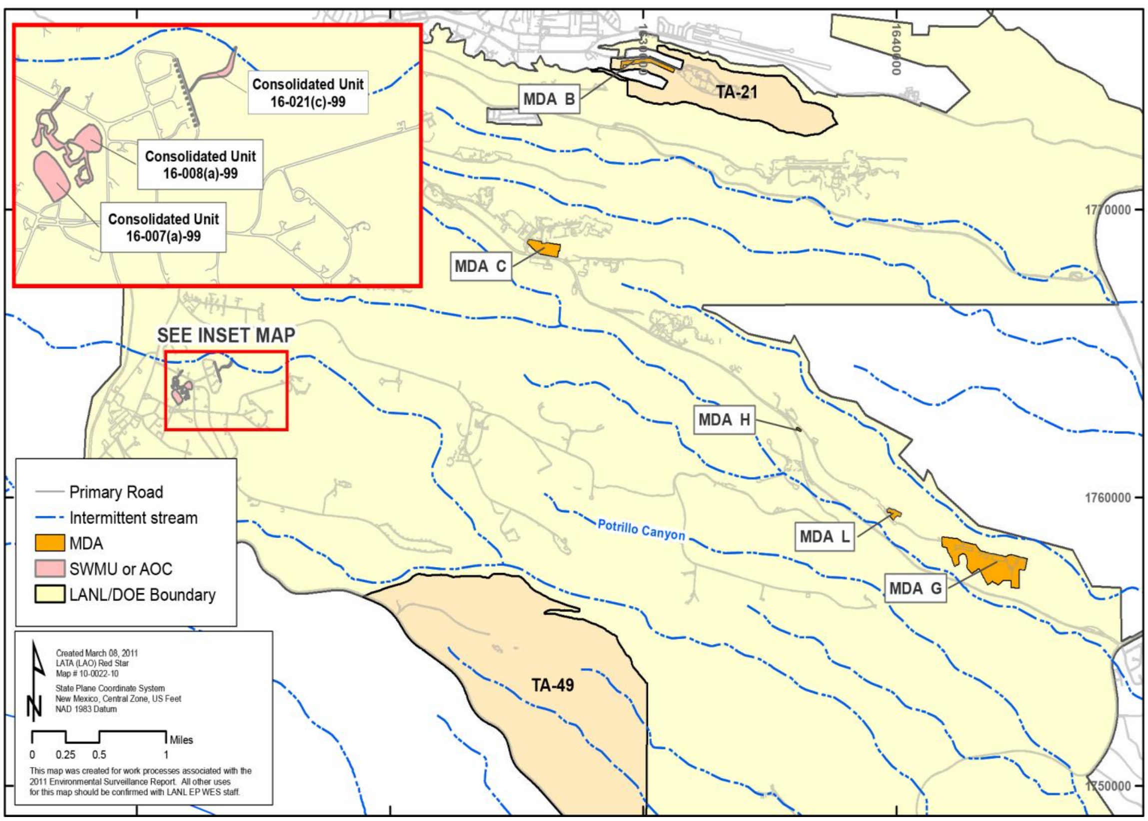

Fig. 4. LANL boundary map displaying TA-21. (LANL 2010a)

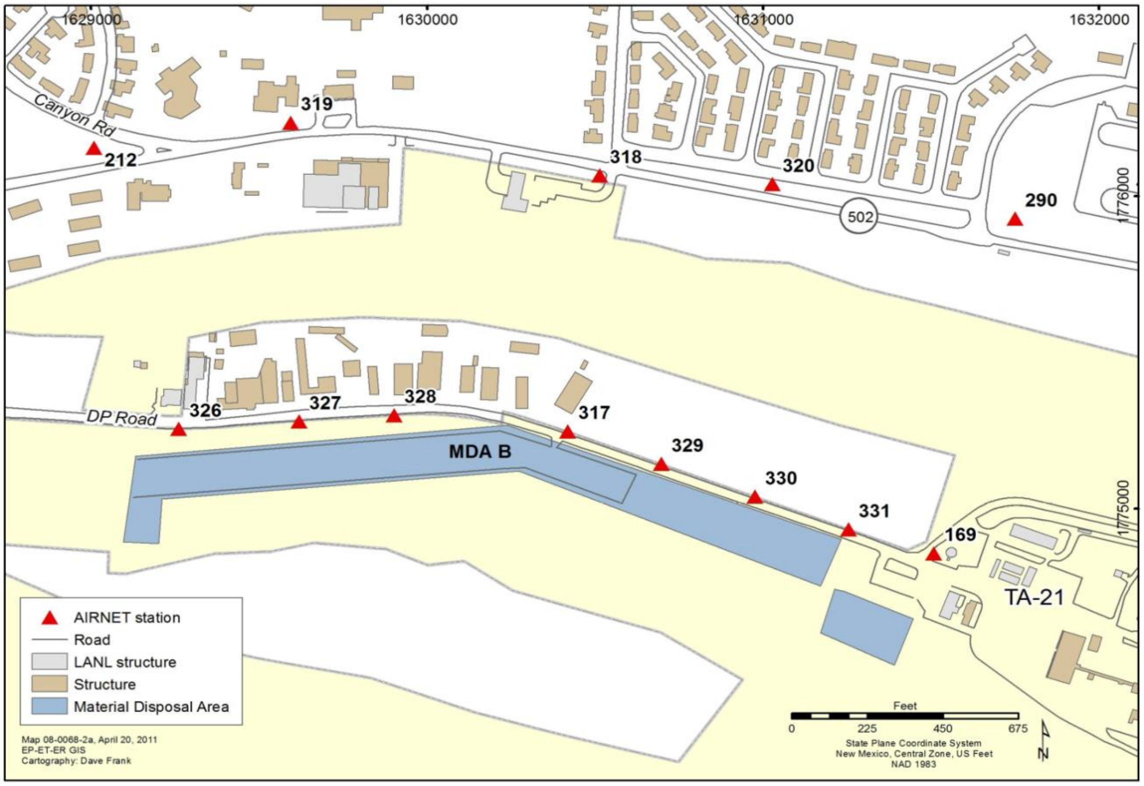

Fig. 5. AIRNET stations along the border of MDA-B. (LANL 2010a)

Area TA-21 is located on Delta Prime (DP) Mesa on the northern boundary of the LANL immediately east to southeast of the Los Alamos town site. Area TA-21 is the site of the Laboratory's original plutonium processing facility and several MDAs. From 1945-1948, plutonium contaminated waste was disposed of within shallow trenches within MDA-B and covered with soil. Since 1948, multiple businesses developed across the street and within tens of meters from the MDA-B site. The inventories of hazardous and radioactive material at the MDAs were not well characterized because there are few records of waste disposal during the 1940s and the Manhattan Project. (LANL 2010a)

Excavation activities at MDA B began on 30 June 2010. The remediation began with the removal of an asphalt cover that was present over 75% of MDA B, followed by the removal of soil. Excavation operations consisted of overburden removal, contaminated soil and waste removal, and confirmation sampling. Approximately 7,265 yd^3 of waste were removed from

MDA B. The lack of knowledge about potential radiation hazards was a great challenge while performing this work. To address those challenges safely, the excavation of MDA B occurred inside large metal structures resembling airplane hangars. These structures were built on the site and contained a number of safeguards, including dust and fire suppression systems and high efficiency particulate air (HEPA) filtering to minimize the emission of contaminated soils during excavation operations. (LANL 2010a)

For compliance, the AIRNET stations collected continuous two-week samples over the 128 week sampling period. Each AIRNET station collected airborne radionuclides on a particulate filter. The particulate filters were changed every 2 weeks. Each calendar quarter, six or seven of the biweekly filters from a given station were assembled into a single composite sample and sent to a commercial laboratory for isotopic analysis using U.S. Environmental Protection Agency (EPA) approved methods. Annual emissions reporting and compliance evaluations for a station are based on the average concentrations of the four quarterly composite samples. Particulate matter was collected at airflow rates around 110 L min^{-1} (4 ft^3 min^{-1}).Within the field, personnel recorded the sampling data on a palm-held microcomputer, including timer readings, and volumetric flow rates at the beginning and end of the sampling period. The data were later transferred to a database and checked thereafter. (LANL 2011)

The measured concentrations for each two-week sample were then averaged over all 64 two-week sampling periods for each AIRNET station. The average values provided a concentration profile over the entire measurement period. From the profile, parameters of importance, such as the shape of the profile, were identified. Furthermore, the average measured values provided a benchmark that the modeled concentration values could be compared against.

The measurement of radiochemical samples requires that background counts be subtracted from the gross counts to yield the net values. Consequently, net values are sometimes obtained which are lower than the minimum detection limit of the sampling (analytical) technique. Additionally, individual measurements can result in both positive and negative values. Though a negative value is not representative of a physical reality, a valid long-term average of many measurements can only be obtained if the very small and negative values are included in the population calculations. (Gilbert 1987).

Uncertainties are reported as one standard deviation for each individual measurement. The standard deviation is estimated from the propagated sources of analytical errors according to the standard equation:

Eqn. 15 $$s = \left(\frac{\Sigma_{i=1}^{N} (ci - \bar{c})^2}{(N - 1)}\right)^{\frac{1}{2}}$$

Where:

ci = sample $_i$,

$\bar{c}$ = mean of samples from a given station or group, and

N = number of samples in the station or group.

This value is reported as one standard deviation for the station and group means.

According to LANL2011, the uncertainties for all data sampling represented a 95% confidence (2σ) interval. As confidence intervals were calculated with data from multiple sites and throughout the year, they included random measurements and analytical errors, in addition to seasonal and spatial variations. Therefore, the compilation of all measured data decreased the overall uncertainty associated with the measured data set. Furthermore, negative values were included within the averages as their omission would introduce bias.

3.2 Site-Meteorology

Figs. 6-7, display the daytime and nighttime wind roses associated with the weather stations for years 2010 and 2011, respectively. From the wind roses associated with tower TA-53, the site closest to MDA-B, we can observe the distribution of wind directions and velocities through the year. As shown in Figs. 6-7, the predominant wind direction ranged from: south southeast during the day for 2010 and 2011, occurring approximately 42% and 45% of the time, respectively; and predominately west and southwest at night for 2010 and 2011, occurring approximately 38% and 36% of the time, respectively. Thus, the potential MEI and AIRNET stations are on average downwind from the facility. The MEI is a hypothetical member of the public, who is not on Department of Energy (DOE) or LANL property, and receives the greatest dose from LANL operations. Also, the greatest wind speeds were associated with these prevailing wind directions. However, the wind also blew toward the direction of the potential MEI associated with DP road and the AIRNET stations. As shown in Figs. 6-7, the wind direction ranged from: just west of north during the day for 2010 and 2011, occurring approximately 18% and 18% of the time, respectively; and predominately west of north to east of north during the night for 2010 and 2011, occurring 29% and 30% of the time, respectively. As shown within Figs. 6-7, the wind speeds associated with these directions were much lower.

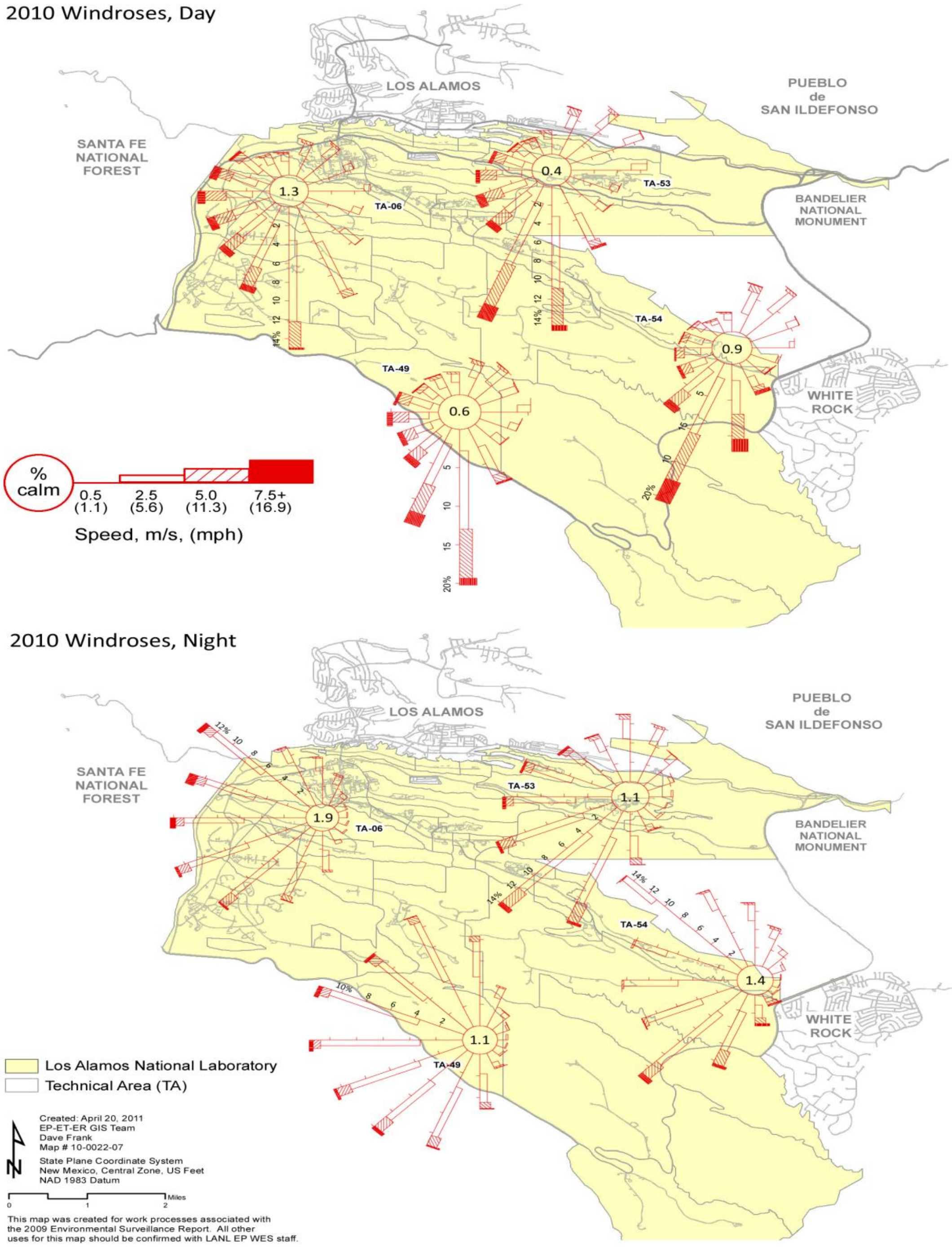

Fig. 6. Wind roses for night and day during the year 2010. (LANL2011)

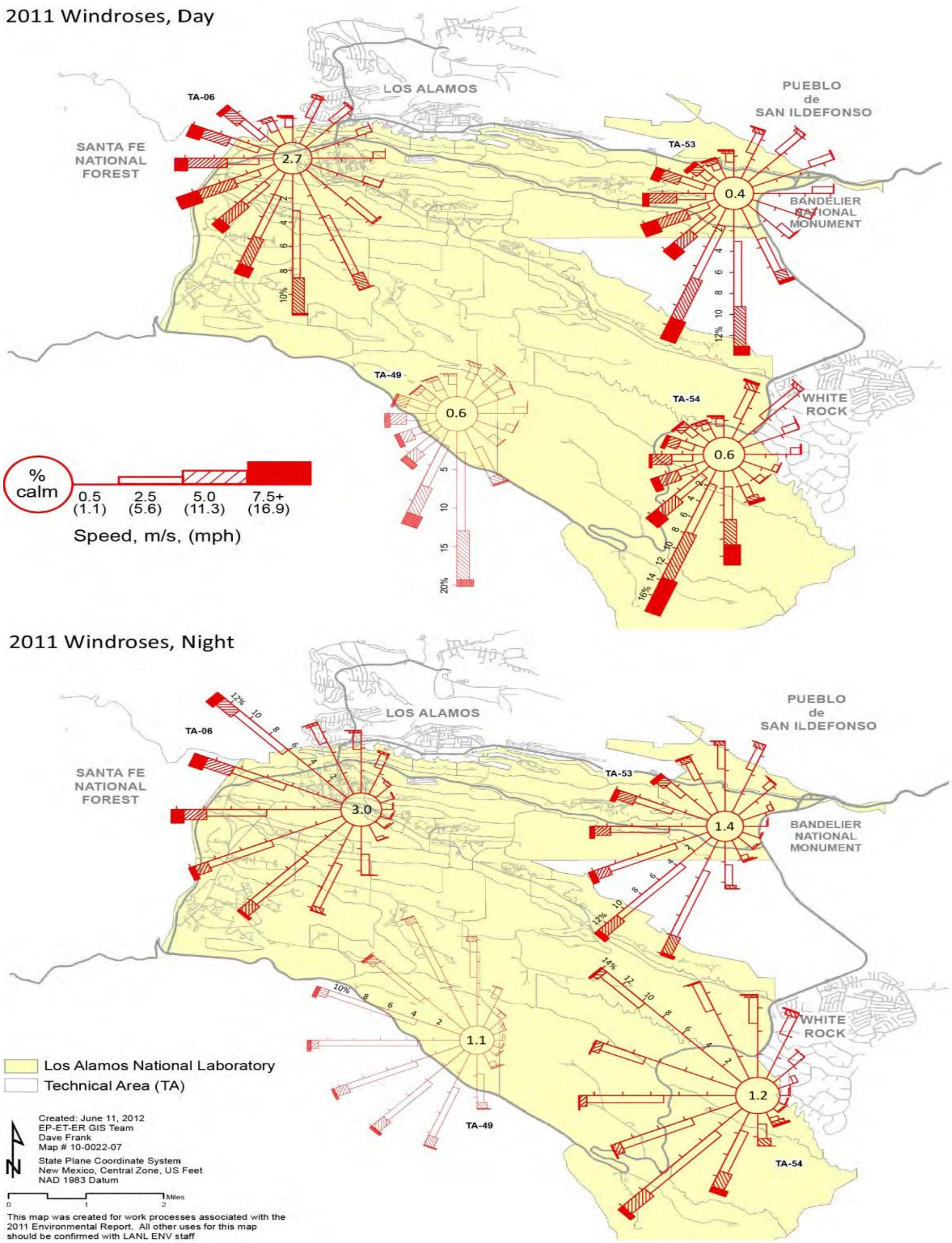

Fig.7. Wind roses for night and day during the year 2011. (LANL 2011)

3.3 Variables of Importance

Distribution parameters may be calculated from available data. The mean and standard deviation are common parameters of interest, however, the type of distribution fit to the data is also very important to consider. An accepted approach for the specification of a model distribution is to choose the distribution which best fits the data (Crawford et al. 2008). However, such an approach takes a large number of observations to distinguish the potential quality of the distribution as a fit to a collection of measured data (Haas 1997). It is pertinent to model development, to evaluate the model parameters, or variables of importance that influence the variability of a selected distribution. (Hattis and Burmaster 1994)

The AIRNET stations sampled particulate matter at a continuous flow rate of 4 ft^3 min^{-1} over 14 day intervals. Filters were analyzed in the laboratory for ^{239}Pu and concentrations were expressed in units of aCi m^{-3} of air. Sampling was completed for 64 time periods ranging from 04/13/2009-09/12/2011, as displayed in Table 5. The average concentrations over all 64 periods for each station, and the average concentrations over all eight stations for each period were then expressed in units of Bq m^{-3}, as displayed in Table 5.

As discussed previously, the excavation of MDA B was split into a grid of cells, each measuring 10 ft long by 10 ft wide. Waste removal operations consisted of the excavation of hundreds of cells, over a time period of 128 weeks. Per the graphs displayed in the variables of importance section below, we are able to visualize the specific concentration distribution per two-week time period, and visualize the concentration distribution averaged over all time periods. This average concentration distribution allowed for the development of a plume centerline model and provided insight into the overall building wake effects created by each excavation facility per excavation evolution.

Meteorological data was obtained from the LANL Weather machine, (http://www.weather.lanl.gov). The data was pulled from tower TA53 and includes the average wind speed (m s^{-1}), the maximum gust (m s^{-1}) and the direction of the gust (degree). The data was then averaged over each sampling period, as shown in Table 2.

Table 2. Wind speed and wind stability per period.

Period Start Date	Wind Speed (m s^{-1})		Average Wind Direction (deg)
	Average Wind	Average Wind Gust	
4/13/2009	3.7	14.1	211.0
4/27/2009	3.8	13.7	233.9
5/11/2009	4.2	14.3	221.7
5/25/2009	3.2	14.8	160.6
6/8/2009	3.3	13.5	208.4
6/22/2009	3.2	11.9	214.1
7/6/2009	3.3	12.5	230.6
7/20/2009	3.5	13.3	175.2
8/3/2009	3.4	13.0	199.4
8/17/2009	3.5	12.3	212.8
8/31/2009	3.1	12.1	208.1
9/14/2009	2.9	11.1	184.9
9/28/2009	4.0	13.2	218.7
10/12/2009	3.1	11.4	200.4
10/26/2009	2.6	8.6	167.3
11/9/2009	2.8	9.4	161.1
11/23/2009	3.0	9.8	201.3
12/7/2009	2.6	9.5	145.3
12/21/2009	1.9	7.2	87.7
1/4/2010	2.0	9.2	160.2

Period Start Date	Wind Speed (m s^{-1})		Average Wind Direction (deg)
	Average Wind	Average Wind Gust	
1/18/2010	2.6	11.6	223.8
2/1/2010	2.1	7.8	203.9
2/15/2010	2.5	9.7	176.9
3/1/2010	2.7	10.3	195.0
3/15/2010	3.2	12.1	140.7
3/29/2010	4.2	14.7	213.3
4/12/2010	4.1	15.3	234.8
4/26/2010	4.7	15.9	245.1
5/10/2010	4.5	15.7	208.5
5/24/2010	3.8	14.3	222.5
6/7/2010	4.2	14.8	203.2
6/21/2010	3.8	14.0	214.7
7/5/2010	3.3	13.0	203.9
7/19/2010	2.9	11.6	203.9
8/2/2010	2.6	12.8	253.5
8/16/2010	3.3	11.7	203.2
8/30/2010	3.7	12.6	250.7
9/13/2010	3.0	10.3	215.2
9/27/2010	3.3	11.7	186.1
10/11/2010	2.8	10.6	206.1
10/25/2010	3.0	11.7	190.1
11/8/2010	3.0	12.1	212.6
11/22/2010	2.9	10.5	200.6
12/6/2010	2.3	8.3	192.4
12/20/2010	2.6	10.0	210.2
1/3/2011	2.0	8.0	121.4

Period Start Date	**Wind Speed (m s^{-1})**		**Average Wind Direction (deg)**
	Average Wind	**Average Wind Gust**	
1/17/2011	2.4	10.9	177.0
1/31/2011	2.9	9.4	161.6
2/14/2011	4.3	15.8	229.9
2/28/2011	3.0	12.0	226.6
3/14/2011	4.3	14.7	235.1
3/28/2011	4.6	16.6	253.5
4/11/2011	4.6	16.2	267.2
4/25/2011	4.3	16.0	225.1
5/9/2011	4.4	16.0	226.9
5/23/2011	5.0	17.6	180.8
6/6/2011	4.7	16.5	219.6
6/20/2011	4.1	14.5	233.6
7/4/2011	3.6	13.7	166.1
7/18/2011	3.2	14.1	190.8
8/1/2011	3.1	13.3	237.3
8/15/2011	3.2	13.1	219.4
8/29/2011	3.0	12.2	238.1
9/12/2011	2.6	10.5	239.6

The variables of possible importance to methodology development are presented within this section, within the units that they were collected in, i.e., aCi m^{-3}. The analyzed variables, which were deemed to be of importance, are those that could affect the developed methodology and will be discussed further within Section 3.4.

The average ^{239}Pu concentrations per period for each station were calculated and graphed, as displayed in Figs. 8-15. The figures show concentration peaks at various periods, and therefore, times throughout the year. The fluctuations observed within the graphs may be tied to a specific activity, or a small break within the containment of the excavation structures. However, we cannot be sure as detailed information on the activities at the time of the peaks is not available.

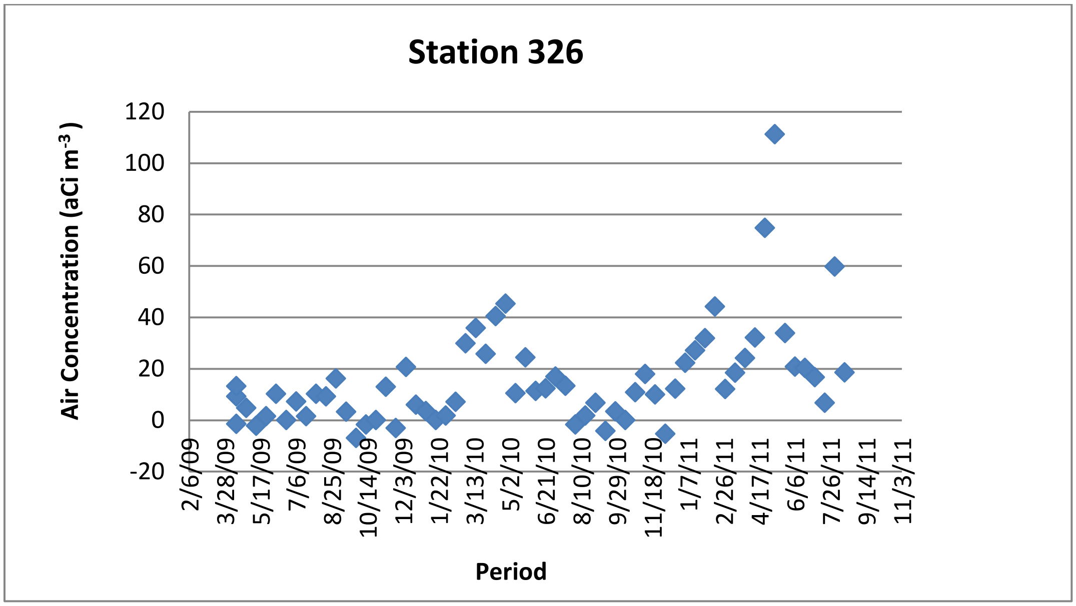

Fig. 8. Station 326 ^{239}Pu concentration per period.

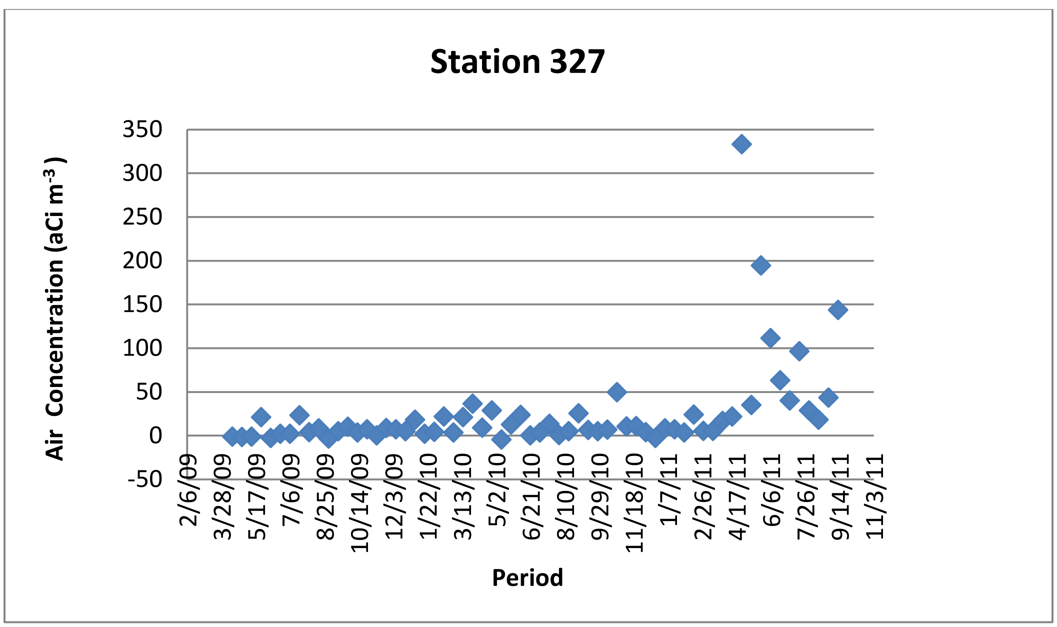

Fig. 9. Station 327 ^{239}Pu concentration per period.

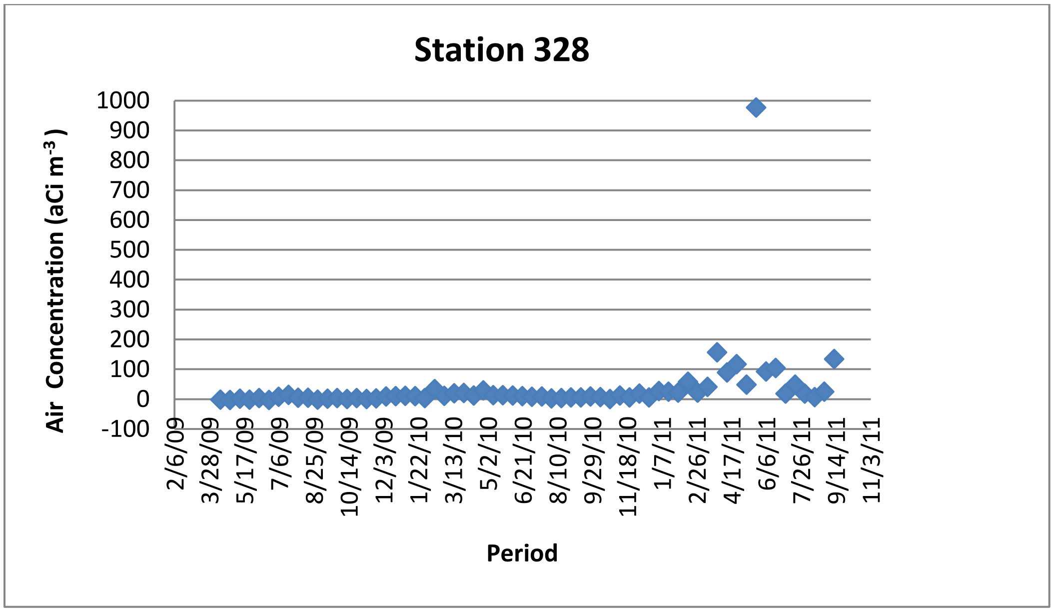

Fig. 10. Station 328 ^{239}Pu concentration per period

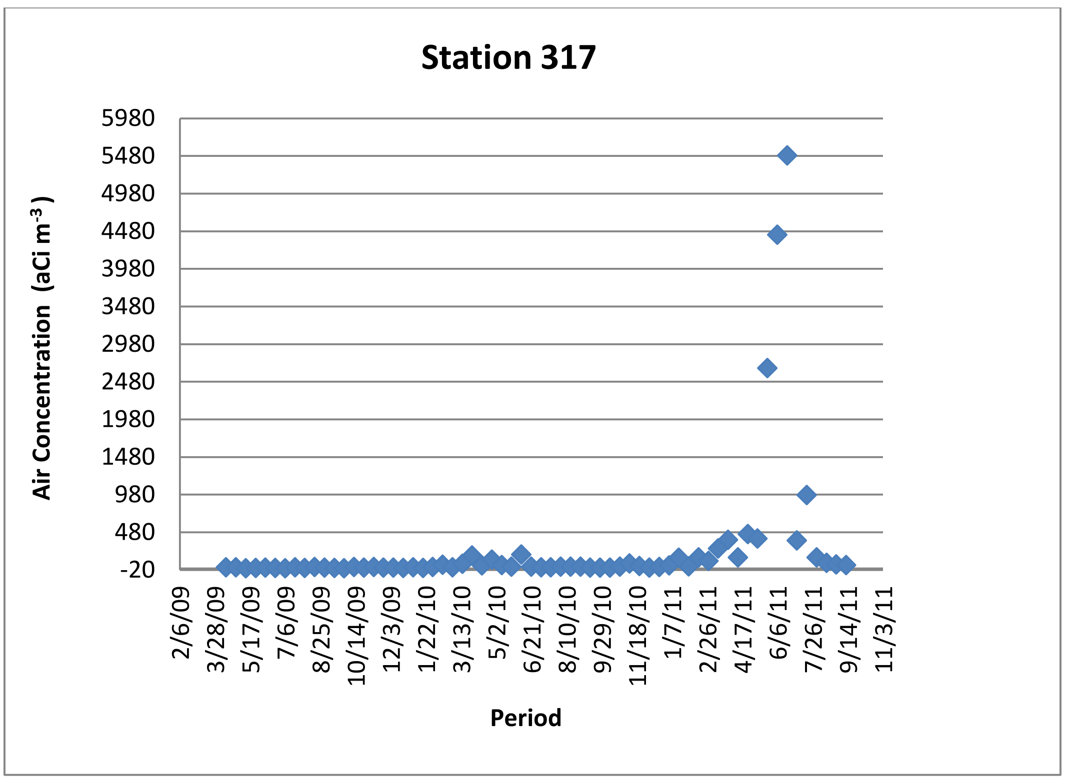

Fig. 11. Station 317 ^{239}Pu concentration per period.

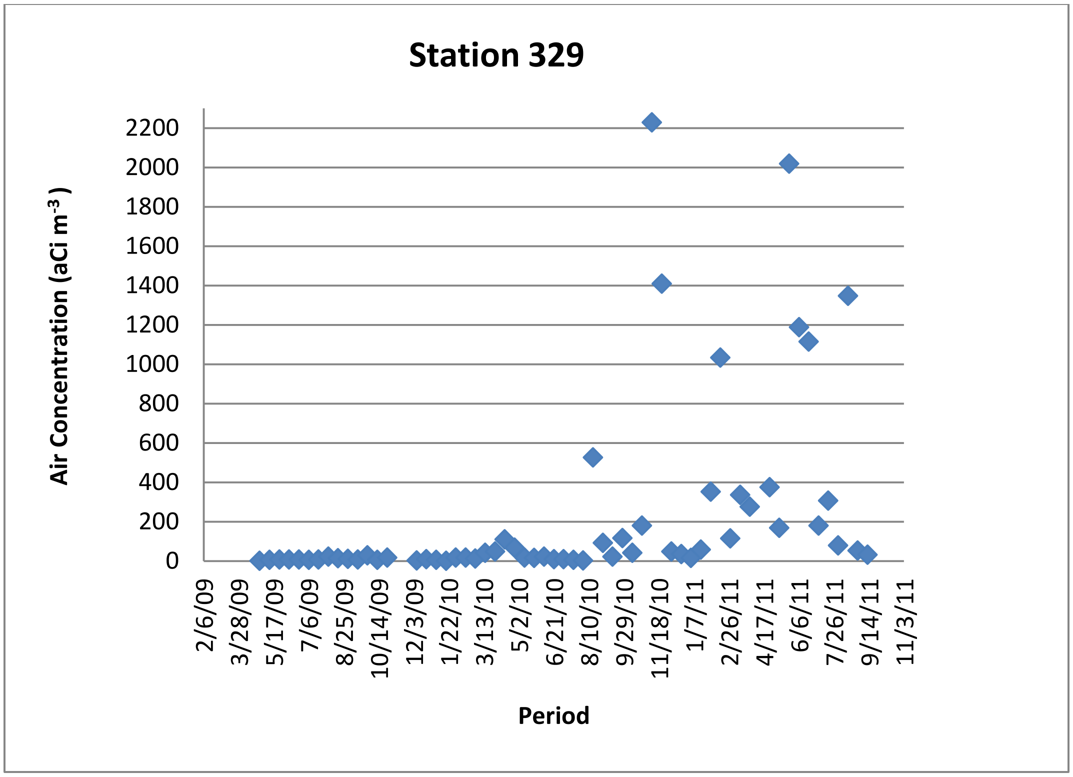

Fig. 12. Station 329 ^{239}Pu concentration per period.

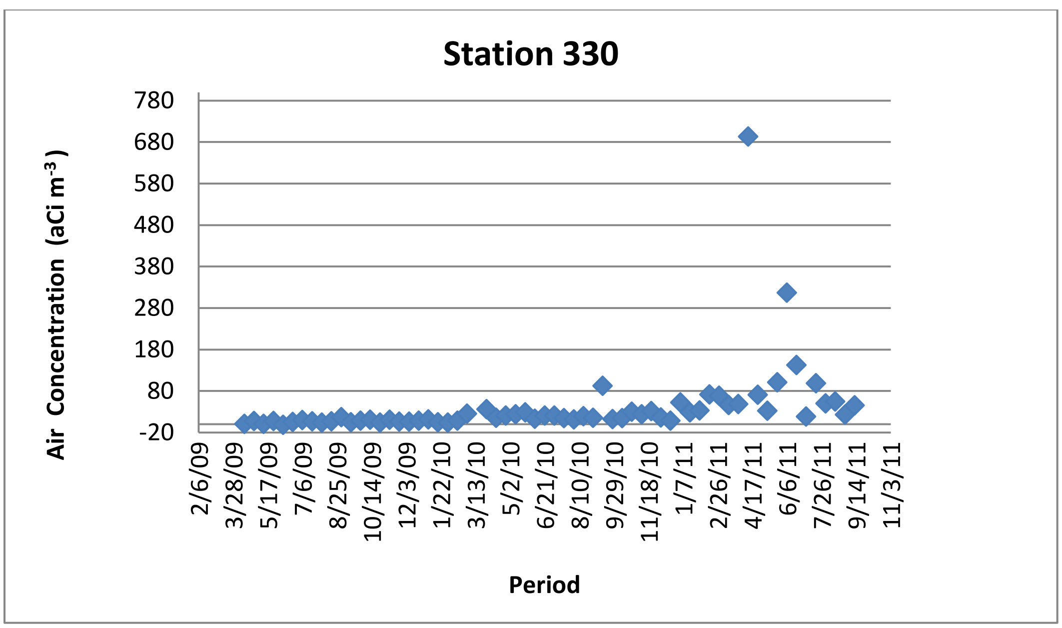

Fig. 13. Station 330 ^{239}Pu concentration per period.

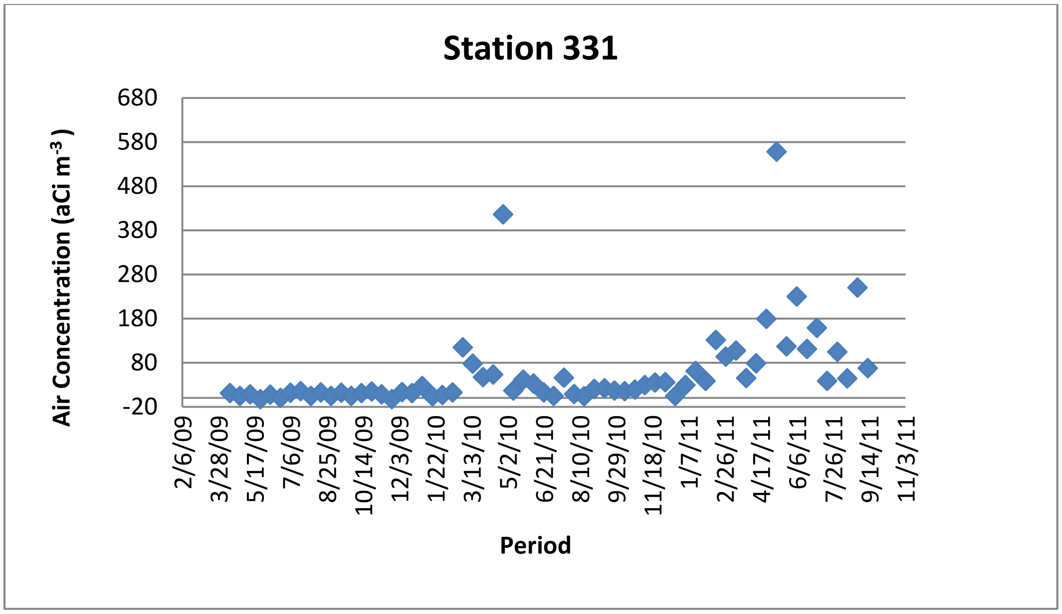

Fig. 14. Station 331 ^{239}Pu concentration per period

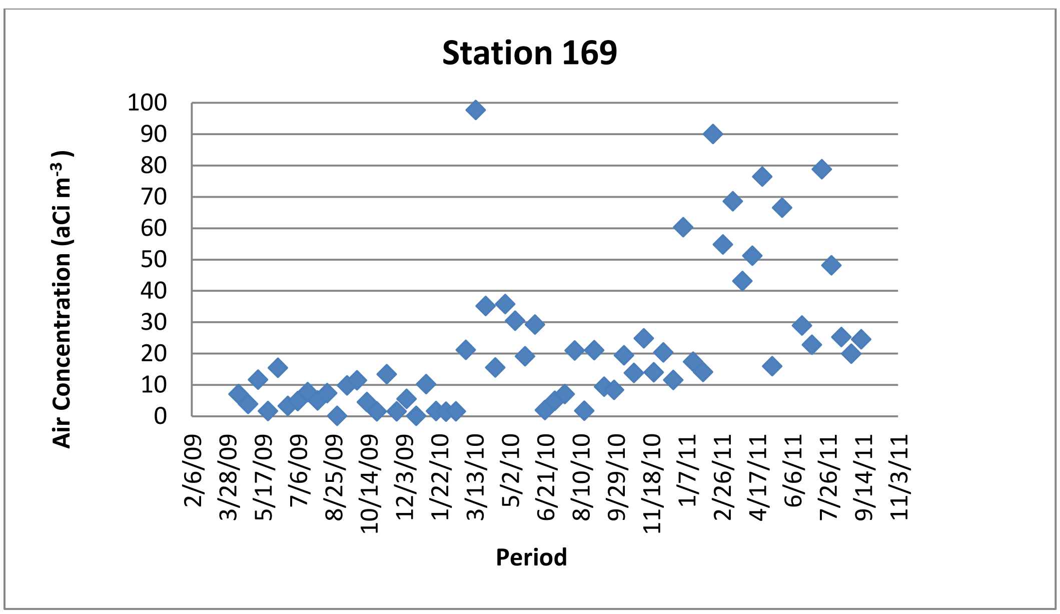

Fig. 15. Station 169 ^{239}Pu concentration per period.

The average concentration of all stations per period were then calculated and graphed, as displayed in Fig. 16, which displays the average concentration per period start date. The average concentrations were shown to peak twice in the year 2010, in April and November. In the year 2011, the average concentrations were shown to peak in April before approaching a maximum peak and nearly plateau from early May to early July. These peaks are factors for consideration because they propagate into an increase in the average concentrations across all periods per station.

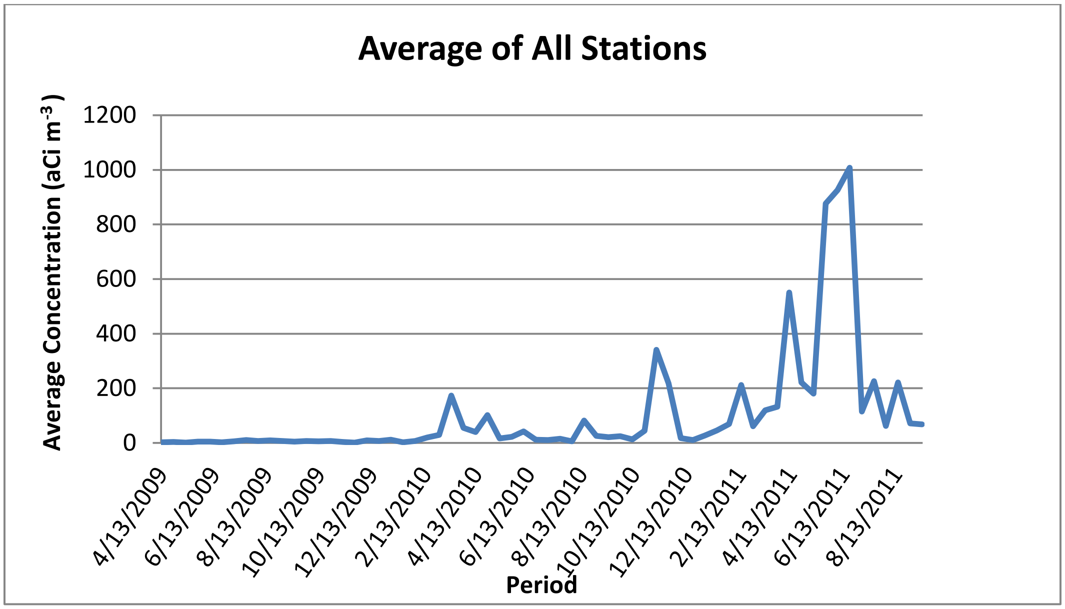

Fig.16. Average ^{239}Pu concentrations per period.

As displayed in Fig. 17, the correlation between the concentrations measured outside the facility and the concentrations measured inside of the facility was investigated for 15 data points across 15 sampling periods which ranged from August of 2008 to January of 2011. The variables in Fig. 17 were shown to have a negligible correlation with an R^2 value of 0.0019. The sampling period that exhibited the largest outside to inside concentration ratio was then removed from the data set, and the remaining 14 sampling periods were compared. The comparison resulted in an improved correlation, with an R^2 value of 0.38, as shown within Fig. 18, and could thus be considered a variable of importance.

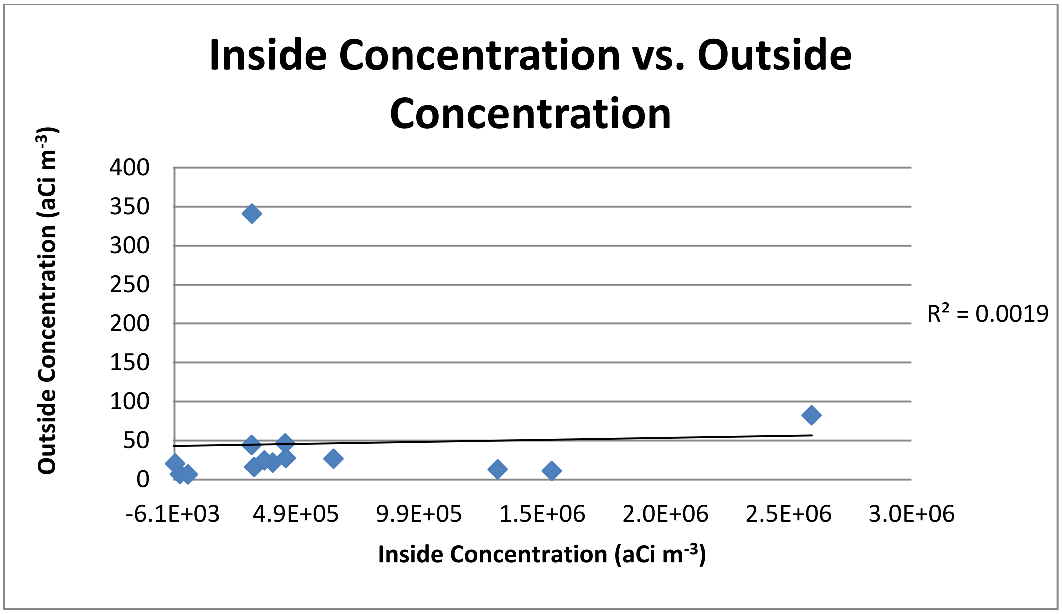

Fig.17. Outside concentration per inside concentration for 15 data points.

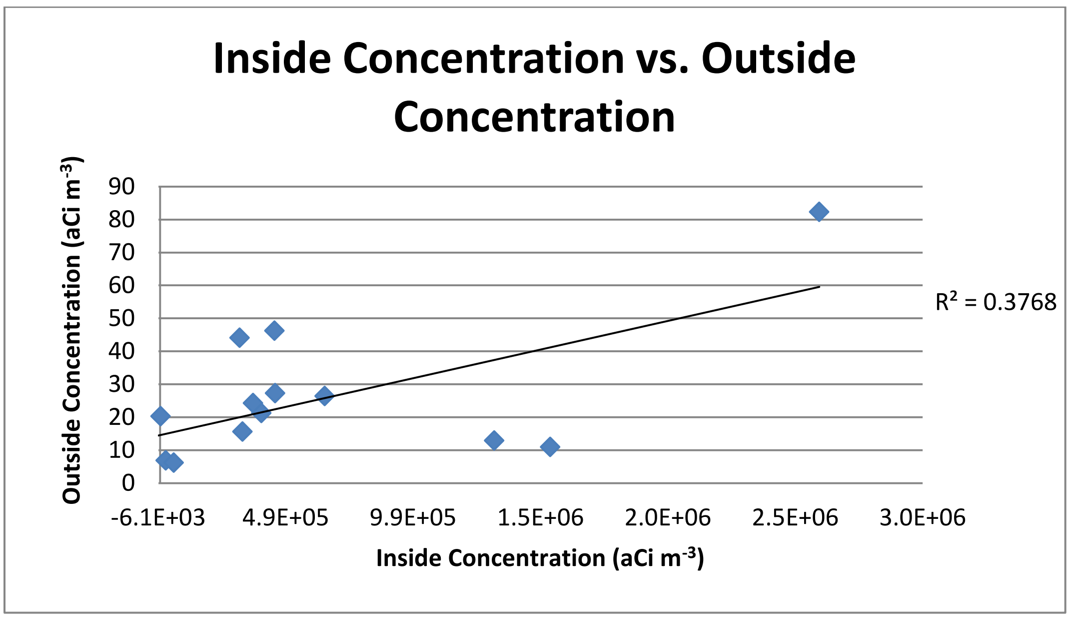

Fig.18. Outside concentration per inside concentration for 14 data points.

As displayed in Fig. 19, the average ^{239}Pu concentration per period was compared against the average wind speed per period, as compiled from the meteorological data. The average wind speed was deemed a variable of importance.

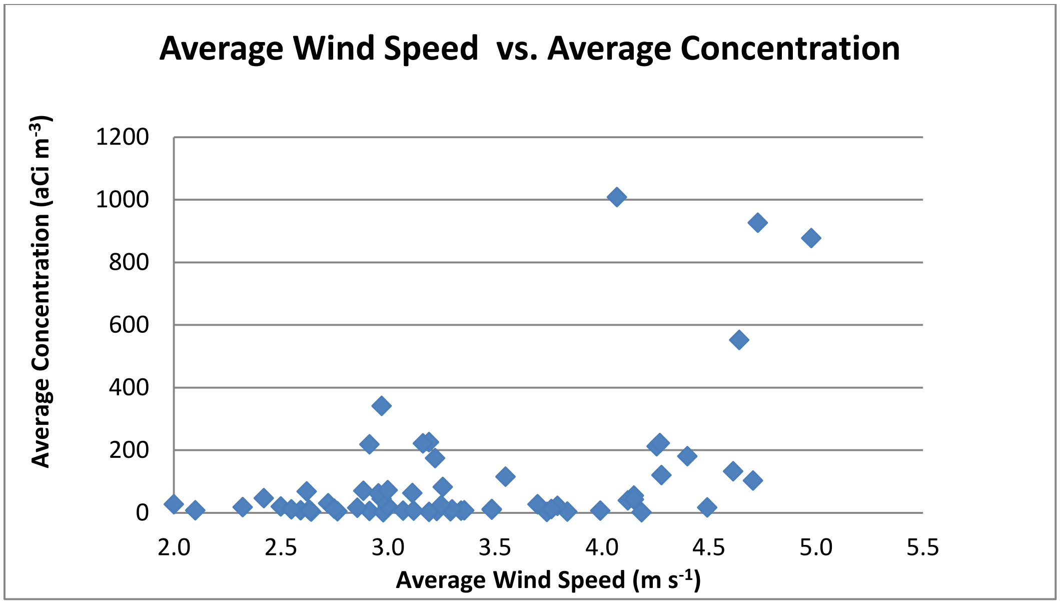

Fig. 19. Average ^{239}Pu concentration per average wind speed per period.

As displayed in Fig. 20, the average Pu-239 concentration per period was compared against the average wind gust speed for each period, as compiled from the meteorological data. The wind gust speed was deemed a variable of importance, yet encompassed by the data in Fig. 19.

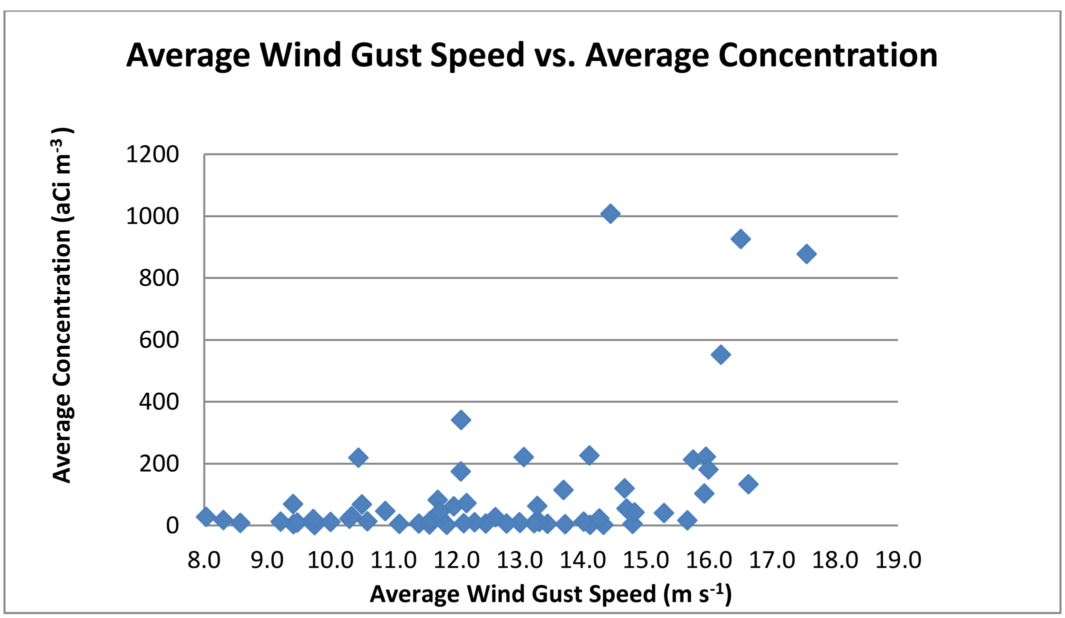

Fig. 20. Average ^{239}Pu concentration per average wind gust speed period.

For this analysis, the average wind gust per period compiled from the meteorological data was analogous to the average wind stability per period. Thus, wind stability represents the delta between the average wind speed over all periods and the average maximum wind speed per period, as such, the greater the departure from the average wind speed over all periods, the greater the wind instability. As displayed in Fig. 21, stability/wind gust speed is cyclical throughout the calendar year, as expected, however, the time periods of greater concentration correlate with a broadening of the peaks and troughs, specifically seen during the broadening associated with the Los Conchas fire which occurred during the summer of 2011. These data points were considered important and will be discussed later in this section.

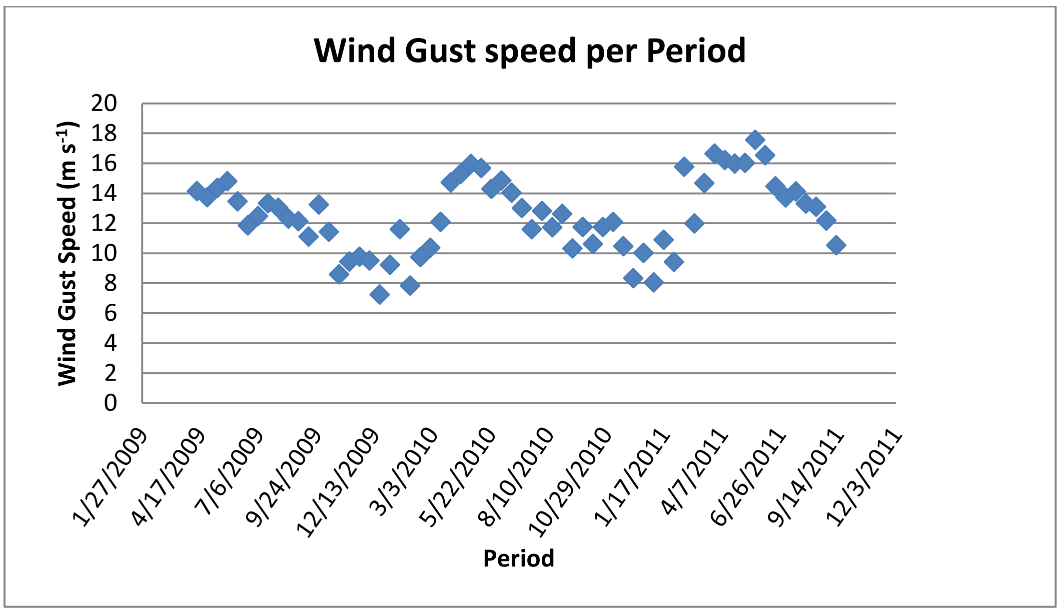

Fig. 21.Wind gust speed for each time period.

The average ^{239}Pu concentration per period was compared against the average wind direction for each period compiled from the meteorological data, as displayed in Fig. 22. The overall correlation for the graph is negligible. However, a possible correlation may exist between the peaks in concentration and average wind direction, which may suggest an increased release to the environment via a related pressure differential across the building, or a concentration at a specific location in the environment as directed by the wind direction.

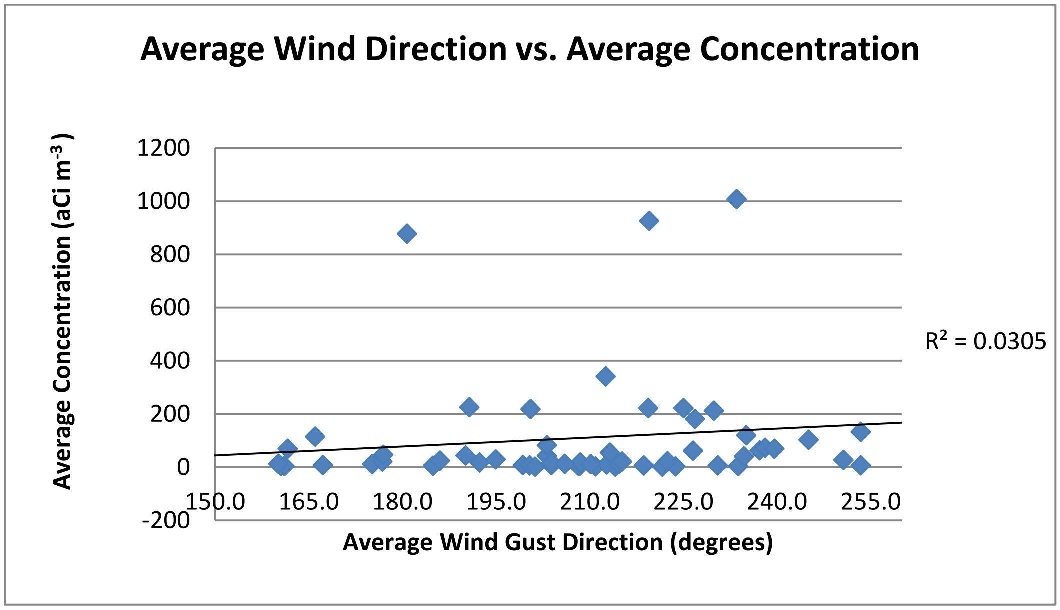

Fig. 22. Average ^{239}Pu concentration per wind gust direction.

The possible correlation between the average concentration and the average wind direction was investigated further. As displayed within Fig. 23, the top 13 average concentrations per period with the greatest concentration values were graphed against the associated wind directions. Note: the data point measured at 203 degrees was not an average value, however, this datum was chosen as it was one of the 13 largest measured values, and the average value was within close proximity to the next largest average value. Fig. 23 shows that the top 13 peaks occur at average wind directions of 141, 203, 213, 201, 230, 267,225, 227, 181, 220, and 234,191, and 220 degrees, with an average of the averages equal to 210 degrees. A wind direction of 210 degrees flows directly through the plume centerline and toward the businesses and MEI. This is of interest, as the concentration peaks are clustered near the plume central line, i.e., stations 317 and 329. This correlation was deemed a variable of importance and will be further investigated during the model development section.

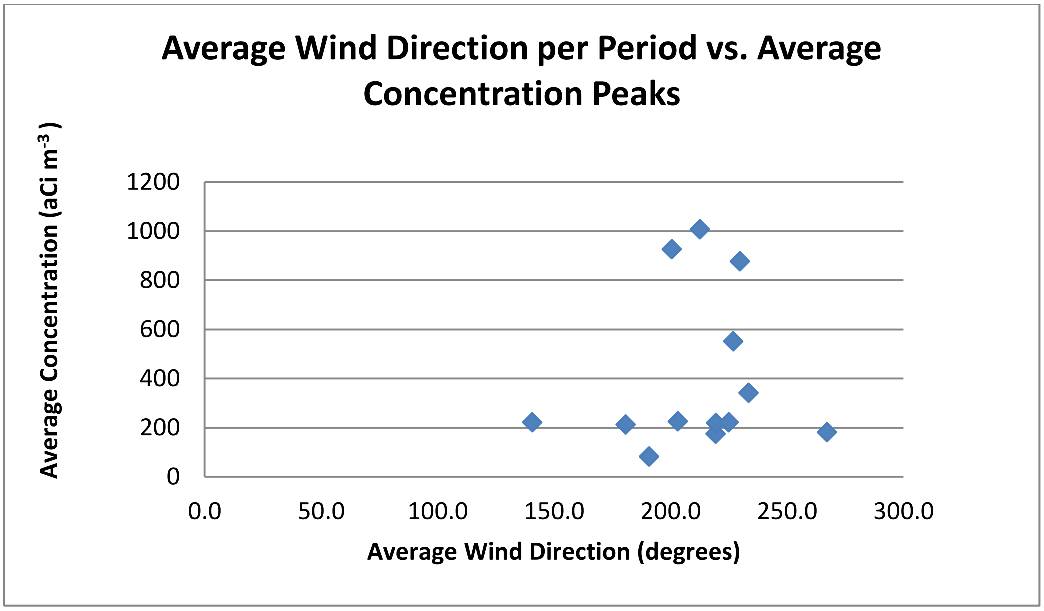

Fig. 23. Average ^{239}Pu concentration peaks per average wind direction.

The ^{239}Pu air concentrations per station for each period are displayed within Appendix A as Figs. A1-A64. The stations were identified according to their horizontal distance relative to the plume central line. Assuming that the plume central line is directly in the middle of stations 317 and 329 yields a horizontal distance of zero meters. Therefore, the horizontal distances perpendicular to the remaining stations, as derived from Fig. 5, are approximately -458 m, -352 m, -233 m, -53 m, 53 m, 159 m, 265 m, and 371 m, for stations 326, 327, 328, 317, 329, 330, 331, and 169, respectively.

For each period, observations were derived from the average concentration distribution across the receptor locations. Graphs of the dispersions display the air concentration per the horizontal distance of the receptor locations for each sampling period.

The Pu-239 average air concentrations per station for all periods within the time period 04/13/2009-09/12/2011, were calculated as shown within Table 5, and displayed within the units that they were collected, i.e., aCi m^{-3}, within Fig. 24. The average concentration distribution presents a unimodal distribution with a concentration peak occurring directly between stations

317 station 329, with concentration peaks of 271.0 aCi m^{-3} (1.0×10^{-5} Bq m^{-3}) and 266.6 aCi m^{-3} (9.9×10^{-6} Bq m^{-3}), for stations 317 and 329, respectively. Fig. 24 will be discussed further within Section 3.4 of this document.

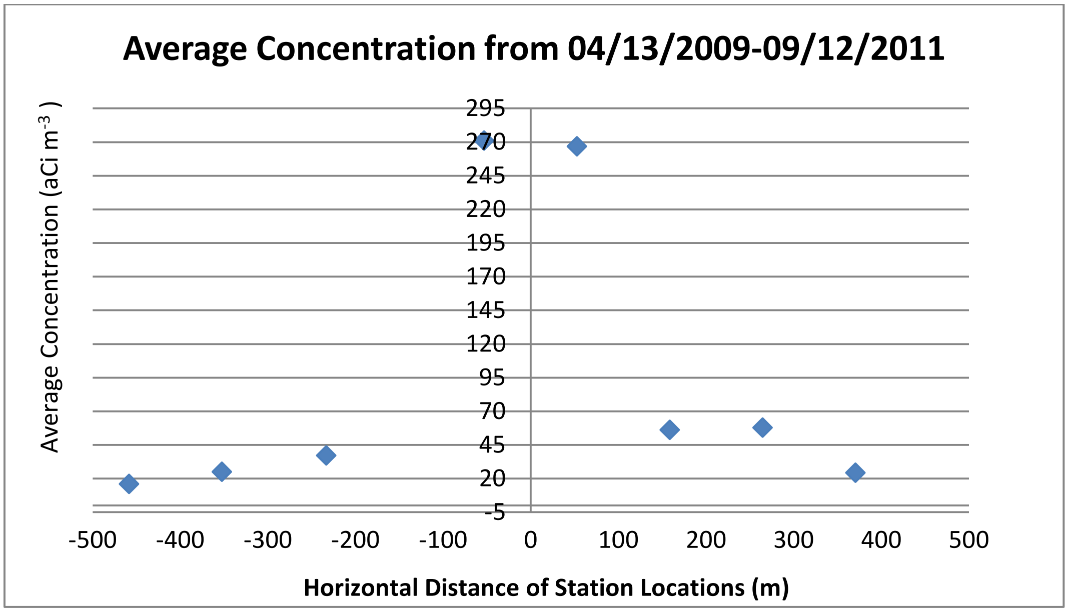

Fig. 24. Average ^{239}Pu concentration per station location for all periods.

Thus the variables of importance carried into Section 3.4 include: the average concentration per period displayed in Fig. 16; the average concentration per average wind speed data points displayed in Figs. 19-20; the average concentration per average wind gust speed data points displayed in Fig. 21; the average concentration peak per average wind direction data points shown in Figs. 23, and Appendix A; and the average concentration over all periods displayed in Fig. 24. As discussed previously, the data presented in Fig. 18 could be interpreted as a variable of importance, and would suggest that the radiological material released into the air within the facility correlates to some degree, with the radiological material measured outside of the facility, thus suggesting a correlation between the radiological material within the soil and the concentrations measured outside the facility, and thus consistent and predictable operational evolutions and condition parameters. However, the complete data set presented in Fig. 17

suggests that we are not able to identify or predict the condition parameters, specifically during unknown conditions, which may have existed during the operational evolutions.

3.4 Methodology Development

All models, regardless of complexity, are only approximations of realty. As such, some level of uncertainty is always associated with any model predication. Two sources of model uncertainty, as described by Hoffman and Miller (1983) are: incorrect parameter values, and failure to account for parameter variability. Uncertainty associated with selection of parameter values can be reduced by using as much site specific information as possible, as documented within Section 3.3. Uncertainty associated with a failure to account for parameter variability may be addressed by allowing for conversion within the radiological assessment model.

Stochastic modeling explicitly addresses the issue of accounting for parameter variability in model output, by treating all uncertain parameters as random variables with a specific probability distribution. (IAEA 1989)

Uncertainty for selection of a parameter value can be represented by a probability density function. The frequency with which a specific value of the parameter is likely to be observed may be tabulated from the collected data. The data may also be combined with subjective knowledge for the derivation of a distribution which describes the parameter of interest (Crawford et al. 2008).

Using the average concentration over all periods displayed in Fig. 24, a model needed to be developed that could be used to predict radionuclide concentration distributions at various horizontal distances within a recirculation zone, and thus allow for assessment for the proper placement of air monitoring stations. Upon first look, the distribution of data displayed in Fig. 24 appeared to approximate a Gaussian distribution. Furthermore, Fig. 24 encompasses the actual location of work within MDA B, as the average data suggests that regardless of work location, the concentrations, averaged over the entire 2-yr project, will peak at the plume centerline.

However, as shown in Fig. 24, the data points did not approach zero at approximately 3σ, which is uncharacteristic of the Gaussian distribution. Therefore, a distribution which may provide a better estimate of the behavior at the tail ends of the distribution was identified as the Lorentzian distribution (also known as the Cauchy distribution). As with the Gaussian distribution, the Lorentzian distribution is a continuous function whereby the probability of observing a value x, is obtained by integrating the probability density over the range of interest. The key distinction between the two distributions is that the Lorentzian does not diminish to zero as quickly as the Gaussian. (Bevington and Robinson 2003)

An investigation into the applicability of applying a Lorentzian based methodology to near field dispersion within the recirculation zone boundaries was performed. Given that atmospheric dispersion calculations are typically based upon the Gaussian distribution, the investigation identified similarities between the Gaussian distribution and the Lorentzian distribution. The Gaussian and Lorentzian distributions are symmetric, bell shaped curves, with the predominant distinction between the two being that the Lorentzian distribution has considerably heavier tales, and therefore does not approach the x-axis as readily, as shown in Fig. 25. The Gaussian and Lorentzian distributions are both special cases of stable distributions and incorporate distributions of independent and similar random variables. Stable distributions have been used as models for many types of physical systems and are described by four characterization parameters: a location parameter and scale parameter μ and c, respectively; and two shape parameters α and β, corresponding to concentration and asymmetry, respectively. Additionally, data sets exhibiting skewness and broader tails are poorly described by a pure

Gaussian model, but may be well described by another stable distribution, such as the Lorentzian distribution. (Nolan 2013)

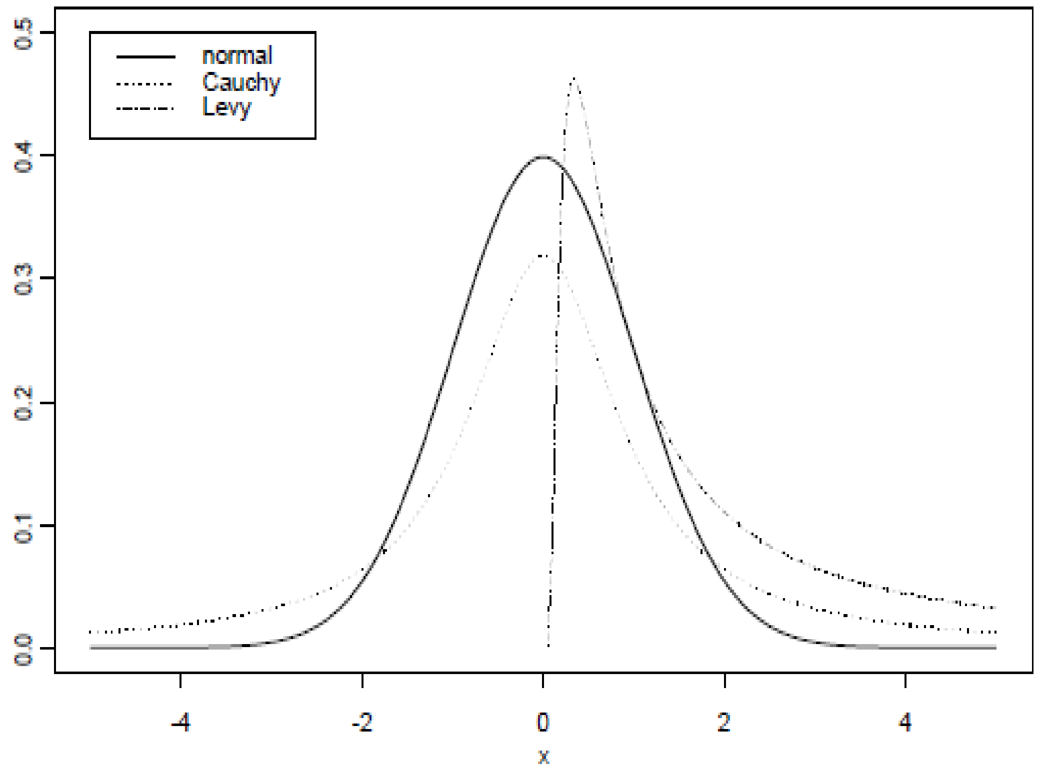

Fig. 25. Standardized Gaussian (0,1), Lorentzian (1,0) and Levy (1,0) distributions (Nolan 2013).

Furthermore, a Lorentzian distribution can be viewed as a mixture of Gaussian random variables distributed around a mean equal to zero, with the variance approximated by an additional stable distribution, i.e., the Lévy distribution. In addition, such a mixture is a special case of a more general theorem, which states that any symmetric stable distribution may be viewed as a mixture. (Nolan 2013)

A Gaussian-Lorentzian mixture, also known as the Gaussian-Lorentzian cross product, combines Gaussian and Lorentzian distributions in a multiplicative form. The shape of the cross product is specified by a shape parameter that varies from 0 to 1, with a pure Lorentzian distribution, occurring with a shape parameter equal to one, and a pure Gaussian distribution occurring with a shape parameter equal to zero. However, the transition from Lorentzian to Gaussian shape is a function of multiple characterization parameters as discussed previously, and is thus not a linear function of the shape parameter. Furthermore, the characterization parameters affect the amplitude, and area under the curve of the cross product. (Huang et al. 2006)

As is consistent with all stable distributions, the location scale family to which the Lorentzian distribution belongs is pertinent to decision theory, whereby the decision may be described in terms of the mean and variance of the distribution (Meyer 1991). However, the Lorentzian scale family was shown to be the only univariate location-scale family to be closed under linear fractional transformation with real coefficients (Knight 1976). Linear fractional transformations are typically classified as hyperbolic, spherical, or elliptic (Schwerdtfeger 1980). This is of importance to this methodology, as the cavity model used within this analysis approximated an ellipsoid control volume (Haltisky 1968), as such, an elliptic transformation was investigated.

Within an elliptic transformation, two distinct points are fixed upon a Riemann sphere. If one stereographically projects the spherical image upon a plane, it can be observed that all other points flow along a family of circles between the two distinct points (Schwerdtfeger 1980), as represented in Fig. 26.

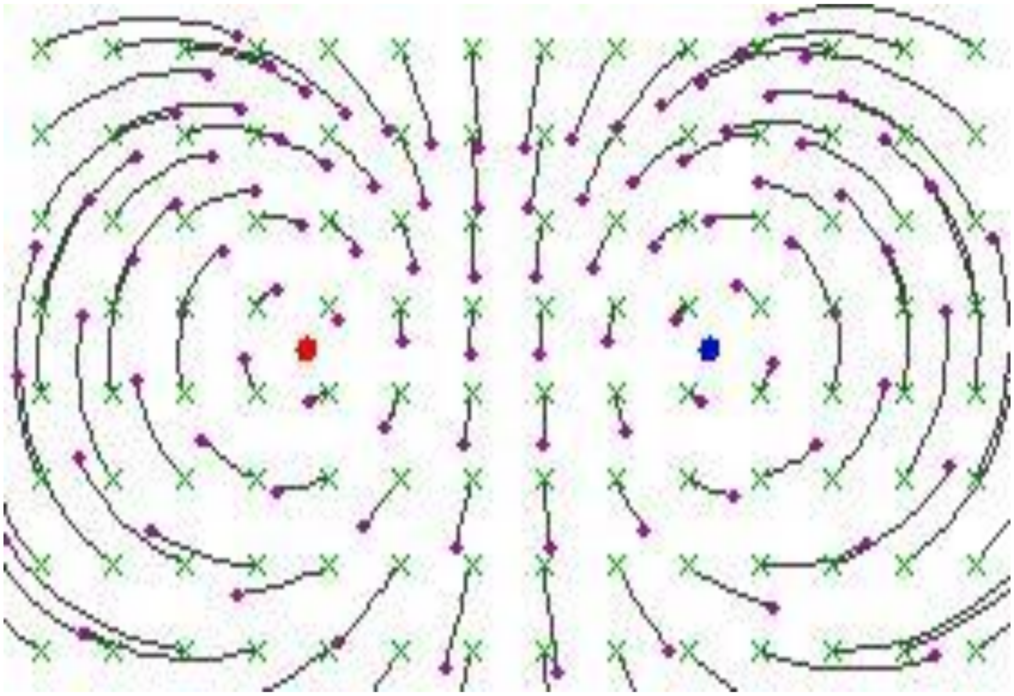

Fig. 26. A representation of stereographic projection of elliptic transformation. (Wikipedia.org)

Interestingly, the projection represented by Fig. 26, also represented the lateral eddy circulation found within the cavity zones, as provided by Halitsky (1968) and displayed in Fig. 27, whereby all points resonate around two distinct points and converge about a central line between the two points, referred to herein as the plume central line. Therefore, given the ability to mix the characterization parameters of the Gaussian and Lorentzian distributions as described previously, in conjunction with the unique qualities of the Lorentzian distribution, aspects of both distributions were utilized within model development as described below.

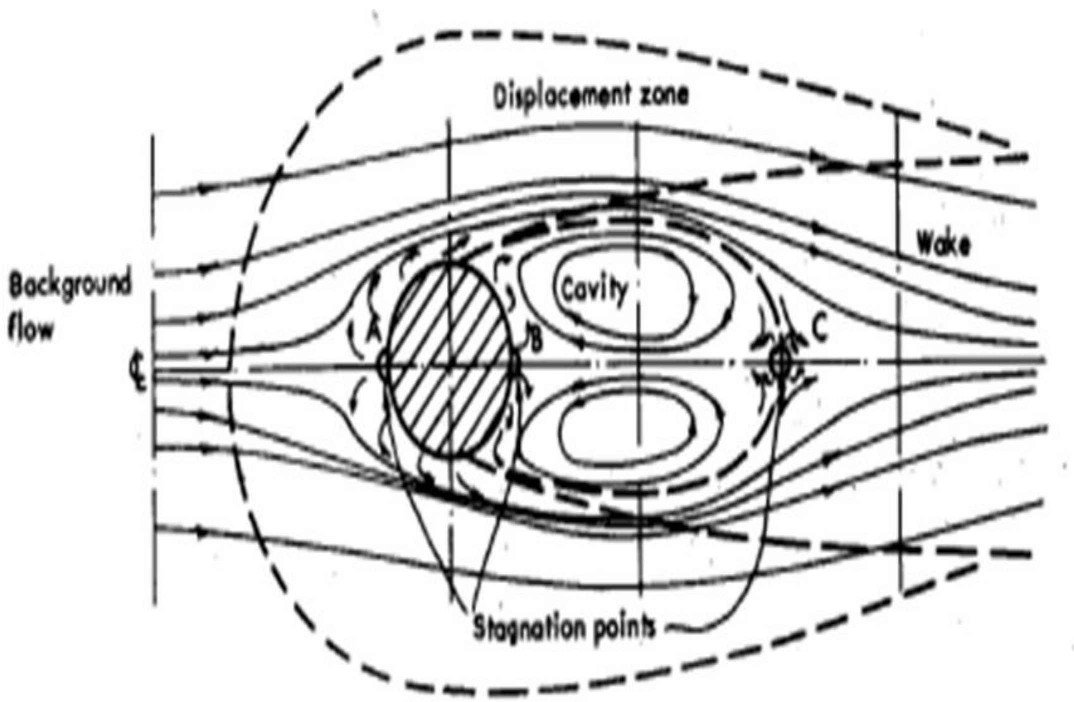

Fig. 27. Flow in a horizontal plane near the ground. (Halitsky 1968)

As displayed in Fig. 28, the Gaussian distribution typically has a greater peak value than the Lorentzian distribution, also, whereby the width of the curve representing the Gaussian distribution is determined by the standard deviation (σ); the width of the Lorentizian distribution is determined by its full-width at half maximum (Γ). Γ is defined as the range of x between values at which the probability is half its maximum value, such that $x = \mu \pm \Gamma/2$, where μ represents the mean within this equation. (Bevington and Robinson 2003)

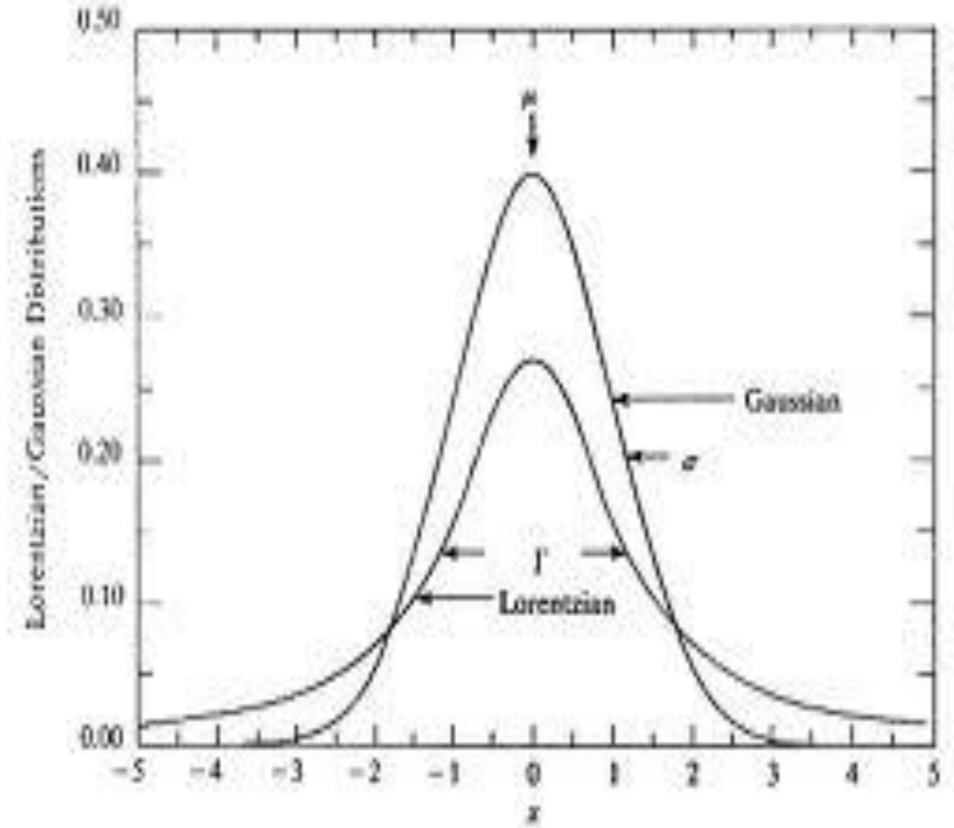

Fig. 28.Comparison of normalized Lorentzian and Gaussian distributions with Γ =2.345σ. (Bevington and Robinson 2003)

The Gaussian distribution representing the probability density is defined as (Bevington and Robinson 2003):

Eqn. 16 $$p_G = \frac{1}{\sigma\sqrt{2\pi}} \exp[-\frac{1}{2}(\frac{x-\mu}{\sigma})^2]$$

The Gaussian based atmospheric diffusion equation can be expressed using the time integrated form of the universal diffusion equation which evaluates the ground level concentration at any distance downwind, as shown in Equation No. 2, and elaborated upon below (Slade 1986). A stable layer which exists above an unstable layer will act to restrict vertical diffusion. Typically, a vertical Gaussian distribution can be assumed to occur at a distance downwind X_L, equal to 0.47 multiplied by the height of the unstable layer L, and vertical uniformity may be assumed to occur at a downwind distance of $2X_L$ (Turner 1970). Given the relatively low height of the cavity zone, and assuming that the height of the mixing depth and the ground are plume reflectors, then when σ_z becomes large compared to the mixing depth, the plume becomes uniformly distributed between the ground and the mixing depth height (Schrader 2010). Given the assumption of uniformity, atmospheric diffusion may then be calculated for any z from 0 to L, using (Yanskey et al. 1966, Turner 1970):

Eqn. 17
$$\frac{\chi}{Q} = \frac{1}{\sigma_y H W \sqrt{2\pi}} \exp[-\frac{1}{2}(\frac{y}{\sigma_y})^2]$$

Where:

H = height of the mixing depth (m)

W = wind speed (m/s)

Through a comparison of Equation No. 16 and Equation No. 17, one can see that multiple differences exist between the two equations which effectively limit the probability of obtaining a given value of χ/Q, specifically: the addition of variables H and W to the denominator of the first term, whereby the resulting χ/Q values are confined within value H and constrained by the value W, thus treating the ground and the height of the mixing depth as plume reflectors per the aforementioned uniformity assumptions, and yielding the proper units of s m^{-3}; the substitution of y for x-μ within the exponent of the second term, thereby specifying the lateral dimension as the dimension of interest per the uniformity assumptions stated previously.

The Lorentzian distribution representing the probability density is defined as (Bevington and Robinson 2003):

Eqn. 18
$$p_L = \frac{1}{\pi} \frac{\Gamma/2}{(x-\mu)^2+(\Gamma/2)^2}$$

Where:

m = median distance, i.e., 0 meters

Given that the solution to Equation No. 18 yielded units of m^{-1}, we then assumed that the distribution was projected onto a three dimensional Cartesian coordinate. This assumption allowed for specification of the x, y, and z coordinates and the establishment of boundary parameters. Furthermore, to calculate a concentration value at a desired point within the coordinate system, and per applicable boundary parameters, the aforementioned uniformity assumptions displayed within Equation No. 17 were applied to Equation No. 18. Thus effectively constraining the probability of obtaining a given χ/Q via the: addition of variables H and W to the denominator of the first term, thereby confining the resulting χ/Q to a value H by specifying the height boundary of the cavity zone, and limiting the χ/Q by a value W thereby specifying the dispersion associated with a given wind speed; substitution of y- μ for x-μ within the denominator of the second term, thereby specifying the lateral dimension as the dimension of interest and providing a Lorentzian based atmospheric diffusion equation with vertical uniformity and the desired units of s m^{-3}, as shown in Equation No. 19.

Eqn. 19
$$\frac{\chi}{Q} = \frac{1}{\pi H W} \frac{\Gamma/2}{(y-\mu)^2 + (\Gamma/2)^2}$$

The value Γ was then calculated to be 266 m according to the data displayed in Fig. 24. The Γ/2 value thus equaled 133 m. As the height of the cavity zone is not defined, the H value was derived from the height of the enclosures which consisted of an arched profile extending from 0 m to a peak height of 10.4 m (LANL 2010b) resulting in a mid-height of 5.2 m, or approximately 5.0 m. A conservative displacement height of 2 m (Slade 1968) was then assumed and summed with the roof heights of the enclosures, yielding a median cavity zone height, H, of approximately 7 m. Additionally, a height of 7 m provided an approximation between the displacement zone heights of a squat one story building and a tall three story building. These values in conjunction with an average wind speed of 3.3 m s^{-1}, as calculated from the average of the average wind speeds per period displayed in Table 2, were subsequently used as input to Equation No. 19.

A χ/Q was then calculated using Equation No. 19, for each horizontal distance relative to the station locations represented by Fig. 25, as displayed within Table 3.

Table 3. Atmospheric diffusion coefficients per station.

Station	**Station Distance from Plume Center Line (m)**	**χ/Q ($s\ m^{-3}$)**
326	458	8.3×10^{-6}
327	352	1.3×10^{-5}
328	233	2.6×10^{-5}
317	53	9.0×10^{-5}
Plume Centerline	0	1.0×10^{-4}
329	53	9.0×10^{-5}
330	159	4.3×10^{-5}
331	265	2.1×10^{-5}
169	371	1.2×10^{-5}

Accident specific parameters are used to evaluate the dose to receptors. Accurate application of the parameters requires that certain assumptions be made which modify the dispersion release fractions to account for the physical aspects of the release. The five components of the following source-term (ST) equation recommended by DOE-HDBK-3010-94 contain the basis for the accident scenario parameters. The ST is the amount of radioactive material, in curies or grams, released airborne during the postulated accident scenario. The airborne pathway is of primary interest for nonreactor nuclear facilities (DOE-STD-1027-92). The airborne ST is estimated by the following linear equation:

Eqn. 20 $$ST = MAR * DR * ARF * RF * LPF$$

Where:

ST = source term (Ci)

MAR = material at risk (Ci)

DR = damage ratio

ARF = airborne release fraction

RF = respirable fraction

LPF = leak path factor

The material at risk (MAR) is the amount of radionuclides in grams or curies, that could be impacted for a given accident scenario and is expressed in terms of the total quantity at risk. For processes, and activities associated with a nuclear facility, the MAR represents the maximum quantity of radionuclides present, or anticipated during the process evolution. Rather than tracking all radionuclides, the masses of all the isotopes of a given element are modeled as a sum; therefore, the total element mass, not its individual isotopes, is modeled.

The damage ratio (DR) represents the fraction of MAR that could be affected by the postulated accident and is a function of the accident initiator and the operational scenario being evaluated.

The airborne release fraction (ARF) is the coefficient used to estimate the fraction of the MAR which is released to the air as an aerosol, thus being available for transport and contribution to the overall dose consequence.

The respirable fraction (RF) is the fraction of the MAR released to the atmosphere that has been transported to a downwind receptor and inhaled into the pulmonary region of the human respiratory system. The RF is applied to particles having a 10-μm aerodynamic equivalent diameter or less, and is affected by humidity, agglomeration, and the propensity of the release to react with the surfaces within immediate proximity.

Leak Path Factor (LFP) is the fraction of the radionuclides released from one control volume to another. The control volumes can be compartmentalized as any volume of interest including: rooms, hallways, ventilation systems, filtration, the environment, etc.; depending on the desired level of specificity. Multiple LPFs can be combined to determine an overall LPF.

For the purposes of this analysis, Equation No. 20 was adjusted to be:

Eqn. 21 $$ST = S_0 * FR_1 * (1 - F_f)$$

Where:

S_0 = amount of ^{239}Pu worked with during each sampling period (represents MAR x DR)

FR_1 = fraction released from soil (represents ARF * RF)

F_f = fraction of air filtered

$1 - F_f$ = the fraction of ^{239}Pu released to the environment (represents LPF)

The variable S_0 from Equation No. 21, can be conservatively thought of as the total inventory that could be impacted for a given release scenario and is expressed in terms of the total quantity at risk in curies (Ci).

The values for each variable within Equation No. 21 were derived from triangular distributions (Whicker and Eisele 2012). The distributions were appropriate as they allowed estimation of the minimum, mean, and maximum of the parameters (Hodak 1994). The distributions also allowed simple linear interpolation over the desired parameter range. The range allows a modeler to express their level of knowledge in regards to an input parameter, in terms of a range of expected values (NRC 1998). The triangular distribution is a continuous distribution with a probability density function defined by three points: point x, the minimum; point y, the maximum; point z, the mode, as represented by the peak (Weisstein 2013). The triangle area equals one, and the mean is calculated from Eqn No. 22:

Eqn. 22 $$\mu = \frac{1}{3}\,(x + y + z).$$

The following data was yielded from the aforementioned triangular distributions (Whicker and Eisele 2012). Within the excavation enclosures, the limiting amount of plutonium in soil (Ci) that had a probability of being disturbed over the two-week sampling periods yielded approximately: a minimum activity equal to 0.0 Bq; a mean of 4.4 x 10^{10} Bq; and a maximum of 1.1 x 10^{11} Bq. The fraction of soil that had a probability of being released into air yielded approximately: a minimum of 0.0; a mean of 0.003; and a maximum of 0.01. The limiting fraction of air filtered, displayed approximately: a minimum equal to 0.9; a mean of 0.95; and a maximum of 0.99. From the mean (approximated as the 50^{th} percentile) values and maximum (100^{th} percentile) values, the 75^{th} percentile values were linearly interpolated. Using this information as input to Equation No. 21, the ST for each percentile was calculated as displayed in Table 4, and provided a range of values for which the sensitivity of the ST parameters could be observed. The minimum values provided were not considered further as the ST associated with these values was negligible and not anticipated to conservatively estimate the release.

Table 4. The 50^{th}, 75^{th}, and 100^{th} percentile source terms.

	S_0 (Bq)	**FR_1**	**$1\text{-}F_f$**	=	**ST (Bq)**	**ST/2 (Bq)**
50^{th} percentile	4.4 x10^{10}	0.003	0.05	=	6.6 x10^{6}	3.3 x10^{6}
75^{th} percentile	7.8 x10^{10}	0.007	0.075	=	4.1 x10^{7}	2.1 x10^{7}
100^{th} percentile	1.1 x10^{11}	0.01	0.10	=	1.1 x10^{8}	5.5 x10^{7}

With exception of the plume centerline, the total ST was then assumed to be evenly divided between the two recirculation volumes which comprise the recirculation zone, and thus divided by two, as shown by the value ST/2 within Table 4. For the plume centerline calculation, the ST/2 value represented the contribution from both recirculation volumes upon the plume centerline, i.e., conservatively assumed that half of the ST/2 from each recirculation zone was concentrated at the plume centerline. Thus, the ST/2 values were used to calculate the concentration at each AIRNET station within their respective recirculation volumes. Note: the control volume approach also bounds any potential lateral diffusion due to pressure differentials from plume centerline to the recirculation zone boundary.

The total volume of the cavity zone was assumed to be approximated as a quadrant of an ellipsoid (Haltisky 1976). First the total ellipsoid volume (m^3) was calculated according to:

Eqn. 23 $$V = \frac{4}{3} * \pi * a * b * c$$

Where:

a = width axis radius (m)

b = length axis radius (m)

c = height axis radius (m)

The value (a) was represented by half of the approximate length of MDA-B, as calculated from Fig. 24, and was shown to be 415 m. The value (c) was conservatively assumed to be equal to the value H, or 7 m. The value (b) was calculated to be 191 m, according to the cavity zone length calculation shown in Equation No. 24 (DOE 2004):

Eqn. 24 $$\textit{Cavity Zone Length} = 2.5\ ((2a) \times c)^{0.5}$$

The value (c) was conservatively assumed to equal the value H, or 7 m.

These values were then input into Equation No. 23, thus yielding a total ellipsoid volume of 2.3×10^6 m^3. This value was then divided by four to obtain one quadrant of the ellipsoid volume, thus approximating the shape of the recirculation cavity and yielding a total cavity volume of 5.8×10^5 m^3. The total zone volume was then divided between the two circulatory volumes of the zone, which lie at both the left and right sides of the plume centerline, by multiplying the total zone volume by ratios of 458 to 829 and 371 to 829, respectively, yielding circulatory volumes of 3.2×10^5 m^3 and 2.6×10^5 m^3, for the left and right volumes, respectively. Additionally, specific volumes were estimated for the calculation of concentration at the plume centerline, whereby the release occurred into a volume equal to a width represented by the Γ derived from Fig. 24, i.e., 5.8×10^5 m^3 multiplied by the ratio of 266 m to 829 m.

The model concentrations (Bq m^{-3}), i.e., the concentrations modeled for each station, were then calculated according to Equation No. 25:

Eqn. 25 $$Concentration_i = \frac{ST}{SV} x \frac{\chi}{Q} x\, SR$$

Where:

SV is the recirculation volume that the station is located within, and SR is the sampling rate, assumed to be equal to the AIRNET station sample flow rate of 0.0019 m^3 s^{-1}.

3.5 Hypothesis to Be Evaluated

The following null hypothesis is evaluated in this research:

H_{01}: The theoretical methodology advanced by Hawkley shows good correlation with the average radiological concentration data measured on the northern boundary of the MDA B area. The methodology is in agreement with empirical results for radiological concentration data sets obtained from the Los Alamos National laboratory.

H_1: The theoretical methodology advanced by Hawkley does not show good correlation with the average radiological concentration data measured on the northern boundary of the MDA B area, and cannot be validated against empirical results from the Los Alamos National Laboratory.

The decision rule used against this evaluation is as follows:

(i) Based on the analysis of the theoretical methodology advanced by Hawkley and the comparison of this methodology validated against Los Alamos National Laboratory data sets, it will be concluded that the null hypothesis H_{01} is supported and the alternate hypothesis H_1 is rejected if the overall values of the EPA recommended Cox and Tikvart (1990) protocol for evaluation of radionuclide concentrations show good correlation. Good correlation is defined as a fractional bias average (FBA) lesser than or equal to 1.0.

4.0 RESULTS AND DISCUSSION

4.1 Data Comparison

Assessment models are created so that the consequences of radionuclides within the environment may be evaluated for decision making purposes. As such, they are comprehensive representations of a natural system which attempts to facilitate critical evaluation (Forrester 1968). A comprehensive methodology was developed within the Methods section which identified parameters of importance capable of describing temporal variations of concentration specific to the eddy diffusivity and large turbulence inherent to a recirculation zone. As such, a multitude of concentration distributions were measured, as observed in Figs. A1-A64. However, the average concentration distribution which encapsulates all variations was used as a tool for understanding, predicting, and bounding the overall flow characteristics, and thus the estimation of modeled effluent concentrations. Furthermore, the goal for this analysis was to derive a methodology which allowed for the calculation of a concentration distribution, based on specific samples of data and meteorological parameters during a specified sampling period. Furthermore, by allowing for the input of site specific parameters, one could ascertain various percentile estimates of concentration.

The ^{239}Pu air concentrations per period as presented in Table 5 were color coded, where: red represented the greatest concentration, gold the second greatest concentration, and black representing remaining concentrations. Of the 64 periods presented, the greatest concentration per period appears 21 times at station 329. Of the 43 remaining periods, 19 of the greatest concentrations appear at stations 317, and five were observed at station 330, which are the stations directly to the right and left of station 329. Thus, 70% of the greatest concentrations per period appear at or in close proximity to station 329. The second greatest concentrations as represented by the color gold appear nine times at station 329, and 19 times at stations 317 and 330. From these observations one can observe that the plume centerline lies central to stations 317 and 329, which correlates very well with Fig. 24, and identifies the greatest concentrations as being proximal to the plume central line.

Table 5. ^{239}Pu concentrations per AIRNET station over all periods of interest (x 10^{-7} Bq m^{-3}).

Period Start Date	Station							
	326	327	328	317	329	330	331	169
13 Apr 09	-0.6	-0.6	-0.6	4.4	-1.1	0	4.0	2.6
27 Apr 09	1.7	-0.7	-1.2	4.7	0	2.6	1.6	1.4
11 May 09	-0.8	-0.6	0.6	0	1.7	0	2.9	4.3
25 May 09	0.6	7.7	-0.6	1.6	2.2	2.7	-1.0	0.6
8 Jun 09	3.8	-1.2	1.2	3.0	2.6	-0.6	2.7	5.7
22 Jun 09	0.0	0.7	1.2	1.2	2.4	1.9	0	1.2
6 Jul 09	2.7	0.7	2.7	0	1.8	3.5	4.1	1.8
20 Jul 09	0.55	8.4	5.2	3.7	2.6	2.4	5.7	2.8
3 Aug 09	3.8	1.3	1.7	1.3	8.1	1.3	1.7	1.8
17 Aug 09	3.4	2.9	1.5	5.2	4.7	2.5	4.6	2.7
31 Aug 09	6.0	-1.4	-0.6	2.2	3.6	6.3	1.7	0
14 Sep 09	1.2	1.7	6.3	0.6	2.7	1.5	4.2	3.6
28 Sep09	-2.6	3.7	1.3	0	10.4	3.0	1.7	4.2
12 Oct 09	-0.6	1.3	0	5.0	1.8	3.9	4.0	1.6
26 Oct 09	0.0	2.5	1.2	2.9	6.2	1.2	5.5	0.6
9 Nov 09	4.8	0	0	5.1	-5.9	3.8	2.8	4.9
23 Nov 09	-1.2	3.0	1.0	1.7	-3.5	2.3	-1.2	0.6
7 Dec 09	7.7	2.6	3.3	2.6	0.74	2.0	5.0	2
21 Dec 09	2.2	1.8	3.6	1.1	2.9	3.0	3.9	0
4 Jan 10	1.3	6.6	3.9	3.4	2.1	4.0	9.9	3.7
18 Jan 10	0.0	0.6	3.7	0.6	0	1.6	1.3	0.6
1 Feb 10	0.6	1.48	1.1	5.5	5.8	1.2	2.3	0.5
15 Feb 10	2.6	8.0	12.2	16.0	5.8	3.0	4.6	0.6
1 Mar 10	11.0	1.2	4.0	4.2	4.2	9.4	42.3	7.8
15 Mar 10	13.3	7.7	7.4	21.0	15.3	358	28.6	36.1
29 Mar 10	9.5	13.3	7.8	63.0	17.5	13.0	17.4	13

Period Start Date	Station							
	326	327	328	317	329	330	331	169
12 Apr 10	15.0	3.2	4.4	14.0	41.0	5.6	19.6	5.7
26 Apr 10	17.0	11.0	11.0	41.0	25.0	7.5	154.0	13.2
10 May 10	3.9	-1.8	4.8	14.9	6.3	8.8	6.1	11.2
24 May 10	9.0	4.6	4.9	7.0	5.6	10.4	15.2	7.0
7 Jun 10	4.2	8.7	4.4	66.8	8.0	4.7	12.1	10.8
21 Jun 10	4.6	0	3.6	6.5	3.3	7.6	4.5	0.7
5 Jul 10	6.3	1.1	2.7	3.9	3.2	7.5	1.6	1.8
19 Jul 10	4.9	4.8	3.4	3.3	2.0	5.3	16.8	2.6
2 Aug 10	-0.6	0.1	0.7	7.3	0.9	4.3	3.1	7.7
16 Aug 10	0.6	1.7	1.2	7.0	194.4	6.8	1.4	0.6
30 Aug 10	2.5	9.3	2.0	7.8	33.8	5.6	7.4	7.8
13 Sep 10	-1.6	2.3	1.9	2.4	7.8	34.0	8.0	3.5
27 Sep 10	1.2	1.7	3.3	3.1	43.0	4.4	6.1	3.1
11 Oct 10	0	2.4	2.3	2.6	14.0	5.2	5.7	7.2
25 Oct 10	4.0	18.3	0	7.9	66	10.9	6.9	5.1
8 Nov 10	6.7	3.7	4.6	23.2	824.7	8.6	10.6	9.1
22 Nov 10	3.7	4.0	2.0	10.4	521.4	11.5	12.8	5.1
6 Dec 10	-2.0	1.3	6.9	2.3	17.5	6.0	13.3	7.5
20 Dec 10	4.5	-1.1	2.2	5.2	12.7	3.1	1.6	4.3
03 Jan 11	8.3	3.0	10.1	14.1	5.4	19.1	10.7	22.2
17 Jan 11	3.4	2.6	9.0	50.1	20.9	10.4	22.6	6.4
31 Jan 11	4.9	1.1	8.1	9.1	130.2	12.0	14.2	5.2
14 Feb 11	10.0	8.8	21.6	52.0	382.4	26.4	48.5	33.3
28 Feb 11	11.8	1.9	7.9	35.6	42.2	25.3	34.6	20.2
14 Mar 11	16.4	1.8	15.3	96.3	124.0	17.1	39.7	25.4
28 Mar 11	4.4	6.1	58.0	139.0	101.6	17.8	16.7	15.9
11 Apr 11	6.8	8.0	32.9	52.0	1,043.0	256.3	288.2	18.9
25 Apr 11	8.9	132.2	43.3	168.2	138.7	26.0	66.2	28.3
9 May 11	11.9	12.8	18.1	145.2	62.2	11.7	206.4	5.9
23 May 11	27.7	71.8	361.4	983.4	747.0	37.1	43.2	24.6
6 Jun 11	41.1	41.1	34.3	1,639.0	439.6	117.2	84.5	55.9
20 Jun 11	13.0	23.2	38.4	2,029.0	412.0	52.6	41.0	10.7
4 Jul 11	7.7	14.7	6.8	136.6	66.1	6.8	58.7	8.4

Period Start Date	Station							
	326	327	328	317	329	330	331	169
18 Jul 11	7.5	35.6	17.7	360.0	113.1	36.5	14.3	29.1
1 Aug 11	6.1	10.6	6.9	52.6	29.1	18.3	38.9	17.8
15 Aug 11	2.5	6.5	2.6	26.0	498.6	20.0	16.4	9.3
29 Aug 11	22.1	15.9	9.4	18.7	19.6	8.5	92.4	7.4
12 Sep 11	6.9	53.0	49.7	14.4	11.3	16.8	24.8	9.1
Station Average	5.9	9.2	13.8	100.3	98.6	20.7	21.4	9.0

Table 6 displays the horizontal distance from the plume centerline for each station, and the average concentration measured for each station. As displayed in Table 7, the average model concentrations were calculated using the 50th percentile source term, the 75th percentile source term, and the 100th percentile source term.

Table 6. Station number, horizontal distance and average measured concentration.

Station	Horizontal Distance of Station Location (m)	Average Measured Concentration (Bq m^{-3})
326	458	5.9 x 10^{-7}
327	352	9.3 x 10^{-7}
328	233	1.4 x 10^{-6}
317	53	1.0 x 10^{-5}
PCL[(a)]	0	1.1 x 10^{-5}
329	53	1.0 x 10^{-5}
330	159	2.1 x 10^{-6}
331	265	2.1 x 10^{-6}
169	371	9.0 x 10^{-7}

(a) Plume Centerline

Table 7. Average Modeled concentrations.

Average Modeled Concentrations (Bq m^{-3})			
Station	**50^{th} percentile**	**75^{th} percentile**	**100^{th} percentile**
326	1.6×10^{-7}	1.0×10^{-6}	2.7×10^{-6}
327	2.6×10^{-7}	1.6×10^{-6}	4.3×10^{-6}
328	5.1×10^{-7}	3.1×10^{-6}	8.6×10^{-6}
317	1.8×10^{-6}	1.1×10^{-5}	2.9×10^{-5}
PCL[a]	3.4×10^{-6}	2.1×10^{-5}	5.7×10^{-5}
329	2.2×10^{-6}	1.3×10^{-5}	3.6×10^{-5}
330	1.1×10^{-6}	6.4×10^{-6}	1.7×10^{-5}
331	5.1×10^{-7}	3.1×10^{-6}	8.5×10^{-6}
169	2.9×10^{-7}	1.8×10^{-6}	4.9×10^{-6}
(a) Plume Centerline			

Fig. 29 displays the average measured concentration against the 50, 75, and 100 percentile modeled concentrations. The 50 and 75 percentile modeled data aligned well with the measured data, with the 75 percentile providing a realistically conservative estimate of the measured data. This result supported the validity of the approach, whereby the cavity zone boundary conditions and recirculation volumes were derived from site specific data, and into which a conservatively estimated source term was released and dispersed according to the aforementioned Lorentzian diffusion coefficient methodology. Essentially, the model yielded the fraction of ST released to the cavity zone, concentrated at distance y, per recirculation zone volume.

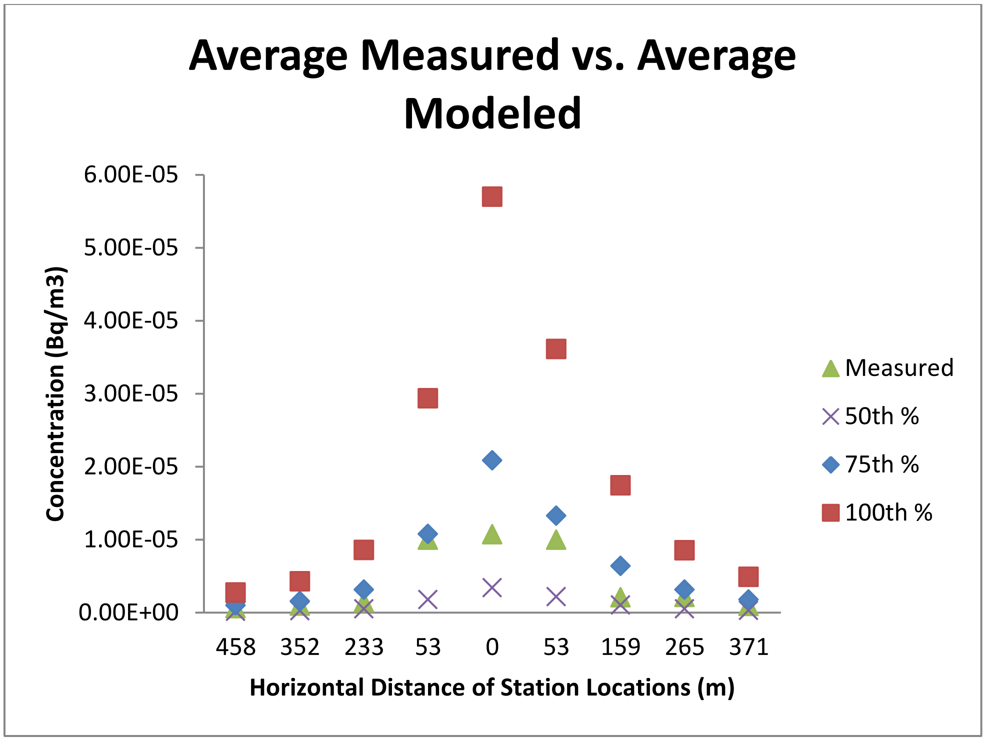

Fig. 29**.** Average measured concentrations compared against the 50, 75, and 100 percentile modeled concentrations.

Each modeled data point represented an estimate of potential measured values, and varied according to the ST input. Furthermore, given the long measurement period, the average concentrations were influenced by upset conditions and operation unknowns. For example, the leak paths may not be fully addressed given upset conditions, i.e., forced flow ventilation loss, multiple point source releases, etc., resulting in concentration magnitudes that are substantially larger over a specific period. Therefore, large data sets which encompass the entire range of conditions were proven necessary for the calculation of one year concentration averages required for reporting public dose to the EPA.

A lack of measured data associated with the plume centerline contributed to model uncertainty. However, given a normalized curve associated with the 128 week average concentrations, an approximate centerline concentration of 1.1 x 10^{-5} Bq m^{-3} was interpolated. This result suggested that placing an air monitoring station at the plume centerline, or between stations 317 and 329, would have been prudent, so that the potential peak concentrations were fully measured. This result places great emphasis upon the location of air monitoring stations around the facility of interest. Additionally, given various site parameters, the location of a site boundary or potential MEI becomes the primary zone of interest. If this zone is not properly accounted for via measurement, the consequence to the MEI may potentially be underestimated, stressing the importance of an adequate number of properly located air monitoring stations within the zone of interest.

4.2 Model Validation

A validation analysis attempts to determine a models domain of applicability (Kirchner 1994, Peterson and Kirchner 1998). The domain of applicability is the condition or conditions under which a model may be assumed to adequately describe the system of interest, and determines the accuracy of a model over a range of input factors for which the model provides accurate estimates. (Grogan 2008)

Accuracy within a model is a measure of how close a model estimate is to a similar measured quantity, and is evaluated by comparing model predictions against an independent set of measurements consisting of like quantities, i.e. radionuclide concentrations. The acceptable level of accuracy is specific to individual judgment and varies depending on the particular questions being addressed by the model (IAEA 1989). According to Grogan (2008), an environmental transport model is performing very well when the modeled data are within a factor of two of the measured data, with typical goals for models to predict concentrations within a factor of 3, 5, or 10, of the measured data, depending upon the assessment question.

Furthermore, the evaluation of model parameters or variables of importance which influence the variability of a selected distribution is pertinent to the quality of fit of a modeled distribution to a collection of data, specifically, when model variation is large (Haas 1997), because variables of importance: influence model outputs; identify or eliminate parameters that can or cannot be safely neglected when constructing the model methodology; increase confidence that the model responds to perturbations similarly to the parent distribution being sampled; reduces the necessary parameters and thus reduces unnecessary uncertainty in the model outputs, thus increasing model performance (Grogan 2008). Additionally, an evaluation of the fit of a distribution based on variability within the modeled parameter is important for the identification of the appropriate distribution, especially when data is scarce (Hattis and Burmaster 1994).

Thus, a model methodology should predict and adequately bound the measured data using model parameters specific to the analysis being performed. The parameter of interest should not be adjusted solely to yield modeled values which exceed the measured values. However, the scope of an assessment analysis includes an investigation into a range of model parameters as signified by the Methods section, Tables 6-7, and Fig. 29. Such an investigation includes a statistical analysis of the modeled parameter.

In addition to Γ being used to determine the width of the Lorentizian distribution as shown in section 3.3, Γ was also investigated as a means for comparing the width of the individual two-week concentration distributions with the greatest peaks. As such, the 13 greatest concentration peaks were further analyzed, and quantified according to Γ, as shown in Table 8

Table 8. Full width at half maximum values associated with the 13 greatest concentration peaks.

Period Start Date	**Full Width at Half Maximum (Γ)**
03/15/2010	115 m
08/16/2010	104 m
11/08/2010	103 m

Period Start Date	Full Width at Half Maximum (Γ)
11/22/2010	112 m
02/14/2011	117 m
04/11/2011	126 m
04/25/2011	260 m
05/09/2011	193 m 124 m
05/23/2011	300 m
06/06/2011	175 m
06/20/2011	171 m
07/18/2011	181 m
08/15/2011	114 m

The 13 greatest peaks displayed within Appendix A, and presented in chronological order within Table 8, displayed distributions centered directly at the PCL, or near the plume centerline, i.e., stations 317 and 329, with the exception of period start date 05/09/2011, which displayed a bimodal distribution with peaks at stations 317 and 331, whereby Γ was calculated for both peaks. The Γ values above were then compared to the Γ value of 266 m calculated for the average concentration distribution displayed in Fig. 25. An interesting result is that the distributions which peaked directly at the PCL, i.e., period start dates 04/25/2011 and 05/23/2011, showed a concentration distributed evenly about the mean, and thus much wider Γs than those associated with peaks at stations 317 and 329. Furthermore, these wider peaks were similar to the Γ value of 266 m measured for the average concentration distribution. Thus allowing for two inferences: if one assumes that the control volume approach is an accurate approximation and that a greater peak would be associated with a smaller Γ, we can conclude that the maximum peak at the PCL is a normalized byproduct of, and may be reasonably approximated from the maximum peaks measured at stations 317 and 329; if we do not assume that the control volume approach is applicable, then we must measure the PCL concentrations and empirically assess the peaks. Also, a smaller Γ could be representative of an acute release to the environment, whereby the release was concentrated near the plume centerline.

Furthermore, this data set suggests that a standard set of Γ could be developed via the ratio of the Γ values provided in Table 10, to the width of the cavity zone. For this analysis, the Γ value was derived from measured data. However, in the absence of measured data, Γ will have to be estimated, and has been shown to be proportional to the width of the cavity zone. For a normalized Lorentzian distribution, the percentage of Γ relative to the x-axis of MDA-B has been shown to be 23 percent (Bevington and Robinson 2003), whereby the x-axis is equivalent to the maximum width of the cavity zone. Within this investigation, the width of the cavity zone was assumed to be equal to the length of MDA-B, approximated as 829 m, and the corresponding percentage of Γ relative to the x-axis was shown to be 30 percent. Furthermore, the cavity zone width rarely exceeds the building width by more than 50 percent (Hanna et al. 1982). Therefore, increasing the MDA-B width by 50 percent yielded an upper range for cavity zone width and a corresponding percentage of Γ relative to the x-axis of 21 percent, thus yielding a range of the percentage of Γ relative to the x-axis of 31 to 21 percent, and correlating well with Bevington and Robinson (2003).

Additionally, to further highlight the effect of unknown conditions upon outside concentrations, environmental data associated with the Las Conchas fire was investigated. The Las Conchas fire began at approximately 1 PM on June 26, 2011 near LANL, and was not 100 percent contained until August 1, 2011 (LANL 2011). During the fire, the outside concentrations per period were shown to be elevated above average outside concentrations. The average outside concentrations per station, were averaged from 128 weeks of measurement data ranging from

April 13, 2009 to September 11, 2011. The increase in outside concentration was believed to be the result of the ventilation system being shut down during the fire when the town and the project people were evacuated. The ventilation system shutdown in addition to the wind may have created a net positive pressure gradient within the enclosures, which then lead to an increased release of contaminated dirt from the enclosures to the environment. A future study comparing inside to outside concentration data would benefit from a greater inside concentration data set. As stated above, the outside concentration data were collected over 128 weeks, via 64 two week sampling periods, whilst the inside concentration data were collected over 15 two week sampling periods. The availability of a larger data set would allow for a more thorough assessment of correlation, and times of operational unknowns.

Furthermore, model validation may involve a comparison of results obtained from different codes for a well-defined hypothetical evolution. The differences amongst the model results require analysis of model, structure, parameter values, and modeling assumptions. As observed from the average concentration data, the distribution approximated a normalized distribution. However, the distribution was assumed to be applied to any downwind distance within the cavity zone, i.e., up to 249 m. This assumption was made to account for eddy diffusion within the circulatory control volumes of the cavity zone and the potential for homogenous dispersion of the effluent in the x direction. Thus, the χ/Q values derived within this analysis were based upon the lateral dispersion (y), from the plume centerline, with a centerline horizontal distance of zero meters. This base application is shown valid when one considers general χ/Q theory, e.g., the χ/Q over the dimensions x, y, and z, is represented by a volume equal to the product of μ x y x z, with μ representing the x dimension, and yields units of s m^{-3}. When we apply uniform mixing within the vertical dimension, we approximate a line dispersion represented by a volume equal to the product of μ x y, and yields units of s m^{-2}. If we then assume a uniform concentration within the dimension x, dispersion is dependent upon μ, but represented by a volume equal to y, and yields units of s m^{-1}. Thus, this one dimensional χ/Q is driven by the inverse of the y dimension, i.e., m^{-1}. Therefore, χ/Q should decrease as the receptor moves further laterally, from y = 0, as was observed and shown within Fig. 29.

Additionally, given that the lateral dispersion approximated a normalized distribution, some of the input parameters identified within this analysis were able to be applied to the Gaussian dispersion model Radiological Safety Analysis Computer (RSAC) program Version 7.2. Using RSAC-7.2, χ/Q values at the plume centerline for various Pasquill-Gifford stability classes were calculated. The trend of these values was then compared to the modeled plume centerline χ/Q value developed within this dissertation. The input parameters utilized were: mixing height = 7 m, equal to H; downwind distance = 191 m, equal to the length of the cavity zone and representative of the enveloping distance within the x direction for which uniformity applies; building wake control with a building width of 829 m and a height of 7 m, representing the building lee side surface area; Pasquill-Gifford stability classes A, B, C, and D; μ = 3.3 m s^{-1}, equal to the average velocity measured over the entire sampling period; an average air density at LANL of 9.58×10^{2} g cm^{-3}.

Table 9. Modeled PCL values versus RSAC-7 PCL values.

Stability Class	**RSAC χ/Q (s m^{-3})**	**Modeled χ/Q (s m^{-3})**
A	3.0×10^{-4}	1.0×10^{-4}
B	3.4×10^{-4}	
C	3.7×10^{-4}	
D	4.0×10^{-4}	

As shown in Table 9, as the stability class decreased from D to A, the value for χ/Q also decreased, and approached the modeled χ/Q. This relationship suggested that our modeled χ/Q was a function of a turbulent control volume with instability greater than that expected for a Gaussian based standard deviation set, thereby over predicting the plume centerline concentration associated with an acute release. The RSAC output files are displayed within Appendix B. Note this comparison represents the effects of stability upon effluent dispersion, with the RSAC values calculated at the zone boundary of x = 191 m. However, the Gaussian model employed by RSAC is unable to represent the recirculation effects and uniformity assumed within the model methodology.

Furthermore, the 1.0×10^{-4} s m^{-3}, plume centerline χ/Q value derived within this analysis, as uniformly appropriate within the length of the cavity zone, i.e., 0 m to 191 m, was compared against an RSAC calculated χ/Q value at a downwind distance of 10 meters. The comparison was performed to analyze a competing approach, as performed within RSAC, against the new methodology described by this dissertation. The RSAC value employed the code specific building wake correction whereby the Gaussian point source was modeled as a plane source via the surface area of the upwind side of the cavity zone, i.e., 829 m by 7 meters. The RSAC generated value was shown to be 5.24×10^{-2} s m^{-3}, or more than two orders of magnitude greater than the modeled value produced within the new methodology. As such, the RSAC calculated value would greatly overestimate the cavity zone concentration, and not be appropriate for realistically bounding the measured data.

4.3 Model Evaluation

The validation of air dispersion models with empirical data is a subjective and generally qualitative process. As such, the EPA recommends using a model evaluation protocol that provides a qualitative methodology which allows for the separation of good performing and poor performing models. One such protocol was developed by Cox and Tikvart (1990), and provides a regulatory approved framework for comparison of the modeled data to the measured data.

Consistent with EPA recommendations (EPA-450/4-84-023), the fractional bias arithmetic mean (FBA) of the modeled values to the set of measured values was used as the measure of model performance and thus the basis for model evaluation. Fractional bias is the "fundamental measure of discrepancy between the measurement-based and prediction based test statistic" (Cox and Tikvart 1990). The performance measures were calculated at each receptor, for both the measured and modeled data sets.

The FBA is calculated according to:

Eqn. 27 $$FBA = 2 * \frac{OB-PR}{OB+PR}$$

Where:

OB = concentration measured at a given receptor

PR = concentration modeled for a given receptor

The FBA was utilized because the bias is symmetrical and bounded, with values ranging from -2.0 (extreme overprediction) and +2.0 (extreme underprediction), as such, the best performing model would have a value of zero. Consistent with EPA recommendations, the separation between good performing and poor performing models was set at 1.0. Because the concentration values reflect the range of expected meteorological parameters and conditions, one fractional bias value for each receptor was deemed representative.

The FBA was calculated for the 50th and 75th percentile average modeled concentrations, displayed in Table 7, and the average measured concentrations displayed in Table 6. The results are shown in Table 10, below.

Table 10. FBA values for the 50th and 75th percentiles.

Receptor	**FBA**	
	50th percentile	**75th percentile**
Station 326	1.1	-0.5
Station 327	1.1	-0.5
Station 328	1.0	-0.8
Station 317	1.0	-0.1
PCL	1.1	-0.6
Station 329	1.3	-0.3
Station 330	0.6	-1.0
Station 331	1.3	-0.3
Station 169	1.0	-0.7

The values displayed within Table 10 highlight the range of model correlation associated with a range in ST, i.e., the FBA values associated with the 50th percentile signified underprediction, while the values associated with the 75th percentile signified overprediction. The 50th percentile FBA values for Stations 328, 317, 330, 169, were ≤ to 1.0, and thus showed good correlation and supported the null hypothesis. The FBA values associated with the remaining receptor locations, excluding Stations 329 and 331, were near the 1.0 cutoff with values of 1.1. All of the 75th percentile FBA values displayed within Table 10were shown to be ≤ 1.0, and thus showed good correlation and supported the null hypothesis. As signified by the FBA values, a correlation of the modeled values to the measured values is dependent upon the ST applied. This result is expected as the modeled and measured values are dependent upon their respective ST. Whereby the modeled ST is an estimate of the range of probable STs associated with the measured values. However, this methodology may also be applied to a bounding evaluation of the MEI. As such, a conservative ST may be applied, such as the 100th percentile, with the goal of bounding all probable measured STs regardless of correlation.

4.4 Evaluation of Tested Hypothesis

The following null hypothesis was evaluated in this research:

H_{01}: The theoretical methodology advanced by Hawkley shows good correlation with the average radiological concentration data measured on the northern boundary of the MDA B area. The methodology is in agreement with empirical results for radiological concentration data sets obtained from the Los Alamos National laboratory.

H_1: The theoretical methodology advanced by Hawkley does not show good correlation with the average radiological concentration data measured on the northern boundary of the MDA B area, and cannot be validated against empirical results from the Los Alamos National Laboratory.

Based upon the decision rule used against this evaluation, as specified in Section 3.5, it was concluded that the null hypothesis H_{01} was supported and the alternate hypothesis H_1 was rejected, as the overall values of the EPA recommended Cox and Tikvart (1990) protocol for evaluation of radionuclide concentrations showed good correlation, i.e., a fractional bias average (FBA) lesser than or equal to 1.0.

4.5 Dose Consequence Evaluation

The methodology identified within this document allowed for the derivation of χ/Q values at specific receptor locations. The methodology further described how to input these values for the development of a modeled concentration profile. The modeled concentration values were then compared to the measured concentration values, and showed good correlation (Table 10). Specifically, the 75th percentile concentrations, which were shown to bound the measured data.

Furthermore, the plume centerline χ/Q value derived using the methodology developed within this document, was compared against RSAC-7.2 derived plume centerline χ/Q values for various stability classes (RSAC-7.2 model parameters were described in section 4.2 above), as shown in Table 9. As the stability class decreased from D to A, the RSAC-7.2 derived χ/Q value decreased, and approached the plume centerline χ/Q value derived using the methodology developed within this document.

Given the aforementioned correlations, a bounding dose consequence analysis was performed using RSAC-7.2. As the inhalation pathway drives the dose consequence, and given a negligible gamma contribution, the total effective dose (TED) was assumed equivalent to the committed effective dose (CED), as determined from the following formula:

Eqn. 28 $$TED = CED = ST \times \chi/Q \times BR \times DCF$$

Where:

ST = source term (Ci)

χ/Q = plume dispersion (s m^{-3})

BR = breathing rate (m^3 s^{-1})

DCF = dose conversion factor (rem Ci^{-1})

For the calculation of the TED, the DCFs provided in the International Commission on Radiological Protection (ICRP)-68 were used. Also, the RSAC-7.2 default DCF for the lung absorption type was selected that would result in the highest dose. Other input parameters included are: the 75^{th} percentile ST (Table 4) as the radionuclide input per Section 4.3; the modeled χ/Q values (Table 3) specific to each receptor; and a breathing rate of 3.33×10^{-4} m^3 s^{-1} (Halitsky 1968, ICRP-1968). The resulting dose consequence values are displayed in Fig. 30. The RSAC files are presented within Appendix C.

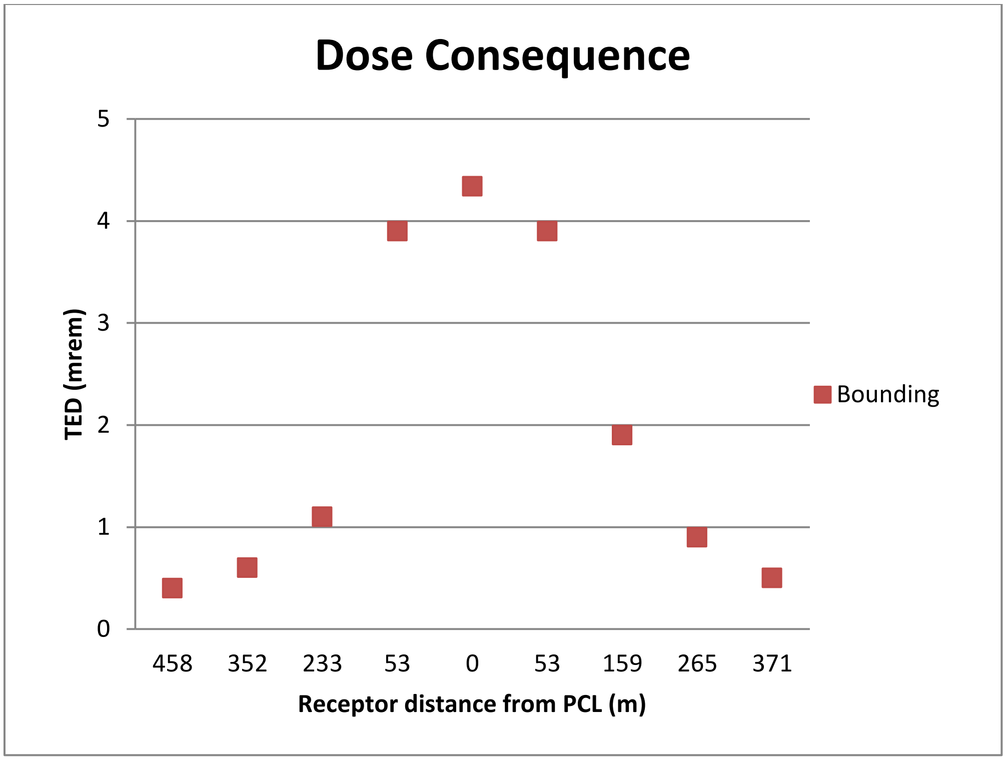

Fig. 30. Dose consequence per receptor.

5.0 CONCLUSION

An investigation into near field atmospheric dispersion around nuclear facilities was performed using a Lorentzian Distribution methodology. Results of the investigation emphasized the importance of AIRNET station placement to completely assess the location of the potential MEI and estimated radiological dose consequence resulting from a single point source release, or a multitude of release locations. The methodology allowed for the estimation of dispersion coefficients within the near field cavity zone, whereby the coefficients were based upon the Lorentzian distribution as opposed to the standard Gaussian distribution. The use of the Lorentzian distribution in lieu of the Gaussian distribution allowed for the derivation of a concentration distribution with considerably heavier tales. Therefore, the x-axis was not approached as readily, as is consistent with the displacement zones within the near field of a radiological release. The modeled concentrations were shown to correlate well with the measured concentrations, as a fractional bias average (FBA) lesser than or equal to 1.0 was calculated for each receptor location.. Thus, the methodology was shown to be appropriate for near field atmospheric dispersion calculations provided that the ST and site specific data are realistically estimated. As such, the methodology was shown to be applicable to operational scoping calculations and dose assessments, in the absence of measurement data.

6.0 FUTURE WORK

A future study which collected additional measurement data released from a facility with a different geometrical configuration would be beneficial. The modeled data could then be calculated from the methodology developed within this work, yet be based upon a different set of inputs. The additional set of inputs would allow for an additional correlation between measured and modeled data.

Furthermore, a future study would benefit from a greater inside concentration data set, for the comparison of inside to outside concentration data. As stated above, the outside concentration data were collected over 128 weeks, via 64 two week sampling periods, whilst the inside concentration data were collected over 15 two week sampling periods. The availability of a larger data set would allow for a more thorough assessment of correlation, and times of operational unknowns. Also, a future study would benefit from the calculation of additional modeled values, according to standard models with near field corrections, and comparison of the results against the modeled values calculated within this work.

7.0 REFERENCES

Batchelor, G.K, (1950). “The Application of the Similarity Theory of Turbulence to Atmospheric Dispersion.” Quarterly Journal of the Royal Meteorological Society, 76(328): Pages 133-146.

Barr, S., and Clements, W.E., (1984). “Diffusion Modeling: Principles of Application,” In Atmospheric Science and Power Production, ed. D. Randerson, DOE/TIC-27601, United States Department of Energy, Pages 584-619.

Bevington, P.R., Robinson, D.K., (2003). *Data Reduction and Error Analysis*, McGraw-Hill.

Briggs, G.A., (1974). “Diffusion Estimation for Small Emissions,” In 1973 Annual Report, Environmental Research Laboratories. Air Resources, Atmospheric Turbulence and Diffusion laboratory. DOE/TIC, U.S Department of Energy, Pages 83-145.

Briggs, G.A., et al., (1977). “Summary of Recommendations made by the AMS Workshop on Stability Classification Schemes and Sigma Curves,” American Meteorological. Society, 58: Pages 1305-1309.

Canepa, E., (2004). “An Overview about the Study of Downwash Effects on Dispersion of Airborne Pollutants,” Environ. Modeling Software 19: Pages 1077–1087.

CFR, 10 CFR 50, “Domestic Licensing of Production and Utilization Facilities,” Title 10 Code of Federal Regulations Part 50, Office of the Federal Register, Washington, DC, 1990.

Chanin, D.I., et al., “MELCOR Accident Consequence Code System (MACCS) User’s Guide, “NUREG/CR-4691, Vol. 1, Sandia National Laboratories, 1990.

Chanin, D., Young, M., “Code Manual for MACCS2: Volume 1, Users Guide; Volume 2, Pre-Processor Codes COMIDA2, FGRDCF, IDCF2.” NUREG/CR-6613, Sandia National Laboratories, 1998.

Chamberlain, A.C., (1953). “Aspects of Travel and Deposition of Aerosol and Vapour Clouds”, AERE-HP/R-1261, Harwell, Great Britain.

Cox, W.M., Tikvart, J.A., (1990). “A Statistical Procedure for Determining the Best Performing Air Quality Simulation Model.” Atmospheric Environment 24: Pages 2387-2395.

Crawford, T.V., et al., “Atmospheric Transport of Radionuclides,” In Radiological Risk Assessment and Environmental Analysis, ed. J.E. Till and H.A Grogan, Oxford University Press, 2008.

DOE. “Hazard Categorization and Accident Analysis Techniques for Compliance with DOE Order 5480.23, Nuclear Safety Analysis Reports,” DOE-STD-1027-92, U.S Department of Energy, December 1992.

DOE. “Airborne Release Fractions/Rates and Respirable Fractions for Nonreactor Nuclear Facilities,” DOE-HDBK-3010-94, U.S Department of Energy, December 1994a.

DOE. “Preparation Guide for U.S Department of Energy Nonreactor Nuclear Facility Documented Safety Analyses,” DOE-STD-3009-94, U.S. Department of Energy, July 1994b.

DOE. “MACCS2 Computer Code Application Guidance for Documented Safety Analysis,” DOE- EH-4.2.1.4-MACCS2-Code Guidance, U.S Department of Energy Office of Environmental, Safety and Health, June 2004.

EPA. “Interim Procedures for Evaluating Air Quality Models,” EPA 450/4-84-023, U.S Environmental Protection Agency, 1984.

EPA. “AERMOD: Description of Model Formulation,” EPA-454/R-03-004, U.S Environmental Protection Agency, 2004.

Fackrell, J.E., (1984). “Parameters Characterizing Dispersion in the Near Wake of Buildings,” J. Wind Eng. Ind. Aerodyn. 16: Pages 97–118.

Forrester, J.W., (1968). *Principles of Systems*. Wright-Allen Press, Cambridge.

Garratt, J.R., “The Atmospheric Boundary Layer,” Cambridge Atmospheric and Space Science Series, 1994.

Gifford, F.A., Jr. “The Problem of Forecasting Dispersion in the Lower Atmosphere, Tech. Information Extension, U.S Atomic Energy Commission, 1961.

Gilbert, R.O, (1987). “Statistical Methods for Environmental Pollution Monitoring.” Van Nostrand Reinhold, New York, Page 320.

Grogan, H.A., “Model Validation,” In Radiological Risk Assessment and Environmental Analysis, ed. J.E. Till and H.A Grogan, Oxford University Press, 2008.

Haas, C.N., (1997). “Importance of Distributional Form in Characterizing Inputs to Monte Carlo Assessments.” Risk Assessment 17: Pages 107-113.

Halitsky, J., (1968). “Gas Diffusion Near Buildings. In Meteorology and Atomic Energy,” ed. Slade, D.H., Report TID-24190. U.S. Atomic Energy Commission.

Halitsky, J., (1976). “Wake and Dispersion Models for the EBR-II Building Complex,” Atmospheric Environment, Vol. 11, Pages 577-596.

Hanna, S.R., et al., “Handbook on Atmospheric Diffusion,” DOE/TIC-11223, United States Department of Energy, 1982.

Hattis, D., Burmaster, D.E., (1994). “Assessment of Variability and Uncertainty for Practical Risk Assessment.” Risk Assessment 14: Pages 713-730.

Hinds W. C. (1999). *Aerosol Technology*, J. Wiley.

Hodak, D.G., (1994). “Adjusting Triangular Distributions for Judgemental Bias.” Risk Assessment 14: Pages 1025-1031.

Hoffman, F.O., Miller, C.W., (1983). “Uncertainties in Environmental Radiological Assessment Models and their Implications.” Environmental Radioactivity, Proceedings No. 5. NCRP: Pages 110-138.

Hoffman, F.O., et al., (1993). “A Risk-based Screening Approach for Prioritizing Contaminants and Exposure Pathways at Superfund Sites.” Environmental Monitoring and Assessment, 28: Pages 221-237.

Huang, S., et al., (2006). “Statistical Study on the States in the Low Temperature Poly-Silicon Films with Thin Film Transistors.” Thin Solid Films 515: Pages 1210-1213.

IAEA. Evaluating the Reliability of Predictions Made Using Environmental Transport Models. Safety Series No. 100. International Atomic Energy Agency, Vienna, Austria. 1989.

ICRP-68, Dose Coefficients for Intakes of Radionuclides by Workers, International Commission on Radiological Protection, 1994.

Kirchner, T.B., (1994). “Data Management and Modeling,” Environmental Information Management, Proceedings of a Symposium: Pages 357-375.

Kirchner, T.B., “Estimating and Applying Uncertainty in Assessment Models,” In Radiological Risk Assessment and Environmental Analysis, ed. J.E. Till and H.A Grogan, Oxford University Press, 2008.

LANL, 2010a. Los Alamos National laboratory. Environmental Report 2010. ERID-207316.

LANL Drawing No. SK10487, “MDA-B Fixed Excavation Enclosures,” Rev. 1, June 2010b.

LANL. Meteorological data for Los Alamos National laboratory weather station TA-53. 2011b. Available at: http://www.weather.lanl.gov. Accessed 01 March 2013.

LANL, 2011a. Los Alamos National Laboratory. Environmental Report 2011. ERID-228615.

Leonard, M. T., and Jordan, H., “Attenuation of Airborne Source Terms in Leak Paths,” LA-UR-03-7945, October 2003.

Little, C.A., (1984). “Comparison of Exposure Pathways.” Models and Parameters for Environmental Radiological Assessments. DOE/TIC-11468. Pages 4-10.

Martin, J., (2006). *Physics for Radiation Protection*, Wiley-VCH.

Meyer, K., (1991). “Estimating Variances and Covariances for Multivariate Animal Models by Restricted Maximum Likelihood.” Genet Sel Evol 23: Pages 67-83.

NCRP. “Uncertainty in NCRP Screening Models Relating to Atmospheric Transport, Deposition and Uptake by Humans,” National Council on Radiation Protection and Measurements, 1993.

NCRP. “Screening Models for Releases of radionuclides to Atmosphere, Surface Water and Ground,” National Council on Radiation Protection and Measurements, 1996.

Knight, F.B., (1976). “A Characterization of the Cauchy Type.” Proceedings of the American Mathematical Society 55.

Knox, J.B., Walton, J.J., (1984). “Modeling Regional to Global Air Pollution.” In Atmospheric Science and Power Production, ed. D. Randerson. DOE/TIC27601. U.S Department of Energy, Pages 621-651.

Nolan, J.P., (2013). “Stable Distributions: Models for Heavy Tailed Data,” American University.

NRC. “Methods for Estimating Atmospheric Transport and Dispersion of Gaseous Effluents in Routine Releases from Light-Water Cooled Reactors,” Regulatory Guide 1.111, U.S Nuclear Regulatory Commission, 1977.

NRC. “Atmospheric Dispersion Models for Potential Accident Consequence Assessments at Nuclear Power Plants,” Regulatory Guide 1.145, U.S Nuclear Regulatory Commission, 1983.

NRC. “Nuclear Fuel Cycle Facility Analysis Handbook,” NUREG/CR-6410, U.S Nuclear Regulatory Commission, March 1998.

NRC. “Atmospheric Relative Concentrations for Control Room Radiological Habitability Assessments at Nuclear Power Plants,” Regulatory Guide 1.194, U.S Nuclear Regulatory Commission, 2003.

Olvera, H.A., et al., (2007). “Effects of Plume Buoyancy and Momentum on the Near Wake Flow Structure and Dispersion behind an Idealized Building,” J. of Wind Eng. and Ind. Aero. 96: Pages 209-228.

Pasquill, F., (1961). *Atmospheric Diffusion*. D. Van Nostrand, London.

Pasquill, F., and Smith, F.B. (1983). *Atmospheric Diffusion*, 3rd edition, John Wiley & Sons.

Peterson, S.R., Kirchner, T.B., (1998). “Data Quality and Validation of Radiological Assessment Models.” Health Physics 74: Pages 147-157.

Ramsdell, J. V., Jr. “Atmospheric Diffusion for Control Room Air Habitability Assessments,” NUREG/CR-5055, U.S. Nuclear Regulatory Commission, 1988.

Ramsdell, J.V., Jr., et al., “Atmospheric Relative Concentrations in Building Wakes,” NUREG/CR-6331, U.S Nuclear Regulatory Commission, 1995.

Richardson, L.F., (1926). “Atmospheric Diffusion Shown on a Distance-Neighbor Graph.” Proceedings Royal Society, Series A: Pages 110:709.

Rosnick, R., “CAP88-PC Version 3.0 User Guide,”2007.

Schrader, B.J., “The Radiological Safety Analysis Computer Program (RSAC-7.2) User’s Manual,” INL/EXT-09-15275, Rev. 1, Idaho National laboratory, October 2010.

Schulman, L.L., et al., (2000). “Development and Evaluation of the PRIME Plume Rise and Building Downwash Model,” J. Air & Waste Manage. Assoc., Vol. 50, Pages 378-390.

Schwerdtfeger, H., (1980). *Geometry of Complex Numbers*. Dover.

Sehmel, G. A. and Sutter, S. L. (1974), “Particle Deposition Rates on Water Surface as a Function of Particle Diameter and Air Velocity, J. Rechs. Atmos., III, Pages 911-918.

Sehmel, G.A., (1980). “Particle and gas Dry Deposition: A Review,” Atmospheric Environment, 14: Pages 983-1011.

Slade, D.H., “Meteorology and Atomic Energy,” AEC/TID-24190. United States Atomic Energy Commission, 1968.

Taylor, G.I., (1959). “The present Position in the Theory of Turbulent Diffusion.” In Atmospheric Diffusion and Air Pollution, Advances in Geophysics, vol. 6, ed. F.N. Freckle and P.A. Sheared. Academic Press. Page 101.

Thuillier, R.H., and Mancuso, R.L., “Building Effects on Effluent Dispersion from Roof Vents at Nuclear Power Plants,” EPRI NP-1380. Electric Power Research Institute, 1980.
Turner, D.B, “Workbook of Atmospheric Dispersion Estimates,” Publication No. AP-26. Unites States Environmental Protection Agency, 1970.

Weisstein EW. Cauchy Distribution. From Math World-A Wolfram Web Resource. 2013. Available at: http://www.mathworld.wolfram.com/CauchyDistribution.html. Accessed 01 April 2013.

Whicker JJ, Eisele WF. Environmental Air Sampling and Monitoring During Cleanup of a Manhattan Project Era Radioactive Waste Site. Presented at the 2011 Air Monitoring Users Group Annual Meeting. 2011. Available at: http://amug.us/Download12.html. Accessed 09 December 2012.

Whicker, F.W., Rood, A.S., “Terrestrial Food Chain Pathways: Concepts and Models,” In Radiological Risk Assessment and Environmental Analysis, ed. J.E. Till and H.A Grogan, Oxford University Press, 2008.

Widner, T.E., et al., (1991). “Improving Radioactive release Readiness using Scale Model Wind Tunnel Tests.” Proceedings, Third Topical meeting on Emergency Preparedness and Response. American Nuclear Society, Pages 110-113.

Wilson, D.J., Britter, R.E., (1982). “Estimates of building surfaces concentrations from nearby point sources,” Atmos.Environ. 16: Pages 2631–2646.

Wikipedia.org. A representation of stereographic projection of elliptic transformation. Available at: http://en.wikipedia.org/wiki/M%C3%B6bius_transformation. Accessed 01 April 2013.

Yanskey, G.R., et al., (1966), “Climatography of the National Reactor Testing Station,” IDO-12045, Idaho National Engineering Laboratory, Idaho Falls, Idaho.

APPENDIX A

Figs. A1-A64

Fig. A1 displays the air concentration per the horizontal distance of the receptor locations for period start date 04/13/2009.

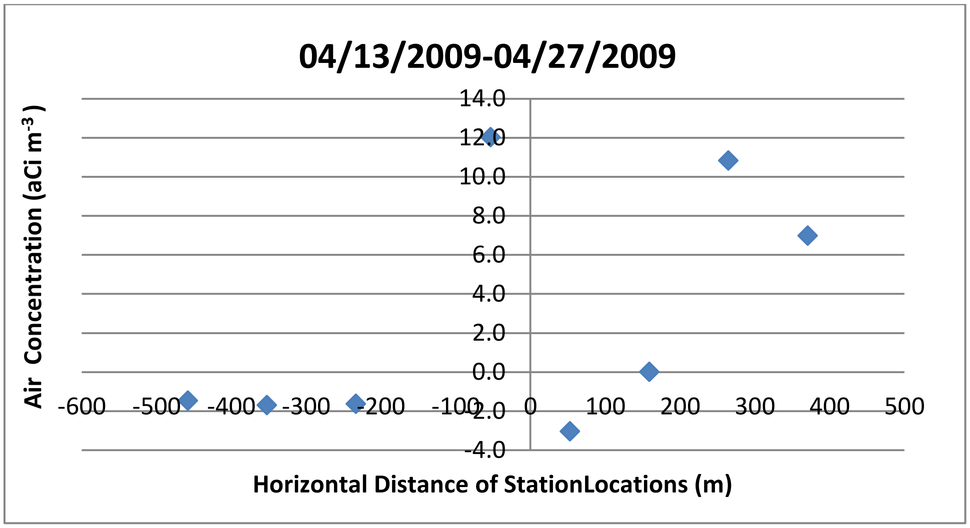

Fig. A1. ^{239}Pu concentrations per station location per period.

Fig. A2 presents the air concentration per the horizontal distance of the receptor locations for period start date 04/27/2009.

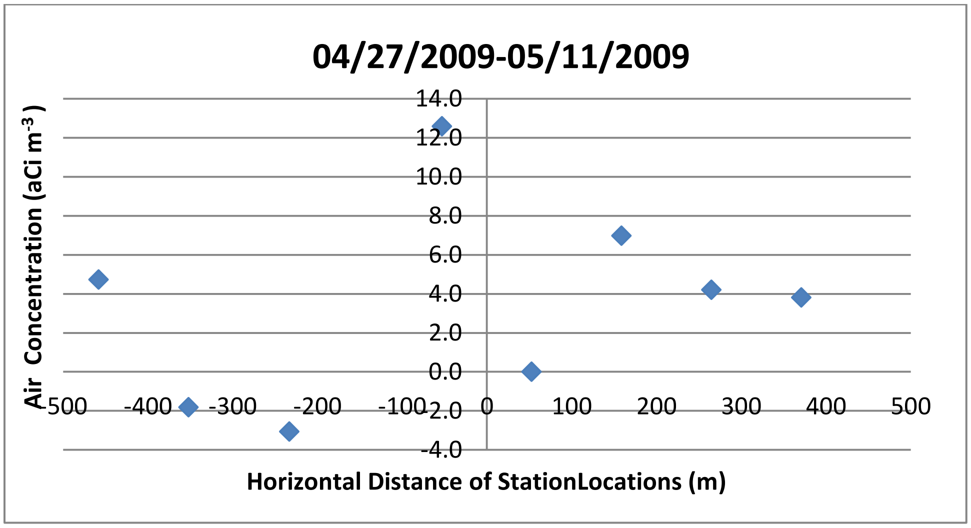

Fig. A2. ^{239}Pu concentrations per station location per period.

Fig. A3 presents the air concentration per the horizontal distance of the receptor locations for period start date 05/11/2009.

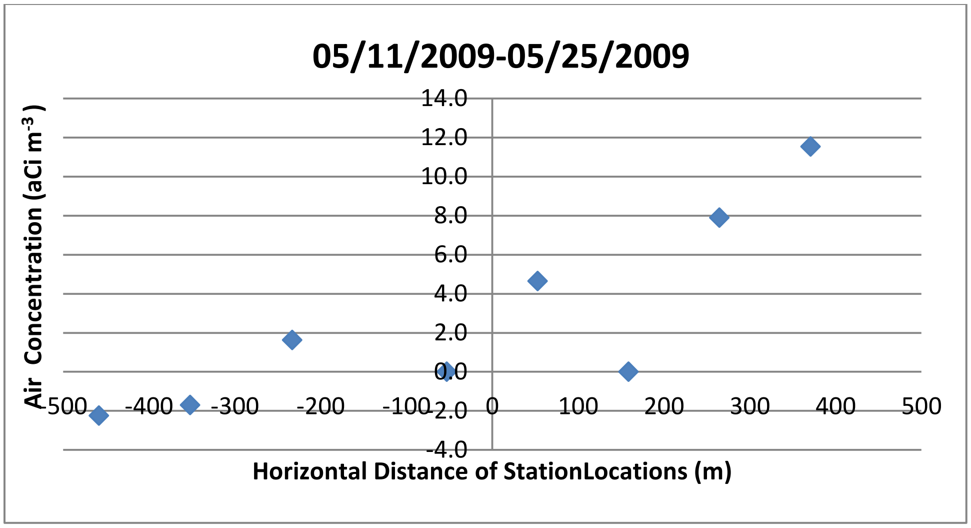

Fig. A3. ^{239}Pu concentrations per station location per period.

Fig. A4 presents the air concentration per the horizontal distance of the receptor locations for period start date 05/25/2009.

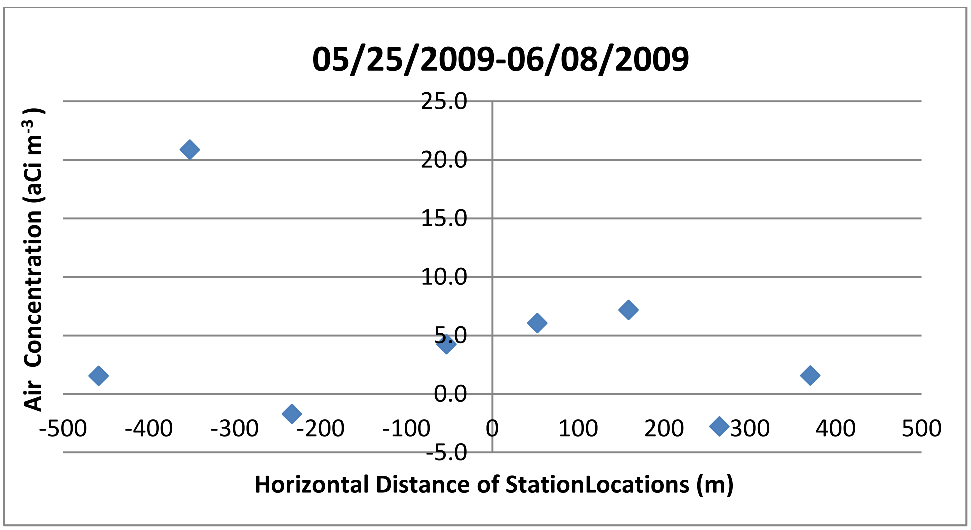

Fig. A4. ^{239}Pu concentrations per station location per period.

Fig. A5 presents the air concentration per the horizontal distance of the receptor locations for period start date 06/08/2009.

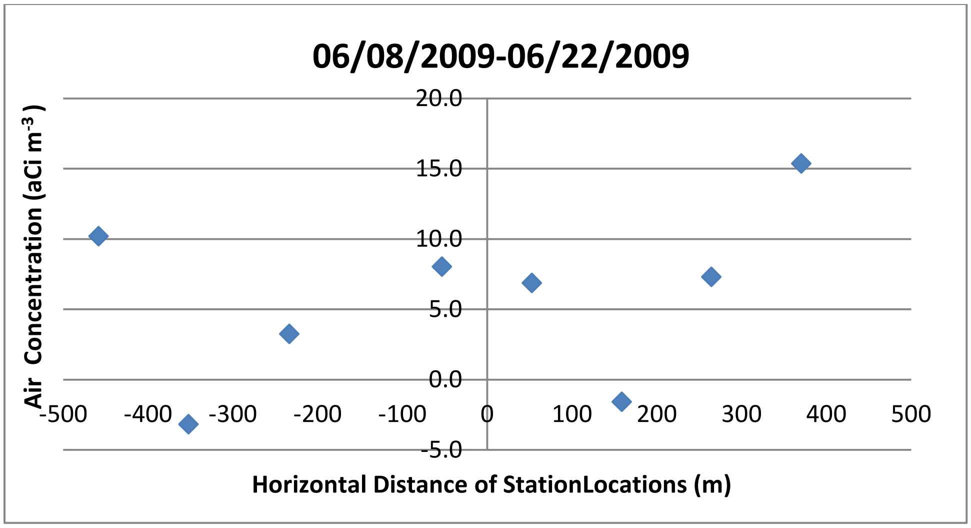

Fig. A5. ^{239}Pu concentrations per station location per period.

Fig. A6 presents the air concentration per the horizontal distance of the receptor locations for period start date 06/22/2009.

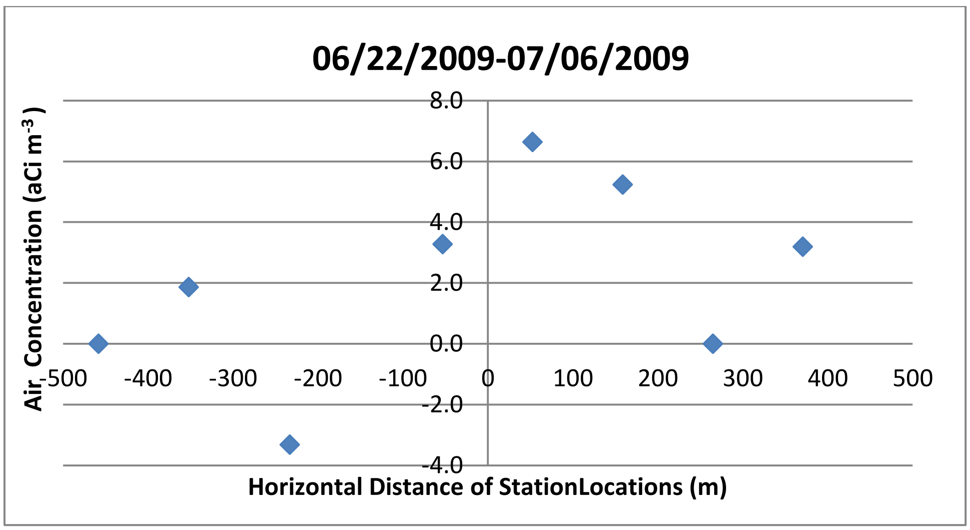

Fig. A6. ^{239}Pu concentrations per station location per period.

Fig. A7 presents the air concentration per the horizontal distance of the receptor locations for period start date 07/06/2009

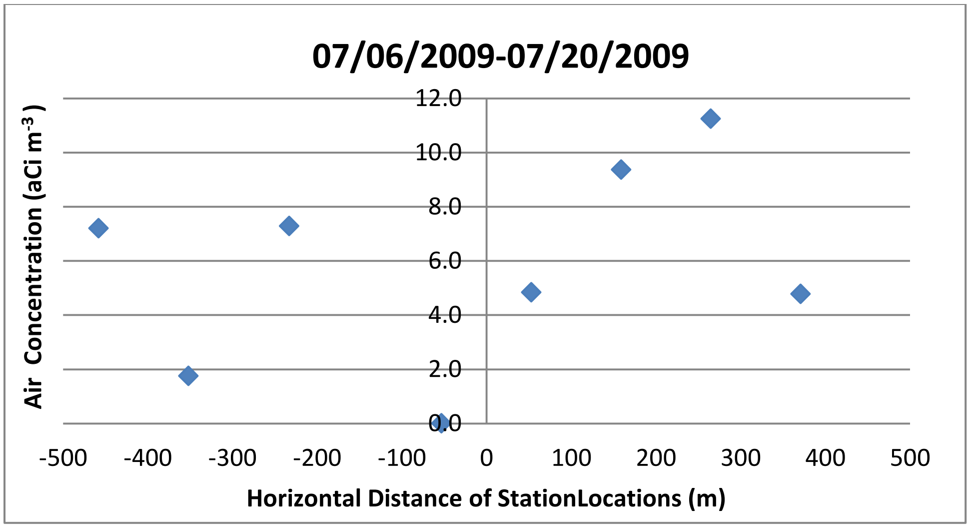

Fig. A7. ^{239}Pu concentrations per station location per period.

Fig. A8 presents the air concentration per the horizontal distance of the receptor locations for period start date 07/20/2009.

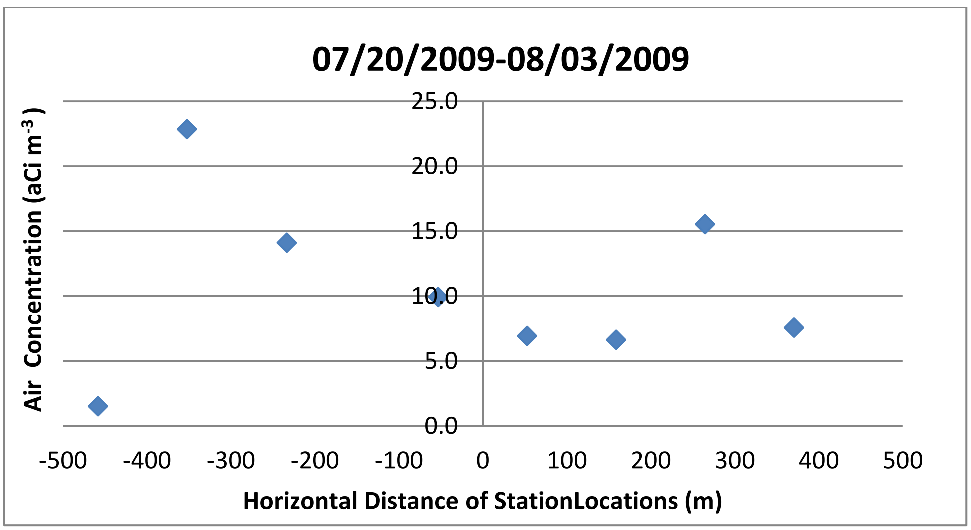

Fig. A8. ^{239}Pu concentrations per station location per period.

Fig. A9 presents the air concentration per the horizontal distance of the receptor locations for period start date 08/03/2009

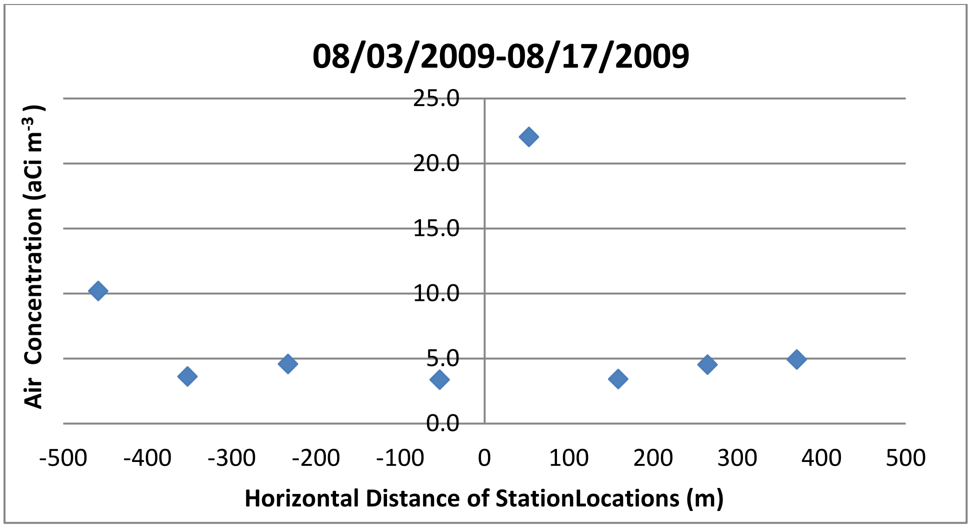

Fig. A9. ^{239}Pu concentrations per station location per period.

Fig. A10 presents the air concentration per the horizontal distance of the receptor locations for period start date 08/17/2009.

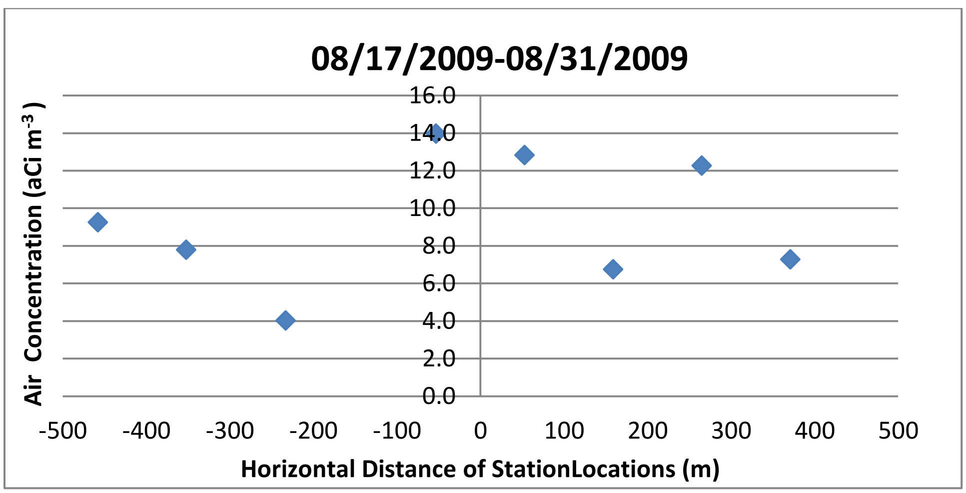

Fig. A10. ^{239}Pu concentrations per station location per period.

Fig. A11 presents the air concentration per the horizontal distance of the receptor locations for period start date 08/31/2009.

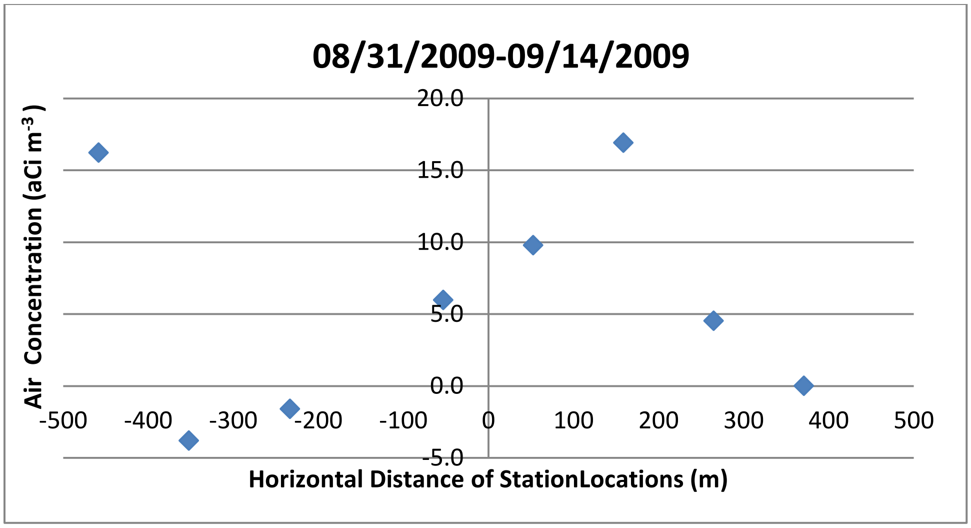

Fig. A11. ^{239}Pu concentrations per station location per period.

Fig. A12 presents the air concentration per the horizontal distance of the receptor locations for period start date 09/14/2009.

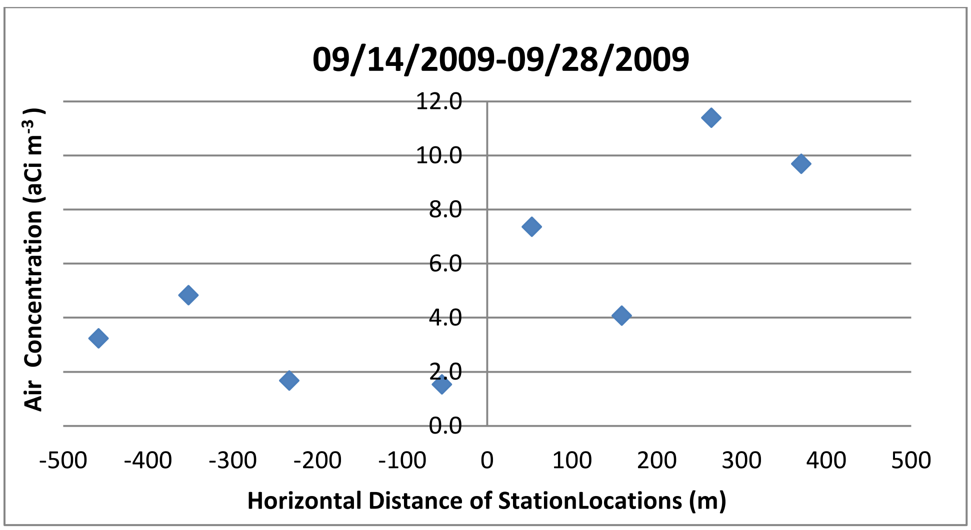

Fig. A12. ^{239}Pu concentrations per station location per period.

Fig. A13 presents the air concentration per the horizontal distance of the receptor locations for period start date 09/28/2009.

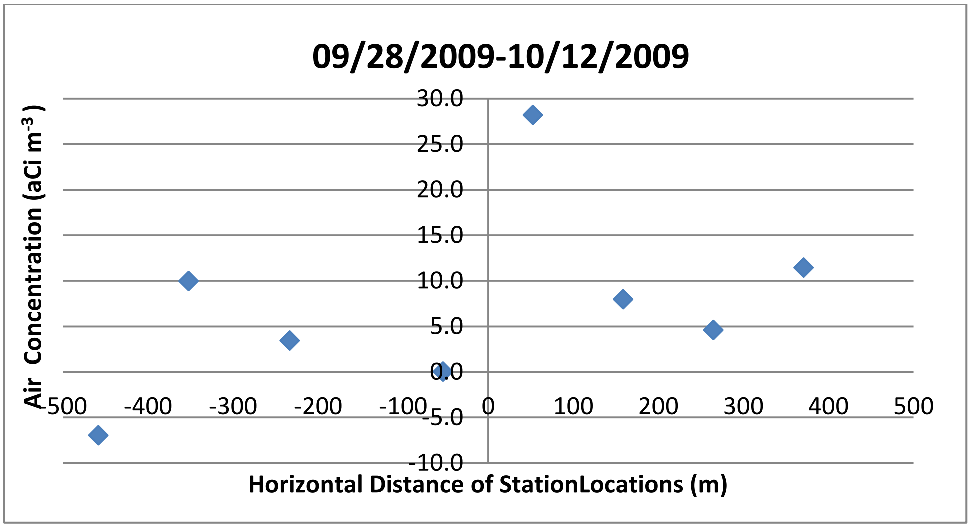

Fig. A13. ^{239}Pu concentrations per station location per period.

Fig. A14 displays the air concentration per the horizontal distance of the receptor locations for period start date 10/12/2009.

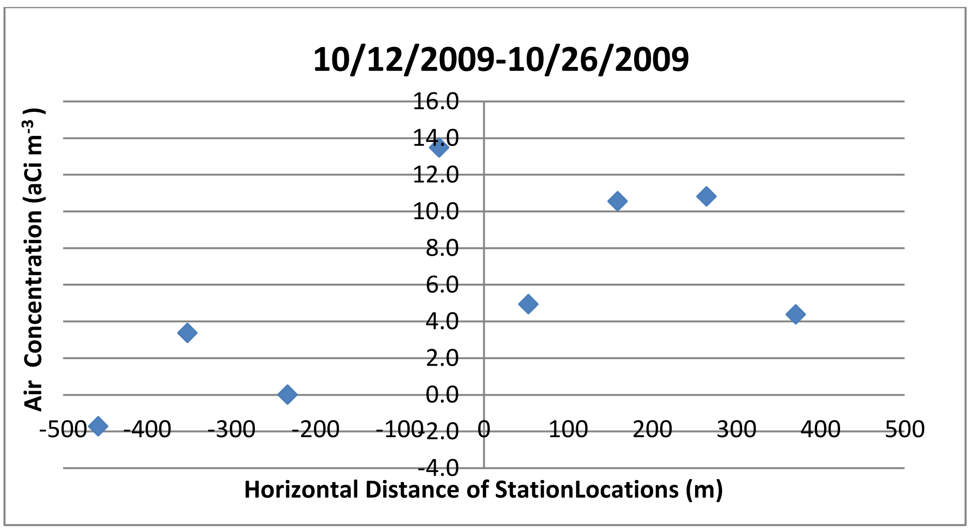

Fig. A14. ^{239}Pu concentrations per station location per period.

Fig. A15 presents the air concentration per the horizontal distance of the receptor locations for period start date 10/26/2009.

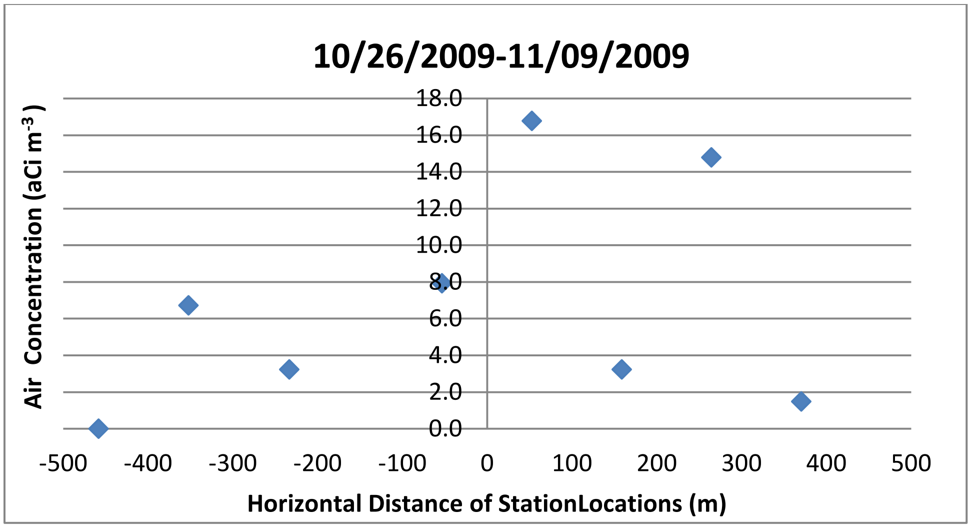

Fig. A15. [239]Pu concentrations per station location per period.

Fig. A16 presents the air concentration per the horizontal distance of the receptor locations for period start date 11/09/2009

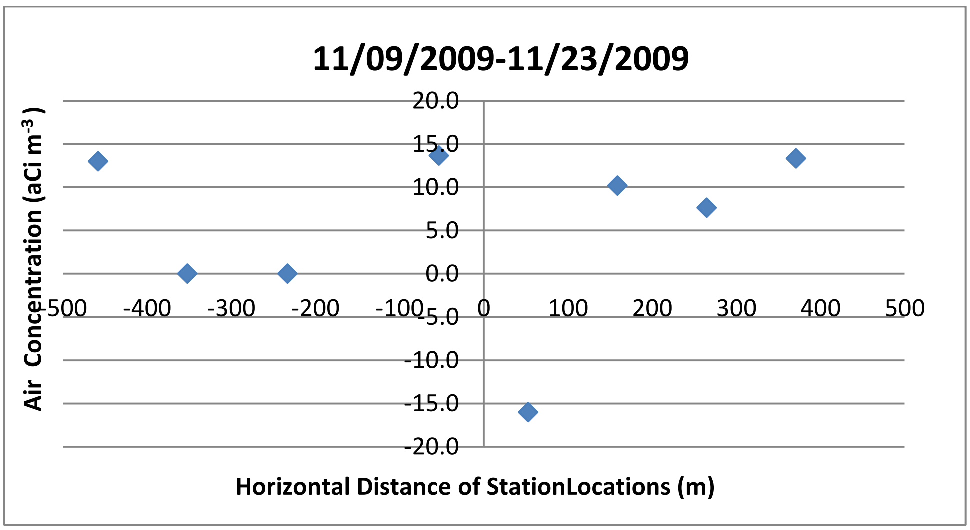

Fig. A16. [239]Pu concentrations per station location per period.

Fig. A17 presents the air concentration per the horizontal distance of the receptor locations for period start date 11/23/2009.

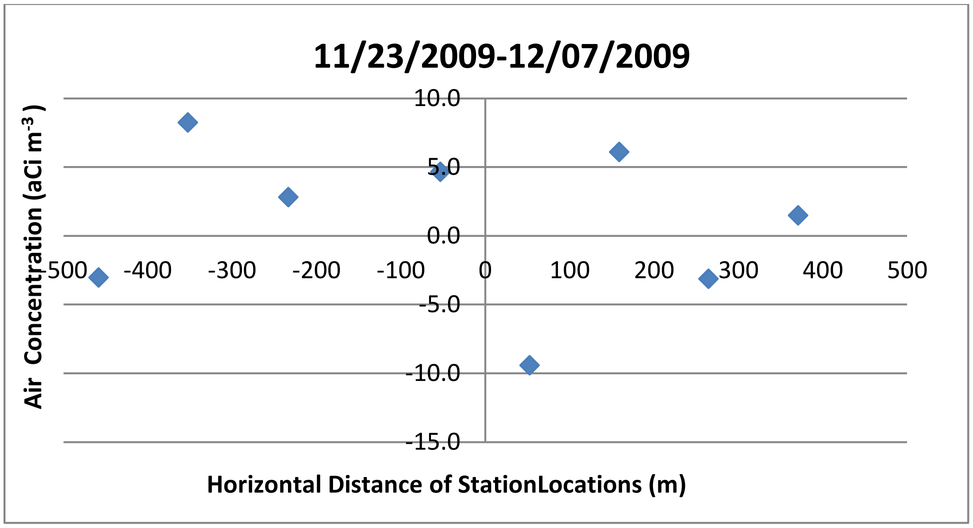

Fig. A17. ^{239}Pu concentrations per station location per period.

Fig. A18 presents the air concentration per the horizontal distance of the receptor locations for period start date 12/07/2009.

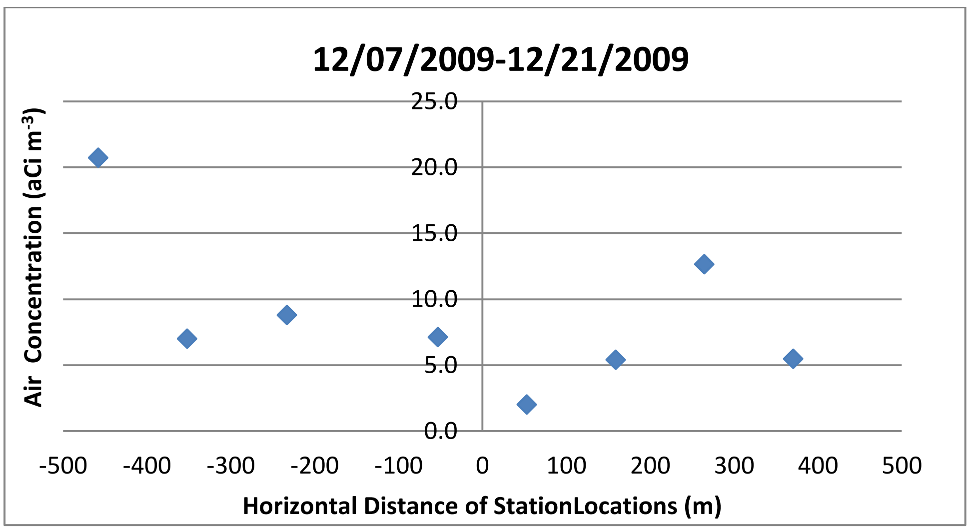

Fig. A18. ^{239}Pu concentrations per station location per period.

Fig. A19 presents the air concentration per the horizontal distance of the receptor locations for period start date 12/21/2009.

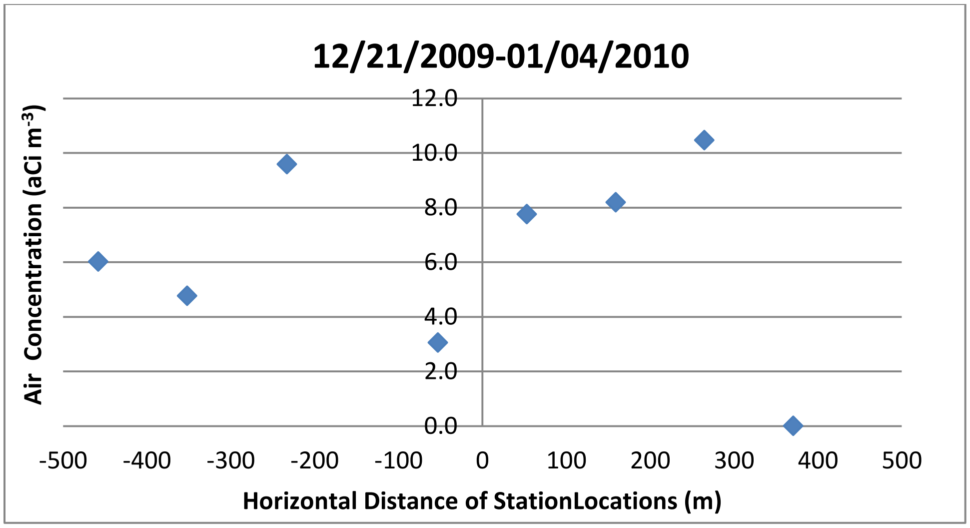

Fig. A19. ^{239}Pu concentrations per station location per period.

Fig. A20 presents the air concentration per the horizontal distance of the receptor locations for period start date 01/04/2010.

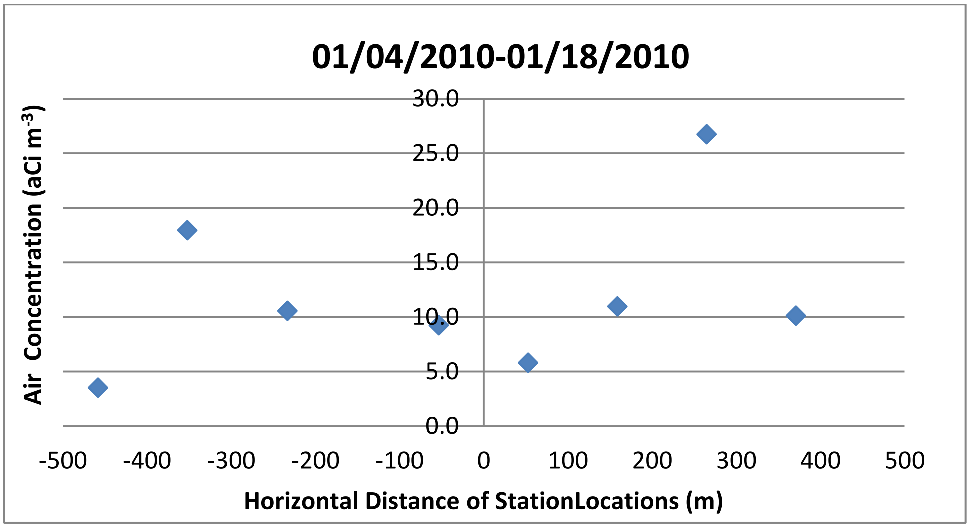

Fig. A20. ^{239}Pu concentrations per station location per period.

Fig. A21 displays the air concentration per the horizontal distance of the receptor locations for period start date 01/18/2010

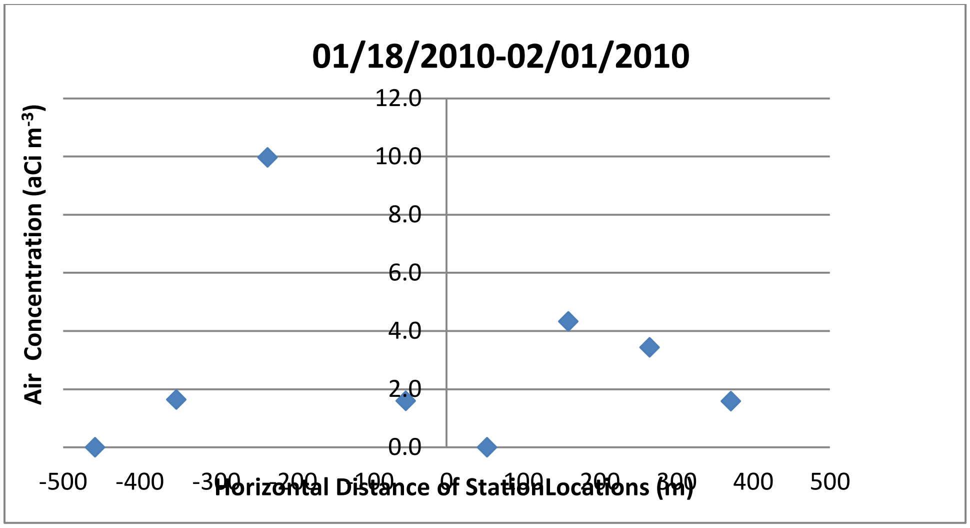

Fig. A21. ^{239}Pu concentrations per station location per period.

Fig. A22 presents the air concentration per the horizontal distance of the receptor locations for period start date 02/01/2010.

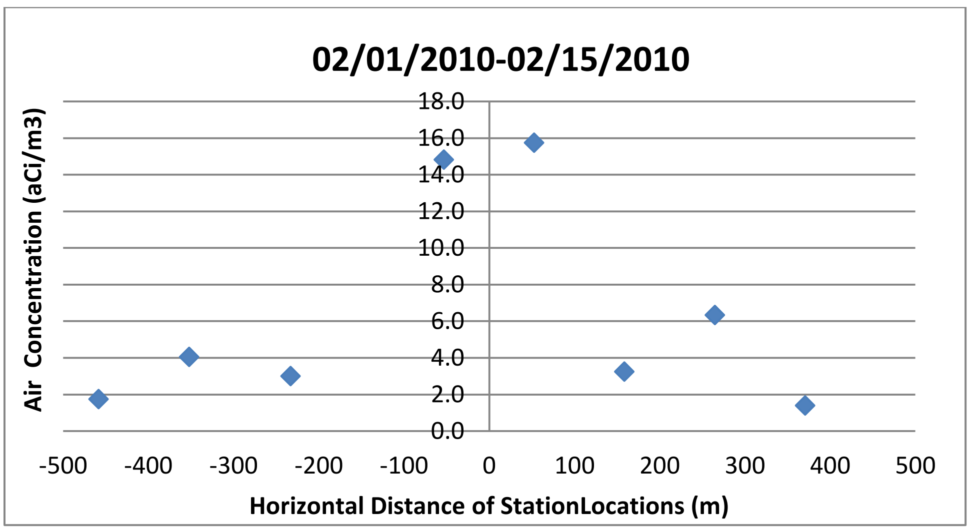

Fig. A22. ^{239}Pu concentrations per station location per period.

Fig. A23presents the air concentration per the horizontal distance of the receptor locations for period start date 02/15/2010.

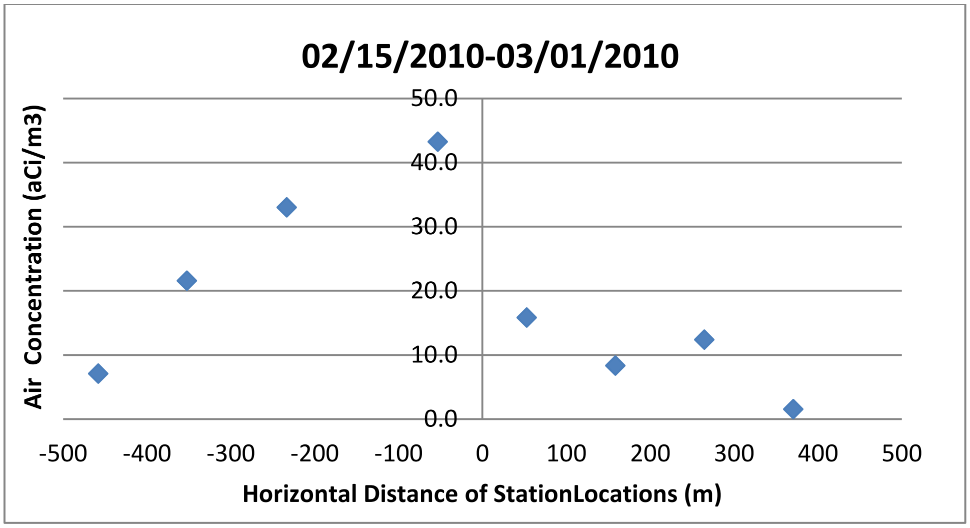

Fig. A23. ^{239}Pu concentrations per station location per period.

Fig. A24 presents the air concentration per the horizontal distance of the receptor locations for period start date 03/01/2010.

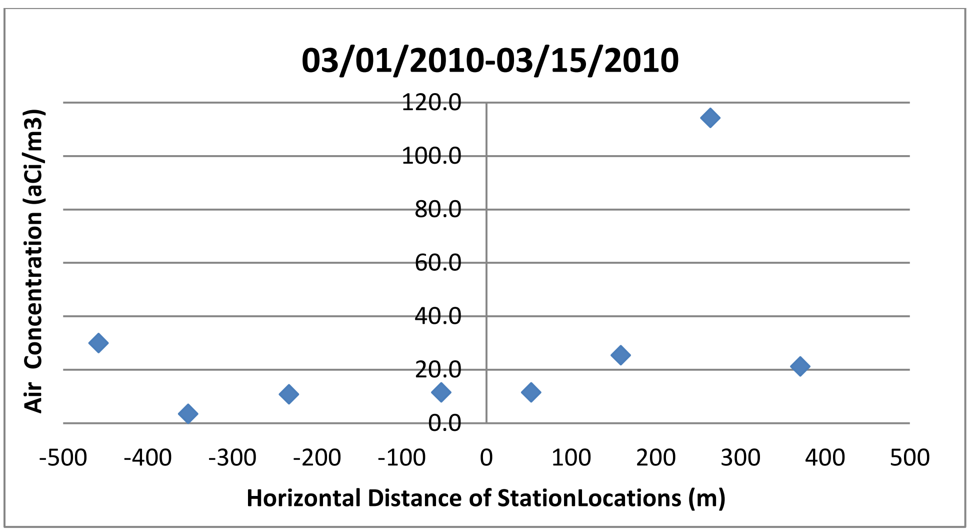

Fig. A24. ^{239}Pu concentrations per station location per period.

Fig. A25 presents the air concentration per the horizontal distance of the receptor locations for period start date 03/15/2010. The concentration peak associated with Fig. A25 was one of the 13 greatest peaks measured.

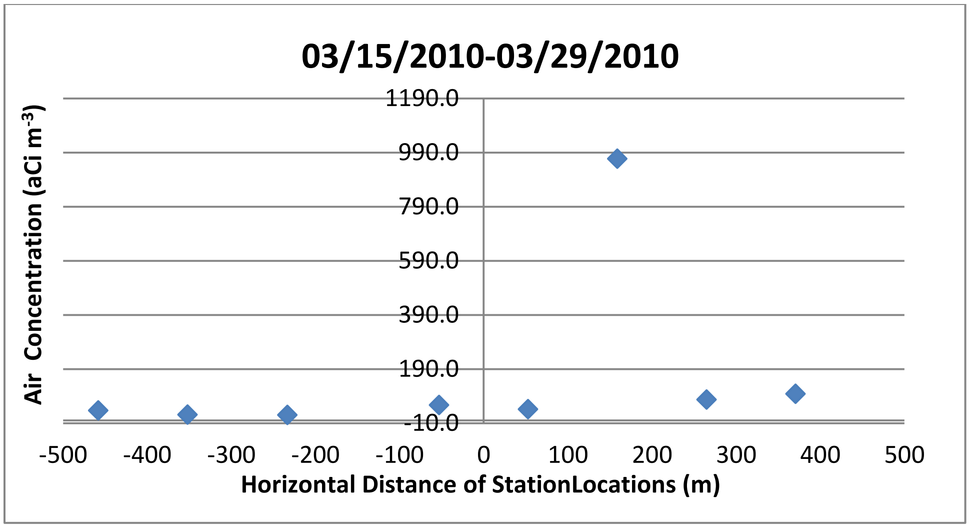

Fig. A25. ^{239}Pu concentrations per station location per period.

Fig. A26 presents the air concentration per the horizontal distance of the receptor locations for period start date 03/29/2010.

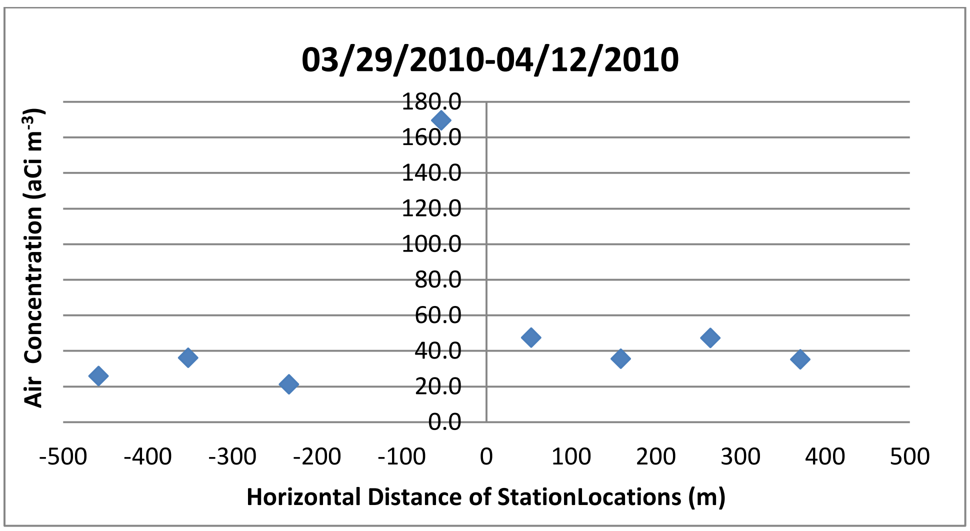

Fig. A26. ^{239}Pu concentrations per station location per period.

Fig. A27 presents the air concentration per the horizontal distance of the receptor locations for period start date 04/12/2009.

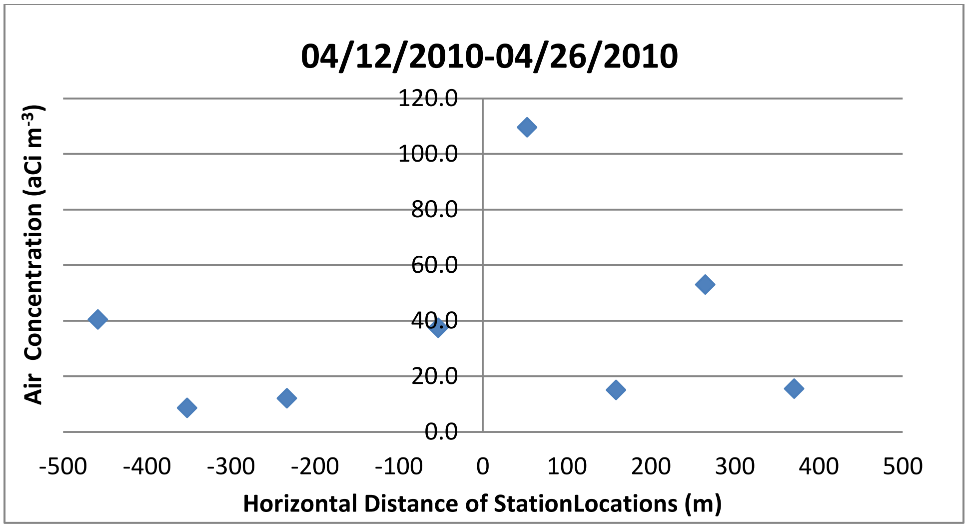

Fig. A27. ^{239}Pu concentrations per station location per period.

Fig. A28 presents the air concentration per the horizontal distance of the receptor locations for period start date 04/26/2010.

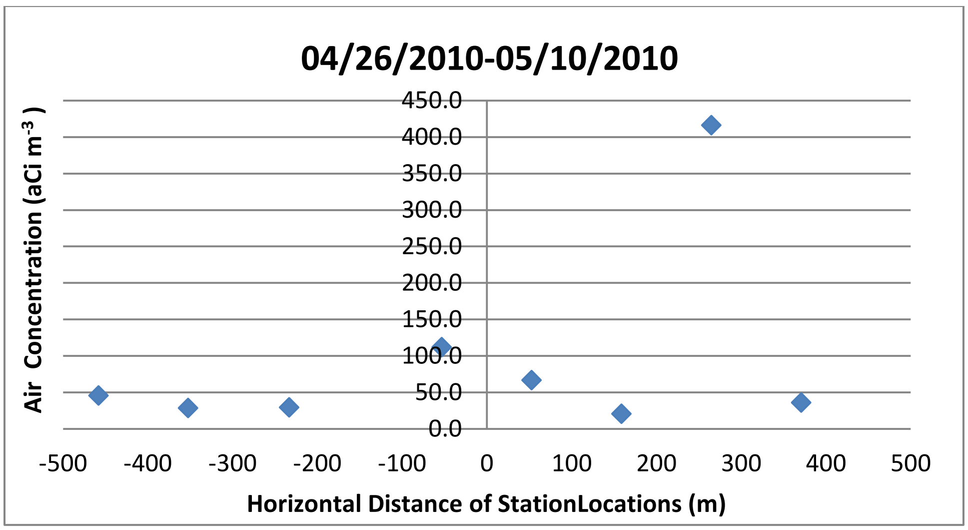

Fig. A28. ^{239}Pu concentrations per station location per period.

Fig. A29 presents the air concentration per the horizontal distance of the receptor locations for period start date 05/10/2010

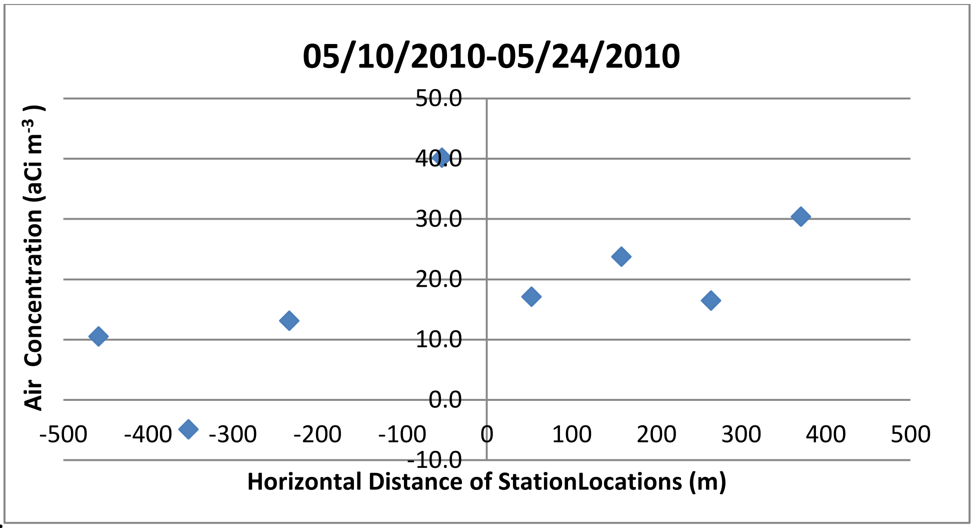

Fig. A29. ^{239}Pu concentrations per station location per period.

Fig. A30 presents the air concentration per the horizontal distance of the receptor locations for period start date 05/24/2010

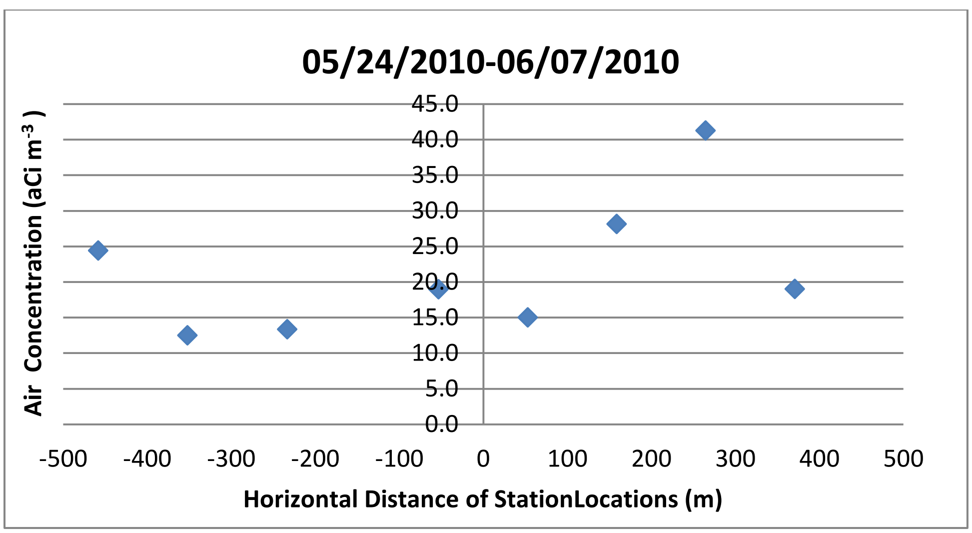

Fig. A30. ^{239}Pu concentrations per station location per period.

Fig. A31 presents the air concentration per the horizontal distance of the receptor locations for period start date 06/07/2010.

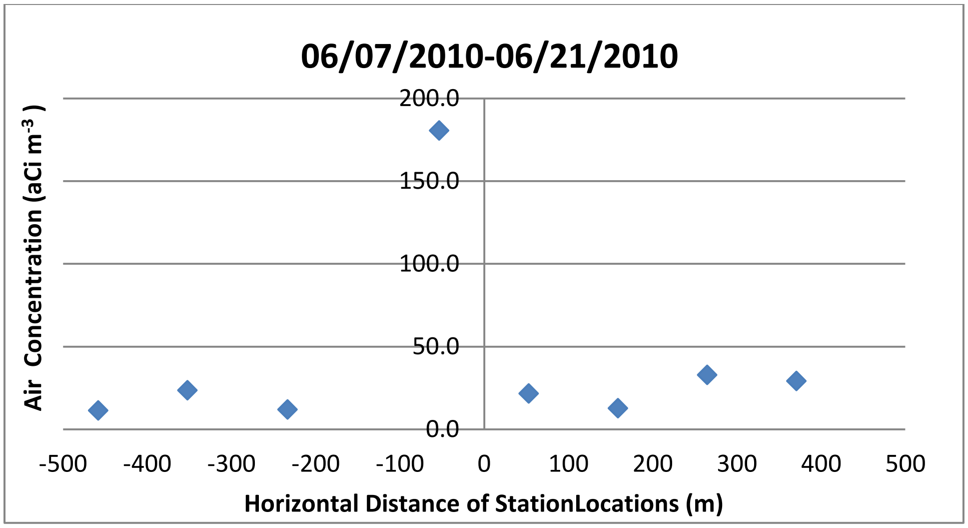

Fig. A31. ^{239}Pu concentrations per station location per period.

Fig. A32 presents the air concentration per the horizontal distance of the receptor locations for period start date 06/21/2010.

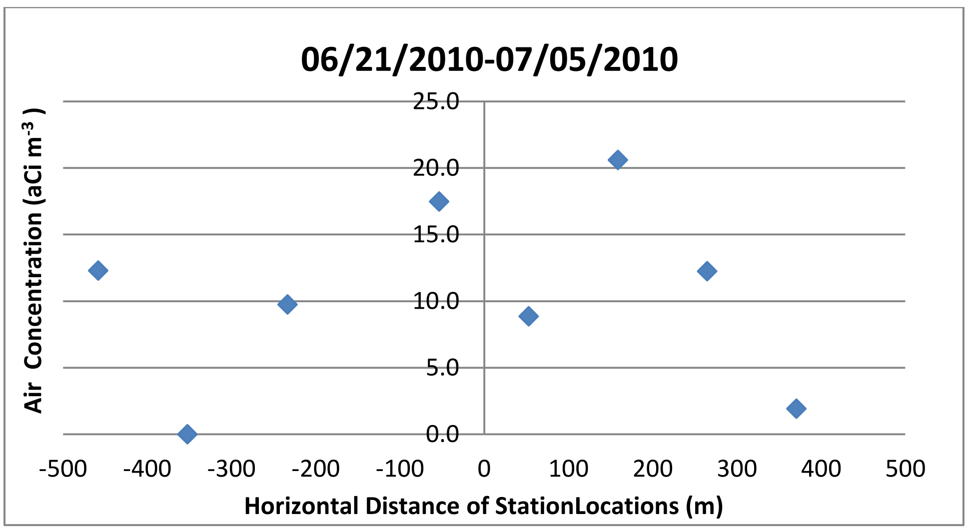

Fig. A32. ^{239}Pu concentrations per station location per period.

Fig. A33 presents the air concentration per the horizontal distance of the receptor locations for period start date 07/05/2010.

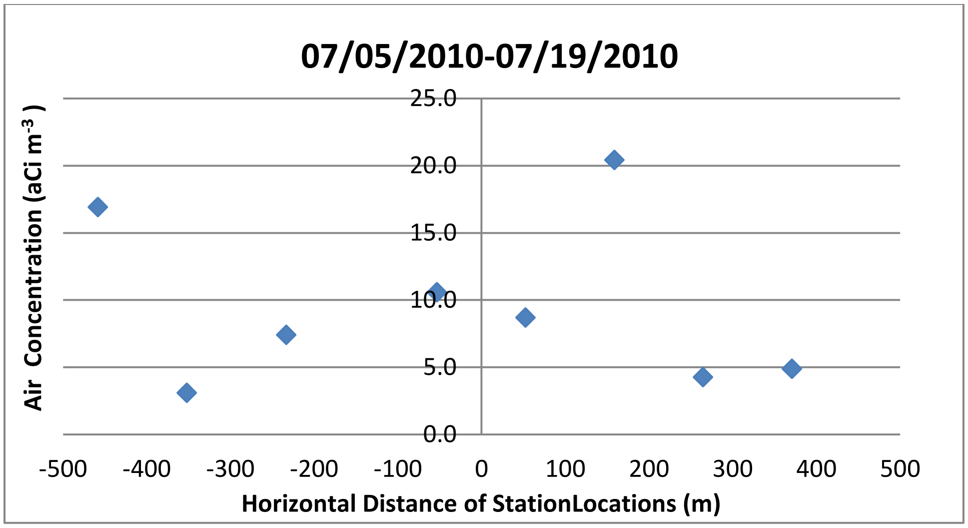

Fig. A33. ^{239}Pu concentrations per station location per period.

Fig. A34 presents the air concentration per the horizontal distance of the receptor locations for period start date 07/19/2010.

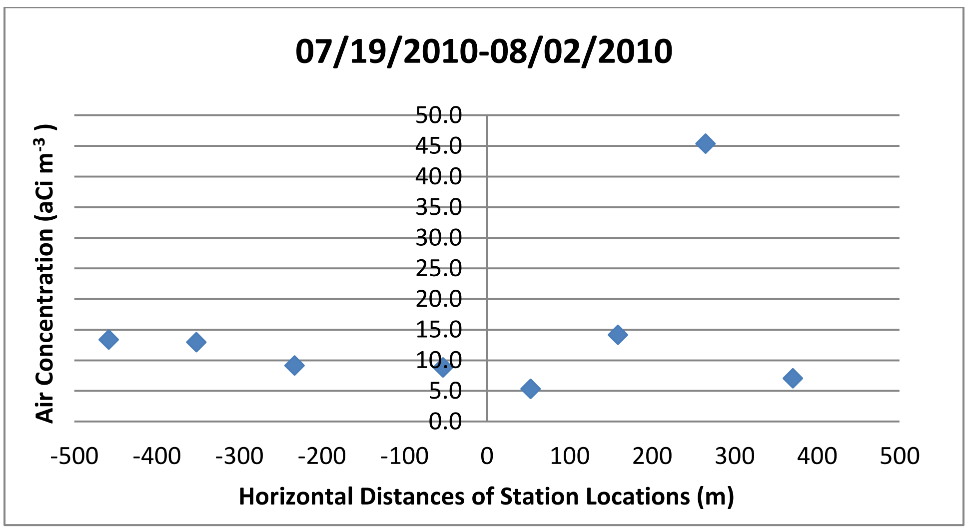

Fig. A34. ^{239}Pu concentration per station location per during period.

Fig. A35 presents the air concentration per the horizontal distance of the receptor locations for period start date 08/02/2010.

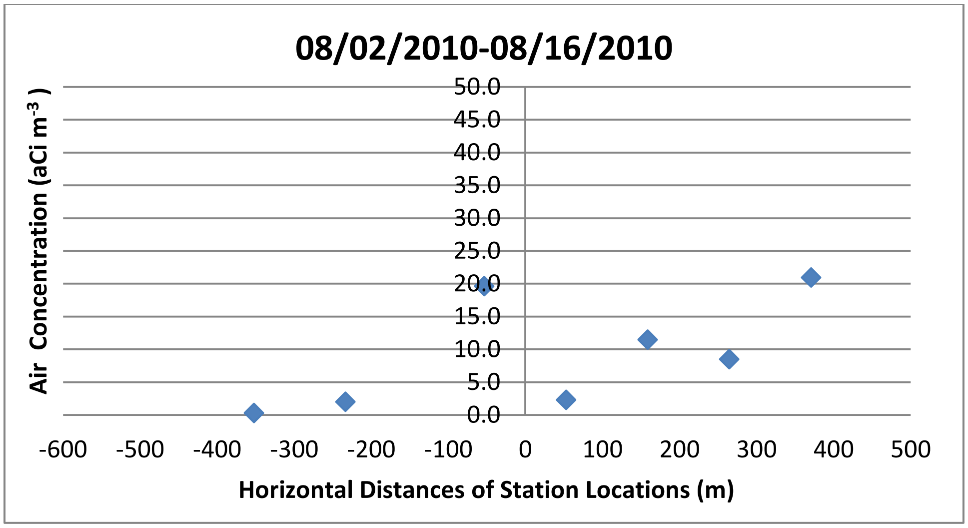

Fig. A35. ^{239}Pu concentration per station location period.

Fig. A36 presents the air concentration per the horizontal distance of the receptor locations for period start date 08/16/2010. The concentration peak associated with Fig. A36 was one of the 13 greatest peaks measured.

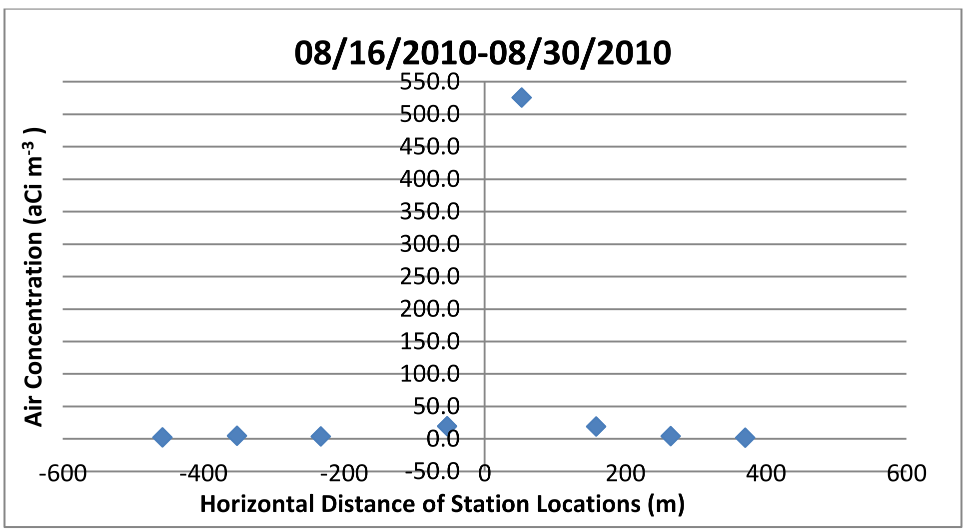

Fig. A36. ^{239}Pu concentrations per station location per period.

Fig. A37 presents the air concentration per the horizontal distance of the receptor locations for period start date 08/30/2010.

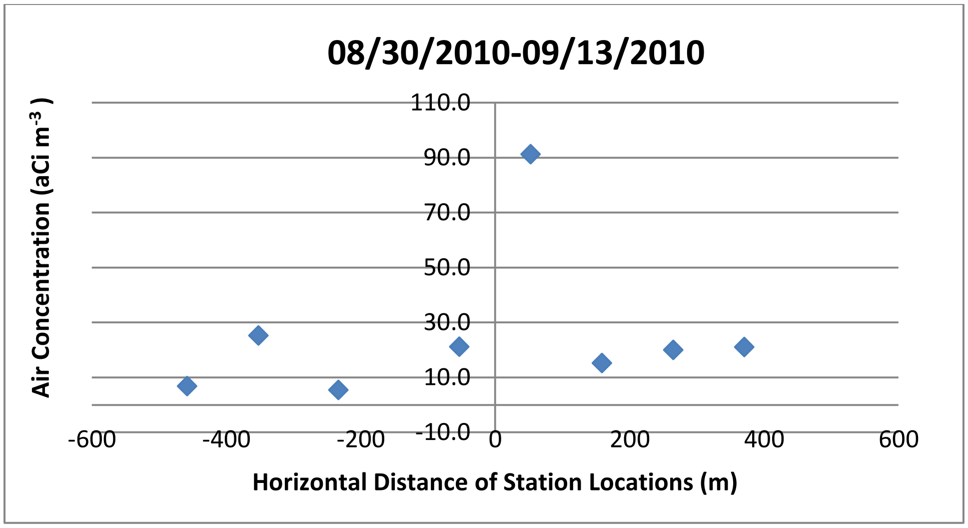

Fig. A37. ^{239}Pu concentrations per station location per period.

Fig. A38 presents the air concentration per the horizontal distance of the receptor locations for period start date 09/13/2010.

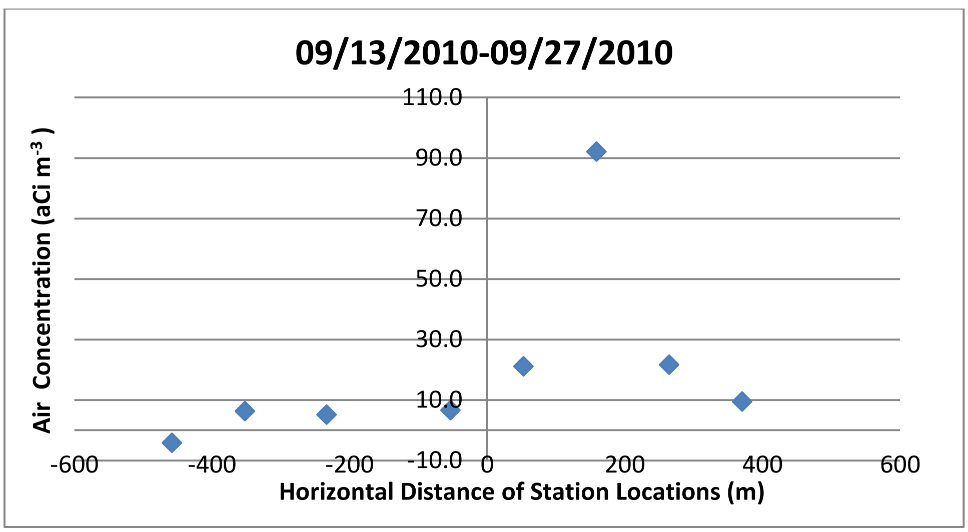

Fig. A38. ^{239}Pu concentrations per station location per period.

Fig. A39 presents the air concentration per the horizontal distance of the receptor locations for period start date 09/27/2010.

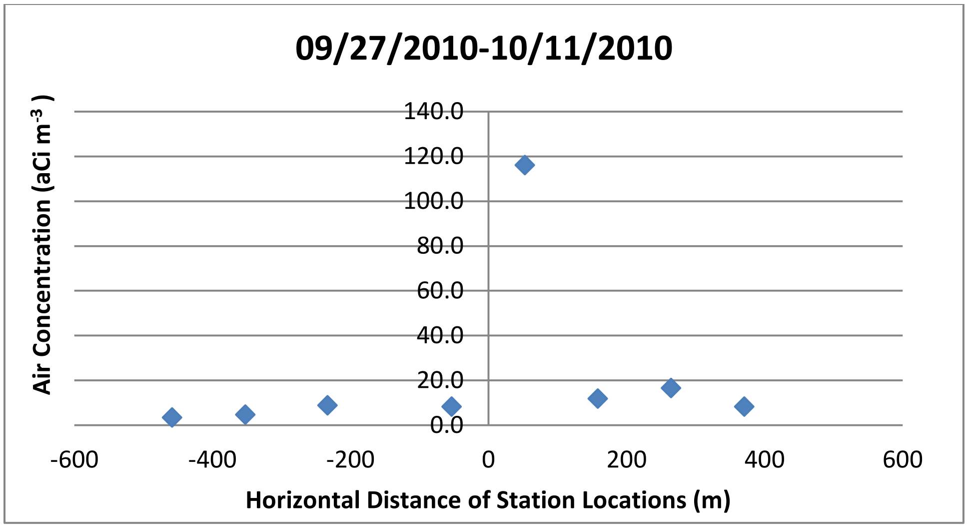

Fig. A39. ^{239}Pu concentration per station location per period.

Fig. A40 presents the air concentration per the horizontal distance of the receptor locations for period start date 10/11/2010.

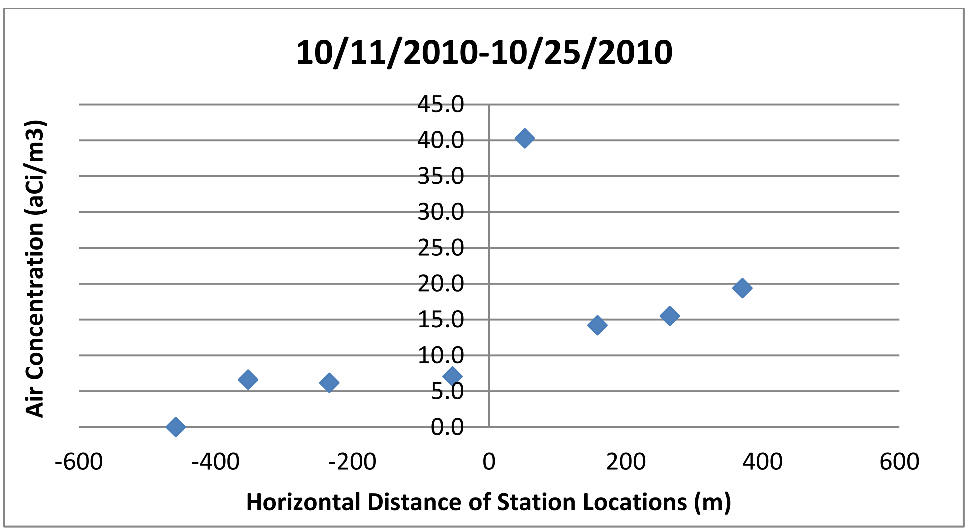

Fig. A40. ^{239}Pu concentration per station location per period.

Fig. A41 presents the air concentration per the horizontal distance of the receptor locations for period start date 10/25/2010.

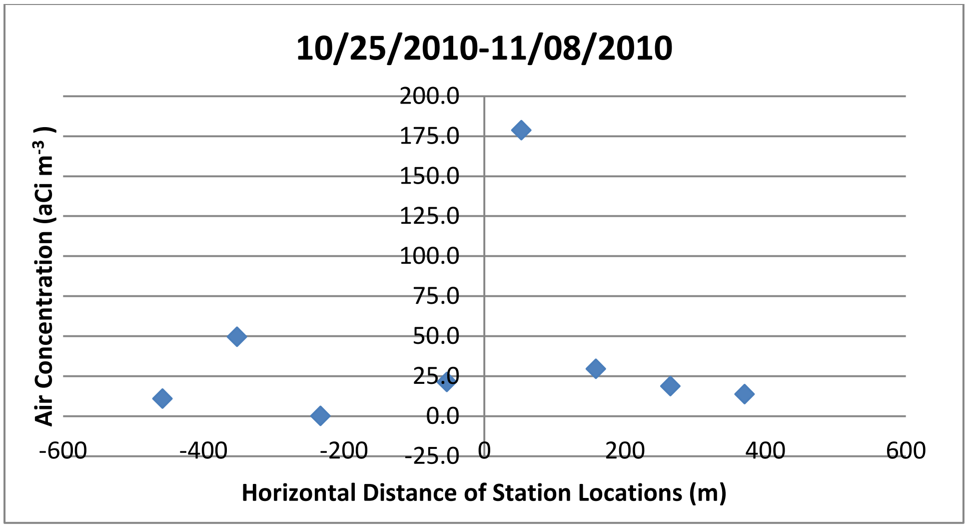

Fig. A41. ^{239}Pu concentration per station location per period.

Fig. A42 presents the air concentration per the horizontal distance of the receptor locations for period start date 11/08/2010. The peak shown in Fig. A42 was one of the 13 greatest peaks measured.

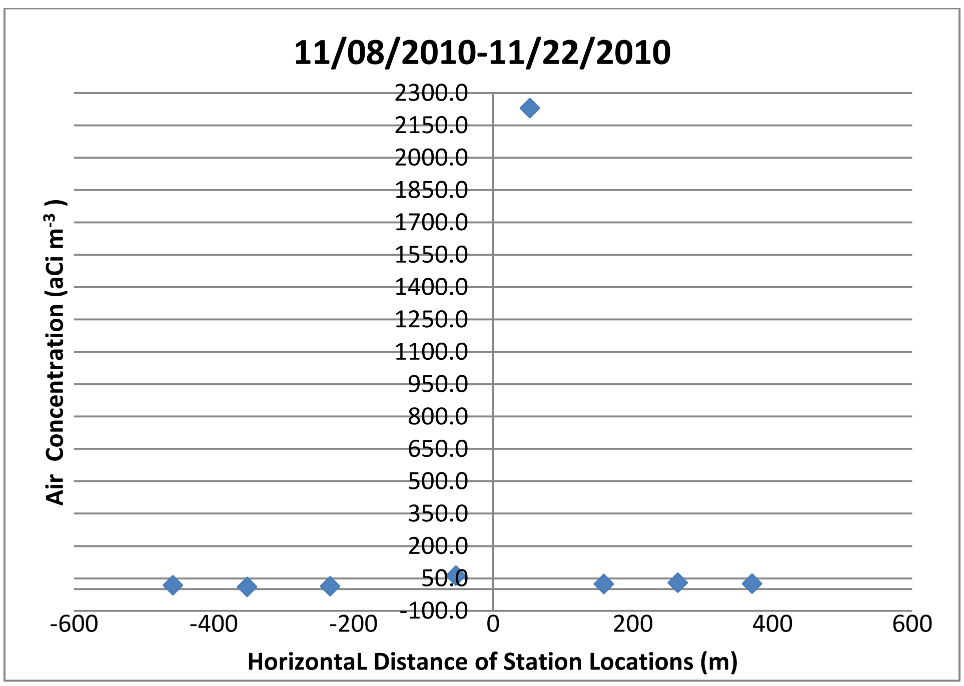

Fig. A42. ^{239}Pu concentration per station per period.

Fig. A43 presents the air concentration per the horizontal distance of the receptor locations for period start date 11/22/2010. The peak shown within Fig. A43 was one of the 13 greatest peaks measured.

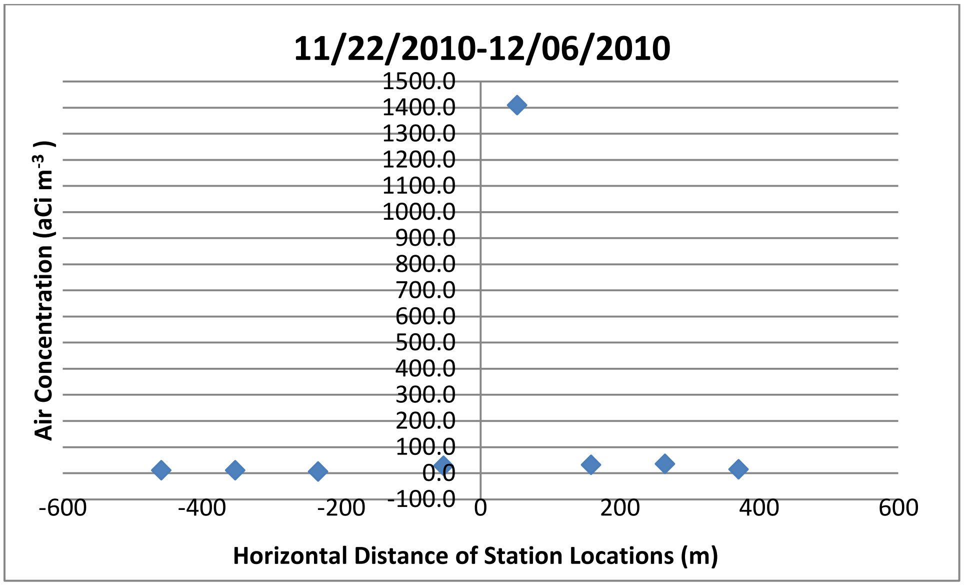

Fig. A43. ^{239}Pu concentration per station per period.

Fig. A44 presents the air concentration per the horizontal distance of the receptor locations for period start date 12/06/2010.

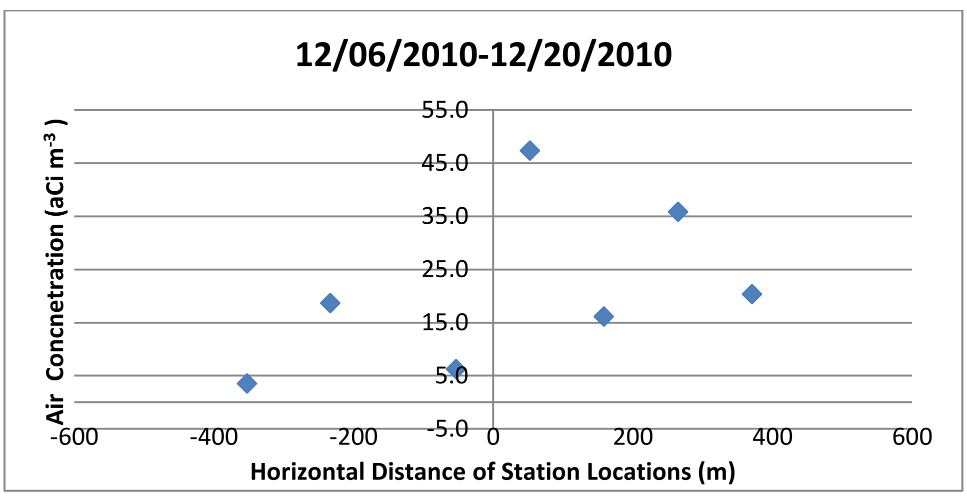

Fig. A44. ^{239}Pu concentration per station location per period.

Fig. A45 presents the air concentration per the horizontal distance of the receptor locations for period start date 12/20/2010.

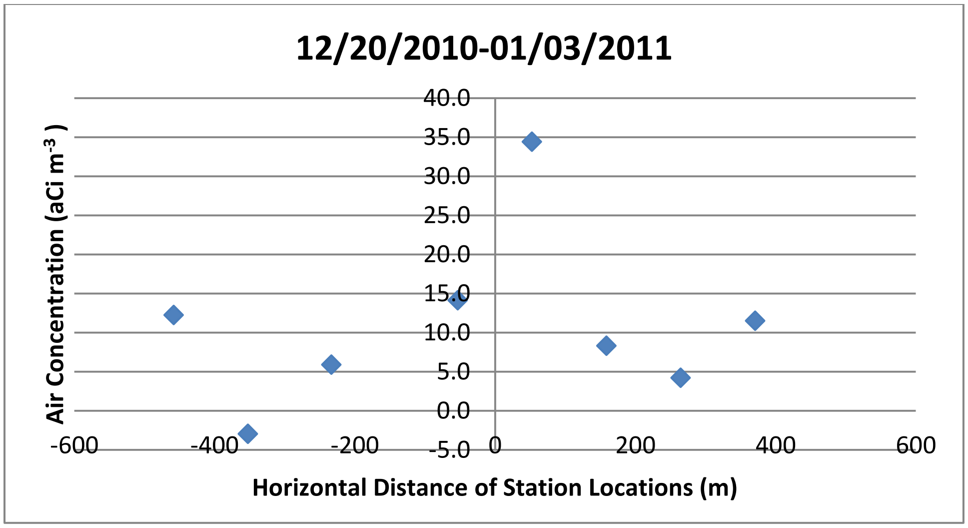

Fig. A45. 239Pu concentration per station location per period.

Fig. A46 presents the air concentration per the horizontal distance of the receptor locations for period start date 01/03/2011.

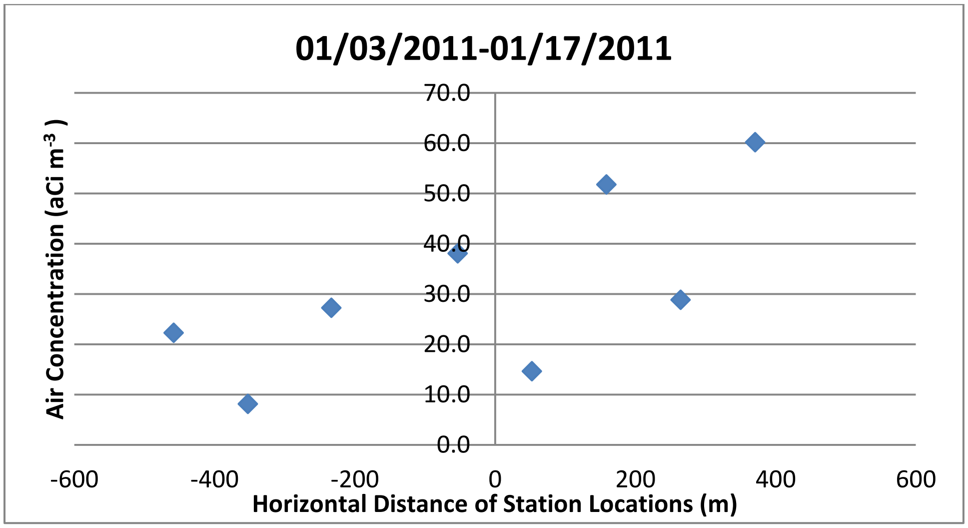

Fig. A46. 239Pu concentration per station location per period.

Fig. A47 presents the air concentration per the horizontal distance of the receptor locations for period start date 01/17/2011.

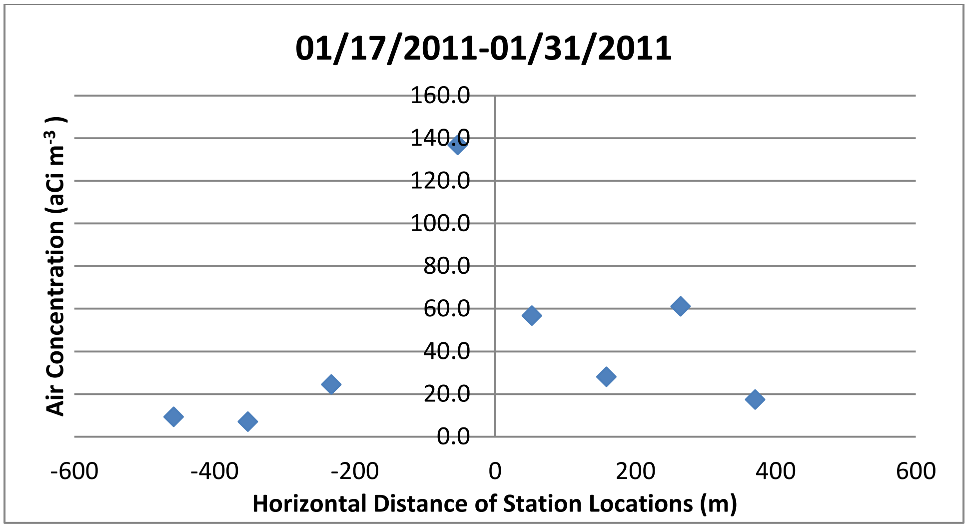

Fig. A47. ^{239}Pu concentration per station location per period.

Fig. A48 presents the air concentration per the horizontal distance of the receptor locations for period start date 01/31/2011,

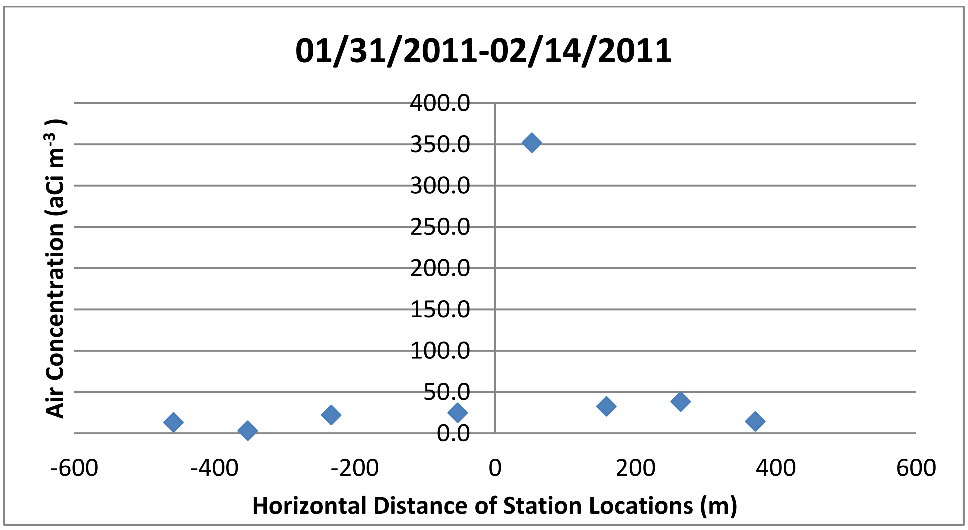

Fig. A48. ^{239}Pu concentration per station location per period.

Fig. A49 presents the air concentration per the horizontal distance of the receptor locations for period start date 02/14/2011. The peak shown within Fig. A49 was one of the 13 greatest peaks measured.

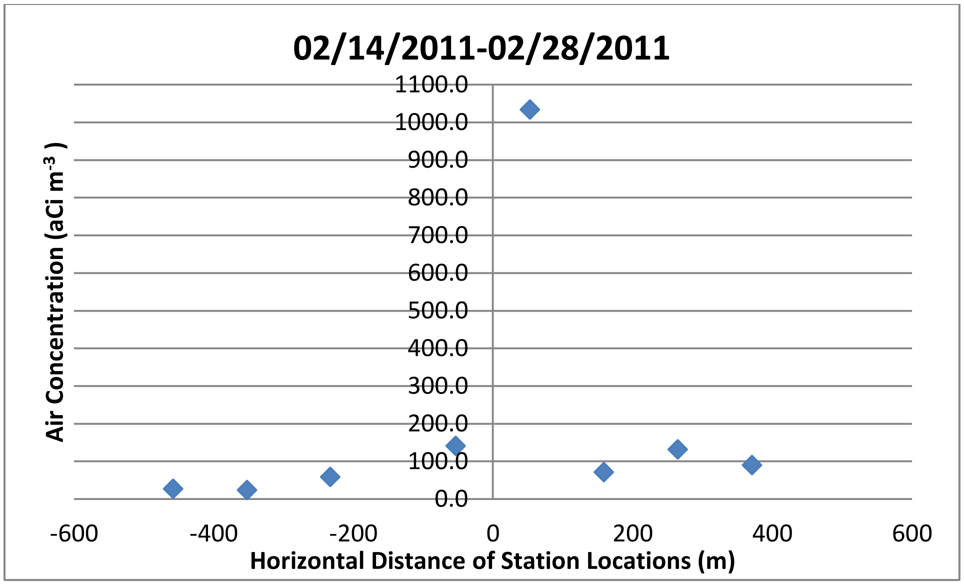

Fig. A49. ^{239}Pu concentration per station location per period.

Fig. A50 presents the air concentration per the horizontal distance of the receptor locations for period start date 02/28/2011.

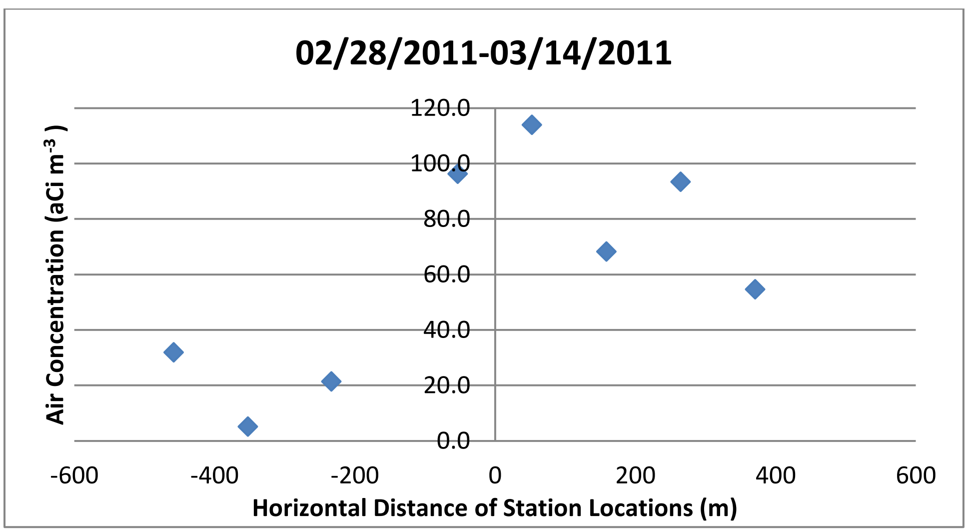

Fig. A50. ^{239}Pu concentration per station location per period.

Fig. A51 presents the air concentration per the horizontal distance of the receptor locations for period start date 03/14/2011.

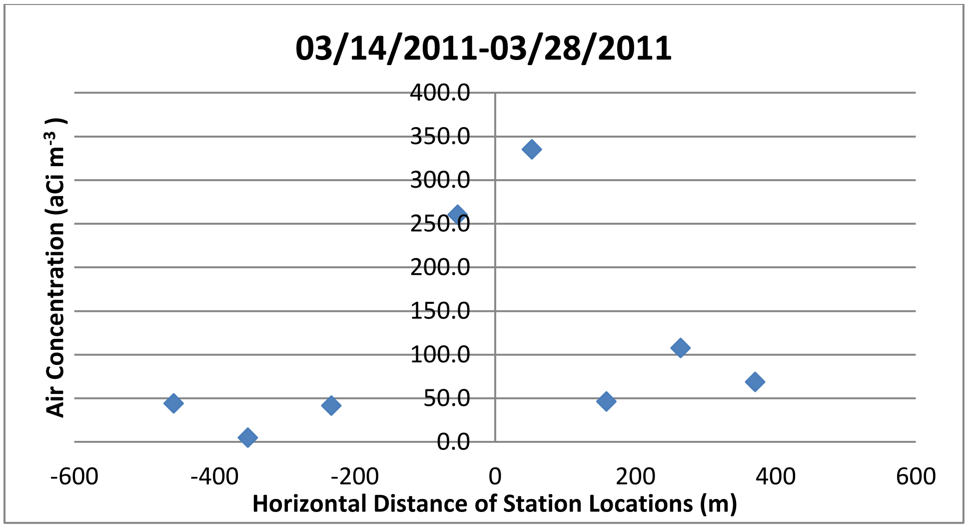

Fig. A51. ^{239}Pu concentration per station location per period.

Fig. A52 presents the air concentration per the horizontal distance of the receptor locations for period start date 03/25/2011.

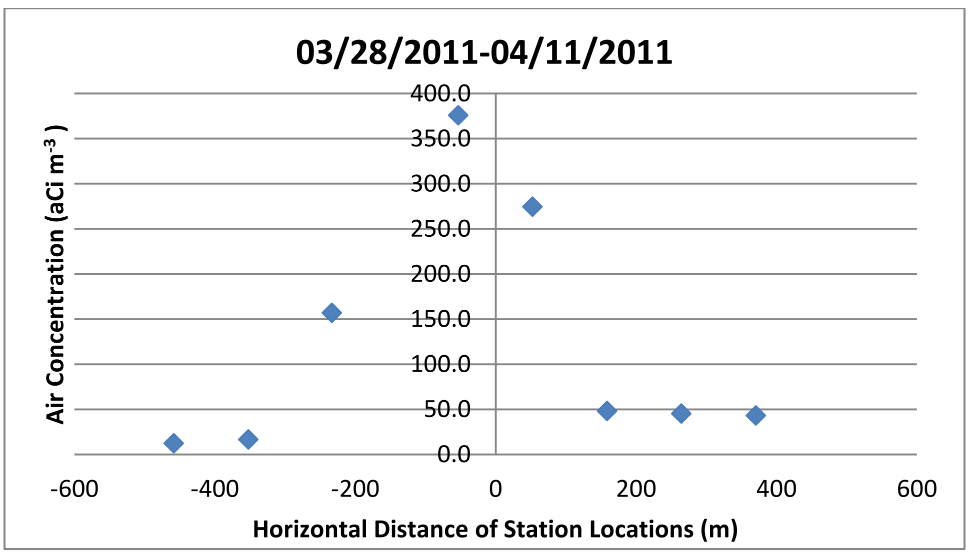

Fig. A52. ^{239}Pu concentration per station location per period.

Fig. A53 presents the air concentration per the horizontal distance of the receptor locations for period start date 04/11/2011. The peak shown within Fig. A53 was one of the 13 greatest peaks measured.

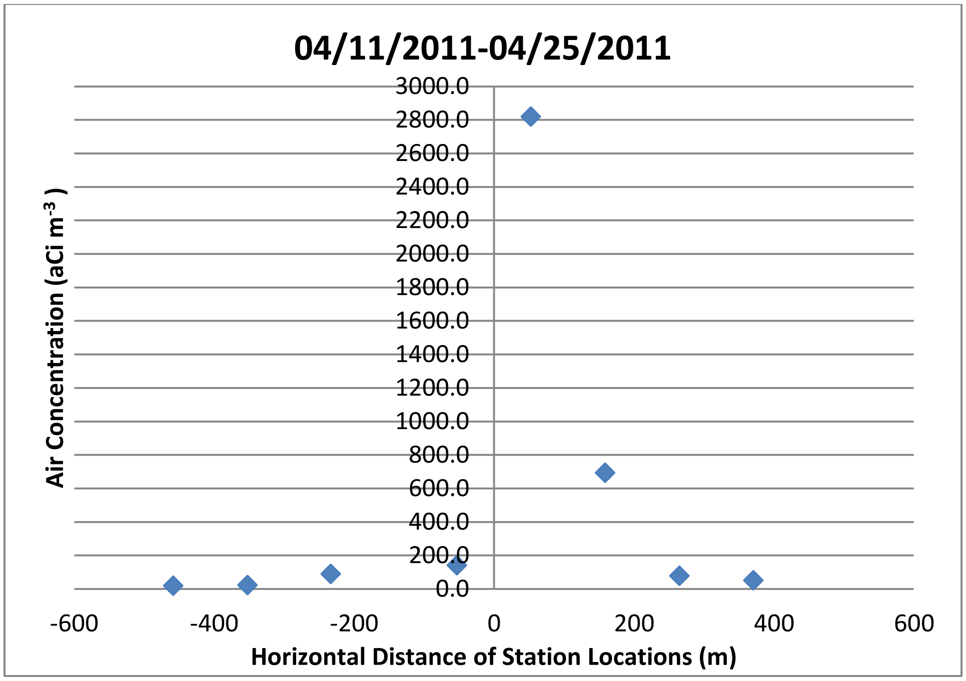

Fig. A53. ^{239}Pu concentration per station location per period.

Fig. A54 presents the air concentration per the horizontal distance of the receptor locations for period start date 04/25/2011. The peak shown in Fig. A54 was one of the 13 greatest peaks measured.

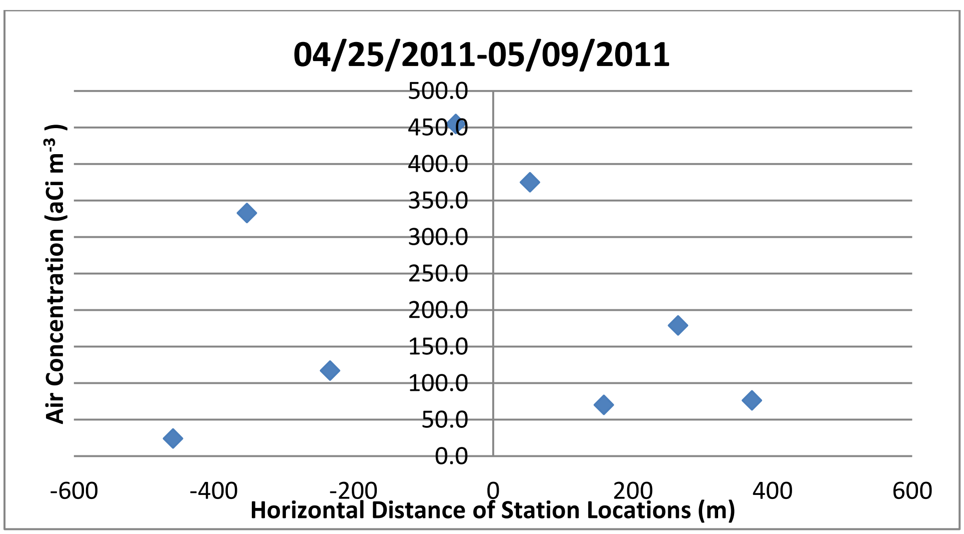

Fig. A54. ^{239}Pu concentration per station location per period.

Fig. A55 presents the air concentration per the horizontal distance of the receptor locations for period start date 05/09/2011. The peak shown in Fig. A55 was one of the 13 greatest peaks measured.

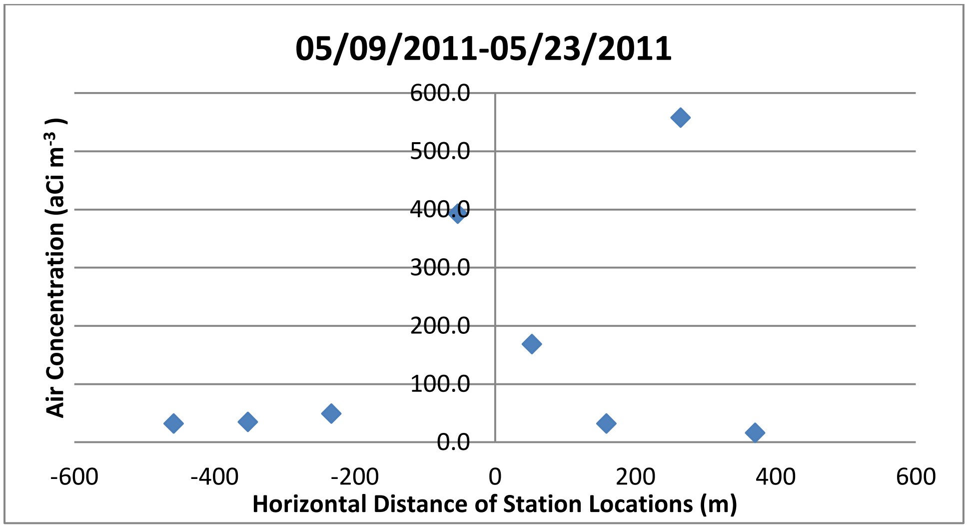

Fig. A55. ^{239}Pu concentration per station location per period.

Fig. A56 presents the air concentration per the horizontal distance of the receptor locations for period start date 05/23/2011. The peak shown within Fig. A56 was one of the 13 greatest peaks measured.

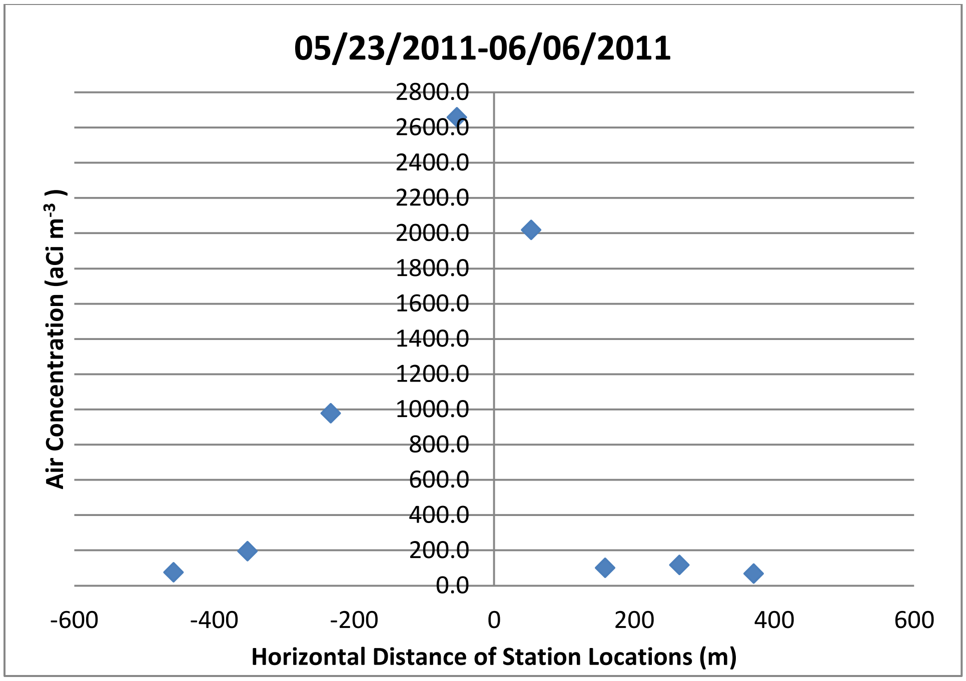

Fig. A56. ^{239}Pu concentration per station location per period.

Fig. A57 presents the air concentration per the horizontal distance of the receptor locations for period start date 06/06/2011. The peak shown within Fig. A57 was one of the 13 greatest peaks measured.

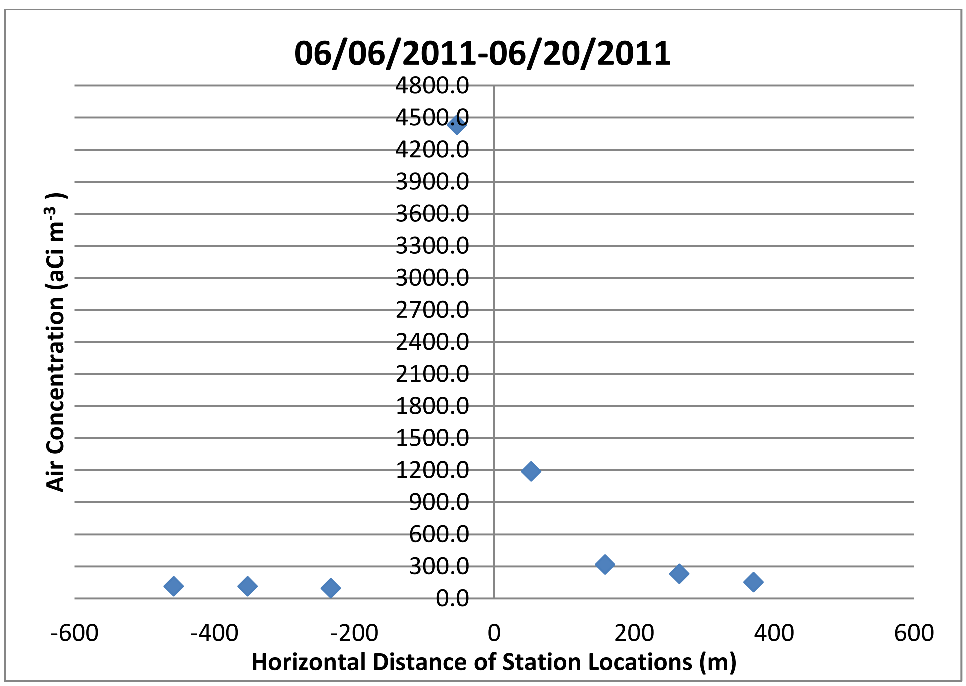

Fig. A57. ^{239}Pu concentration per station location per period.

Fig. A58 presents the air concentration per the horizontal distance of the receptor locations for period start date 06/20/2011. The peak shown within Fig. A58 was one of the 13 greatest peaks measured.

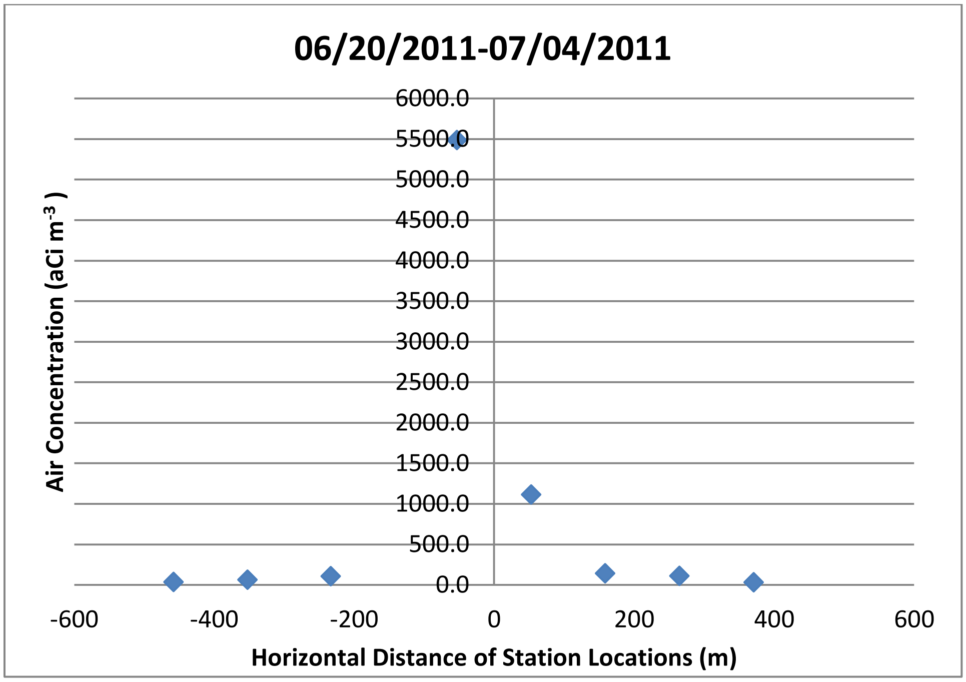

Fig. A58. ^{239}Pu concentration per station location per period.

Fig. A59 presents the air concentration per the horizontal distance of the receptor locations for period start date 07/04/2011.

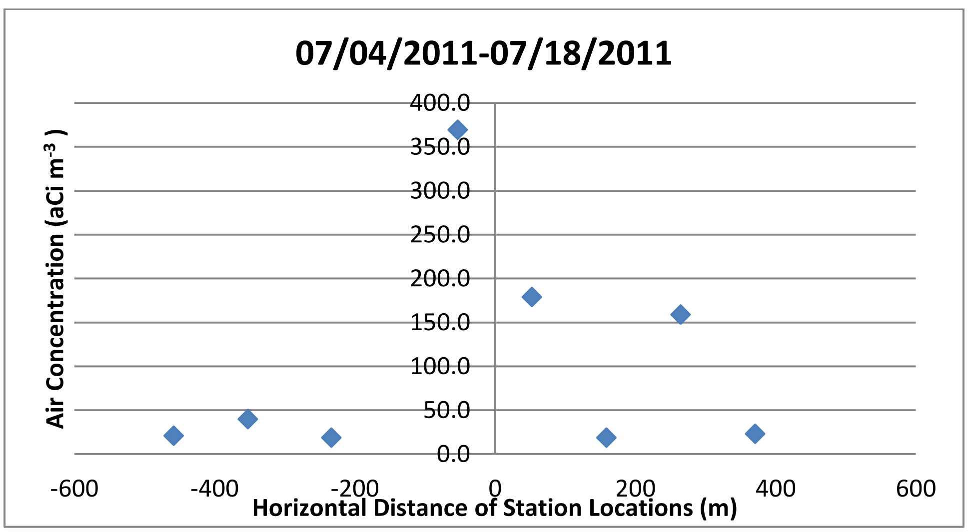

Fig. A59. ^{239}Pu concentration per station location per period.

Fig. A60 presents the air concentration per the horizontal distance of the receptor locations for period start date 07/18/2011. The peak shown within Fig. A60 was one of the 13 greatest peaks measured.

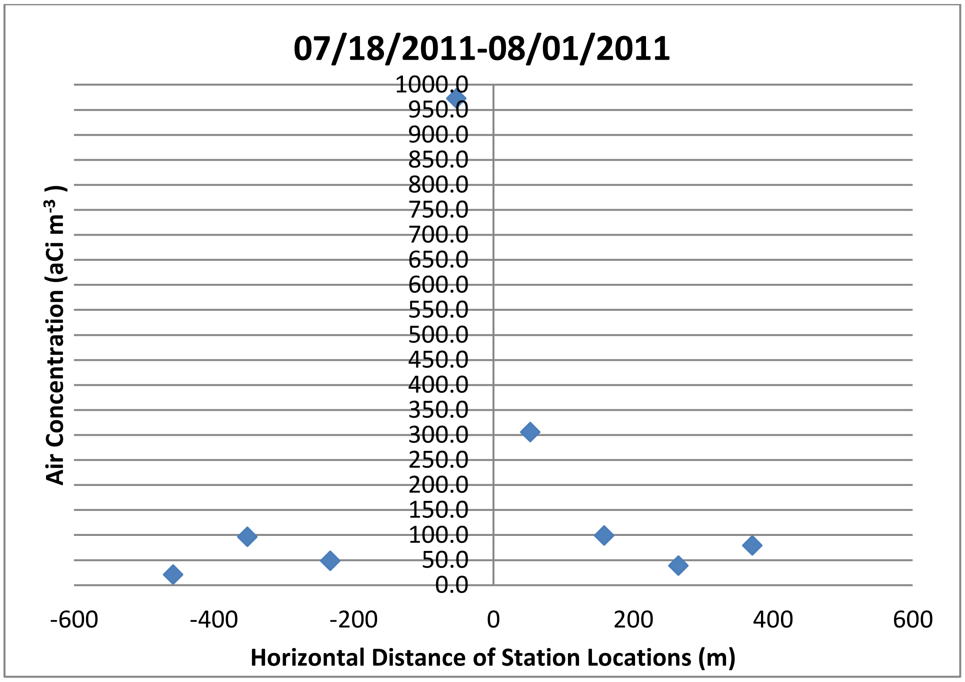

Fig. A60. ^{239}Pu concentration per station location per period.

Fig. A61 presents the air concentration per the horizontal distance of the receptor locations for period start date 08/01/2011.

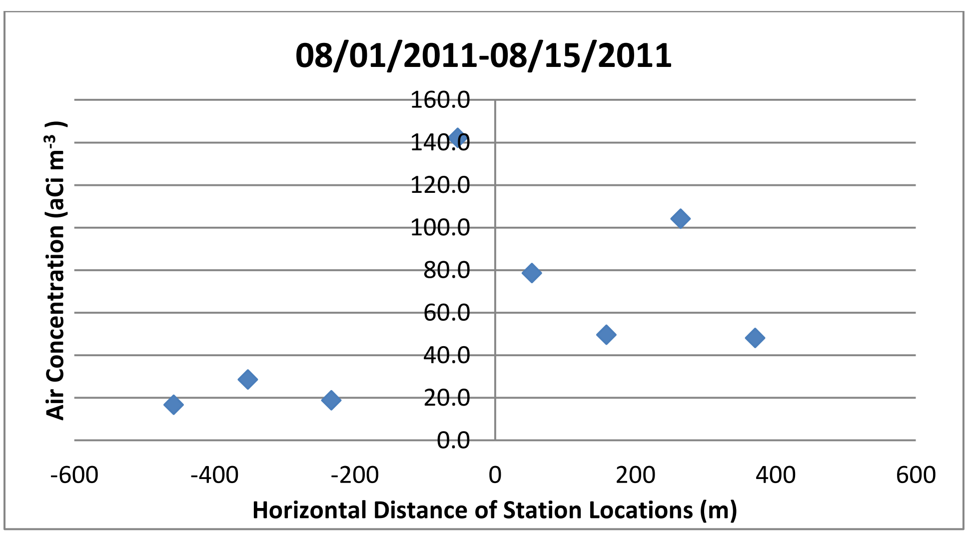

Fig. A61. ^{239}Pu concentration per station location per period.

Fig. A62 presents the air concentration per the horizontal distance of the receptor locations for period start date 08/15/2011. The peak shown within Fig. A62 was one of the 13 greatest peaks measured.

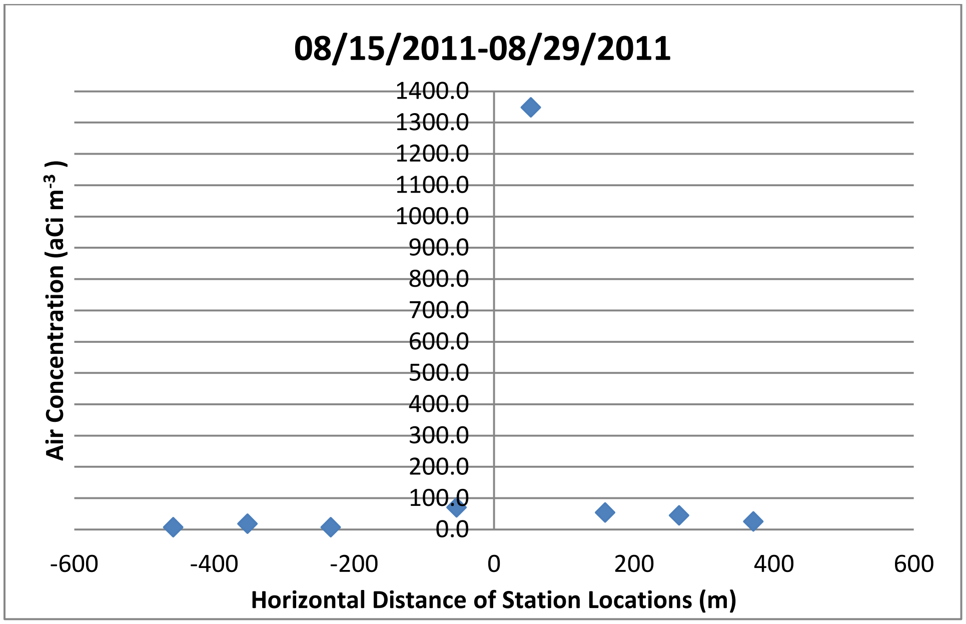

Fig. A62. ^{239}Pu concentration per station location per period.

Fig. A63 presents the air concentration per the horizontal distance of the receptor locations for period start date 08/29/2011.

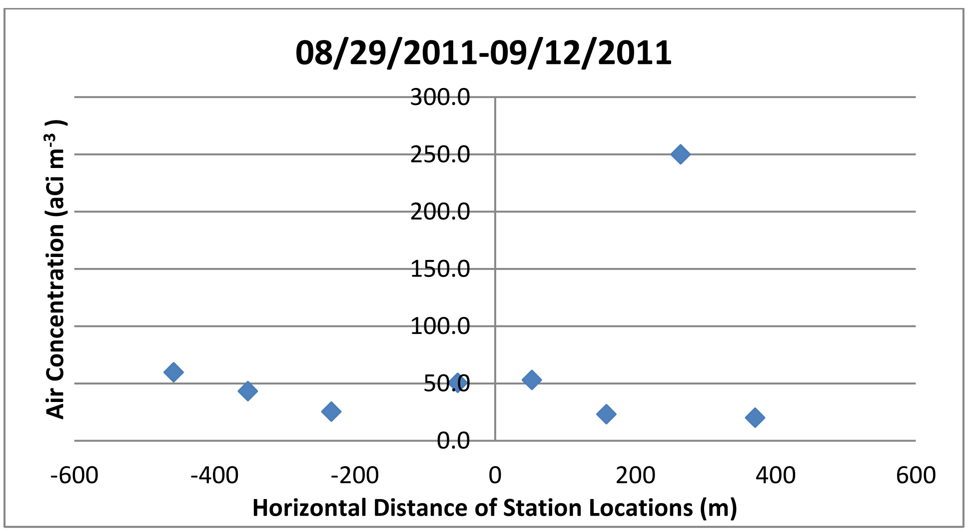

Fig. A63. ^{239}Pu concentration per station location per period.

Fig. A64 presents the air concentration per the horizontal distance of the receptor locations for period start date 09/12/2011.

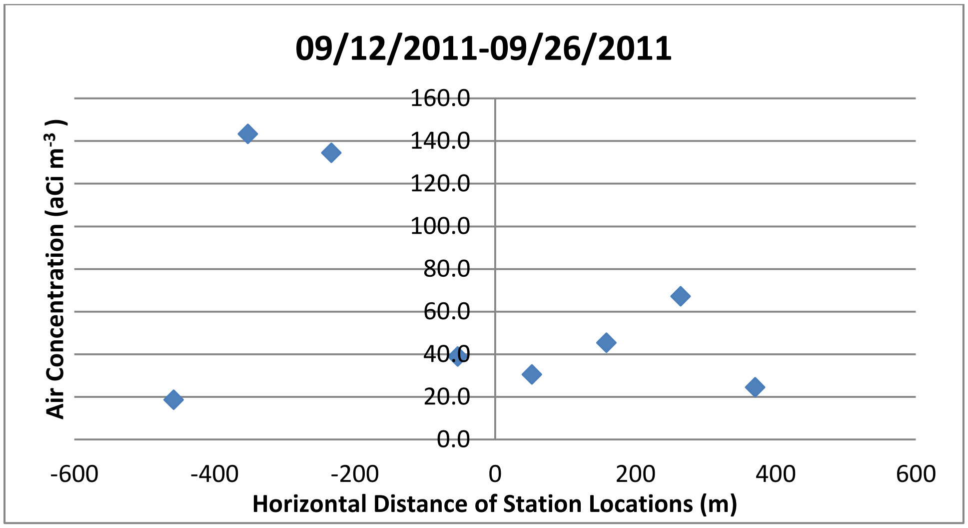

Fig. A64. ^{239}Pu concentration per station location per period.

APPENDIX B

RSAC files associated with Table 9

Class A stability with building wake:

Radiological Safety Analysis Computer Program (RSAC 7.2.0)

Name: INL	**Company:** Idaho National Laboratory	**Serial:** HR688-8449C-M4N6G-E
Computer: INL418751	**Run Date:** 07/17/2013	**Run Time:** 08:13:01

File: Class A_BW.rsac

Input

```
* Class A Stability with Building Wake
#
#
# Radionuclides
2000,0,1
Pu-239,1.
2999
# Met Data stability class A
5000,0
5001,3.3,0.,7.,9.58E2,0.,0
5101,191.
5201,1.,0.
5400,2,829.,7.
5410,3,1,0,0.
5999
10000
```

Direct Radionuclide Input

```
ANY PREVIOUS INVENTORY HAS BEEN ZEROED
NUCLIDE HALF LIFE GRAM CURIE
942390 Pu239 2.411E+04 yr 1.000E+00 6.204E-02
```

Meteorological Data

```
MEAN WIND SPEED = 3.300E+00 (m/s) STACK HEIGHT = 0.000E+00 (m)
MIXING LAYER HEIGHT = 7.000E+00 (m) AIR DENSITY = 9.580E+02
(g/cu m)
```

```
WET DEPOSITION SCAVENGING COEFFICIENT = 0.000E+00 (1/s)
THERE IS 1 SET OF LEAKAGE CONSTANTS (K1,K2)
1.000E+00 0.000E+00
PLUME MEANDER FACTOR = 1.00E+00
PASQUILL CLASS A METEOROLOGY, P-G SIGMA VALUES
BUILDING WIDTH = 8.290E+02 (m) BUILDING HEIGHT = 7.000E+00 (m)
DOWNWIND DISTANCE STACK SIGY SIGZ CHI/Q
HEIGHT (m) (m) (m) (s/m^3)
1.91E+02 0.000E+00 7.391E+01 5.585E+00 2.996E-04
```

Execution Time

```
0.00E+00 SECONDS
```

Class B stability with building wake:

Radiological Safety Analysis Computer Program (RSAC 7.2.0)

Name: INL	**Company:** Idaho National Laboratory	**Serial:** HR688-8449C-M4N6G-E
Computer: INL418751	**Run Date:** 07/17/2013	**Run Time:** 08:19:37

File: Class B_BW.rsac

Input

```
* Class B stability with building wake
#
#
# Radionuclides
2000,0,1
Pu-239,1.
2999
# Met Data stability class B
5000,0
5001,3.3,0.,7.,9.58E2,0.,0
5101,191.
5201,1.,0.
5400,2,829.,7.
5410,3,2,0,0.
5999
10000
```

Direct Radionuclide Input

```
ANY PREVIOUS INVENTORY HAS BEEN ZEROED
NUCLIDE HALF LIFE GRAM CURIE
942390 Pu239 2.411E+04 yr 1.000E+00 6.204E-02
```

Meteorological Data

```
MEAN WIND SPEED = 3.300E+00 (m/s) STACK HEIGHT = 0.000E+00 (m)
MIXING LAYER HEIGHT = 7.000E+00 (m) AIR DENSITY = 9.580E+02
(g/cu m)
```

```
WET DEPOSITION SCAVENGING COEFFICIENT = 0.000E+00 (1/s)
THERE IS 1 SET OF LEAKAGE CONSTANTS (K1,K2)
1.000E+00 0.000E+00
PLUME MEANDER FACTOR = 1.00E+00
PASQUILL CLASS B METEOROLOGY, P-G SIGMA VALUES
BUILDING WIDTH = 8.290E+02 (m) BUILDING HEIGHT = 7.000E+00 (m)
DOWNWIND DISTANCE STACK SIGY SIGZ CHI/Q
HEIGHT (m) (m) (m) (s/m^3)
1.91E+02 0.000E+00 6.500E+01 5.585E+00 3.415E-04
```

Execution Time

```
0.00E+00 SECONDS
```

Class C stability with building wake:

Radiological Safety Analysis Computer Program (RSAC 7.2.0)

Name: INL	**Company:** Idaho National Laboratory	**Serial:** HR688-8449C-M4N6G-E
Computer: INL418751	**Run Date:** 07/17/2013	**Run Time:** 08:21:37
File: Class C_BW.rsac		

Input

```
* Class C stability with building wake
#
#
# Radionuclides
2000,0,1
Pu-239,1.
2999
# Met Data stability class C
5000,0
5001,3.3,0.,7.,9.58E2,0.,0
5101,191.
5201,1.,0.
5400,2,829.,7.
5410,3,3,0,0.
5999
10000
```

Direct Radionuclide Input

```
ANY PREVIOUS INVENTORY HAS BEEN ZEROED
NUCLIDE HALF LIFE GRAM CURIE
942390 Pu239 2.411E+04 yr 1.000E+00 6.204E-02
```

Meteorological Data

```
MEAN WIND SPEED = 3.300E+00 (m/s) STACK HEIGHT = 0.000E+00 (m)
MIXING LAYER HEIGHT = 7.000E+00 (m) AIR DENSITY = 9.580E+02
(g/cu m)
```

```
WET DEPOSITION SCAVENGING COEFFICIENT = 0.000E+00 (1/s)
THERE IS 1 SET OF LEAKAGE CONSTANTS (K1,K2)
1.000E+00 0.000E+00
PLUME MEANDER FACTOR = 1.00E+00
PASQUILL CLASS C METEOROLOGY, P-G SIGMA VALUES
BUILDING WIDTH = 8.290E+02 (m) BUILDING HEIGHT = 7.000E+00 (m)
DOWNWIND DISTANCE STACK SIGY SIGZ CHI/Q
HEIGHT (m) (m) (m) (s/m^3)
1.91E+02 0.000E+00 5.953E+01 5.585E+00 3.738E-04
```

Execution Time

```
0.00E+00 SECONDS
```

Class D stability with building wake:

Radiological Safety Analysis Computer Program (RSAC 7.2.0)

Name: INL	**Company:** Idaho National Laboratory	**Serial:** HR688-8449C-M4N6G-E
Computer: INL418751	**Run Date:** 07/17/2013	**Run Time:** 08:24:16

File: Class D_BW.rsac

Input

```
* Class D stability with building wake.
#
#
# Radionuclides
2000,0,1
Pu-239,1.
2999
# Met Data stability class D
5000,0
5001,3.3,0.,7.,9.58E2,0.,0
5101,191.
5201,1.,0.
5400,2,829.,7.
5410,3,4,0,0.
5999
10000
```

Direct Radionuclide Input

```
ANY PREVIOUS INVENTORY HAS BEEN ZEROED
NUCLIDE HALF LIFE GRAM CURIE
942390 Pu239 2.411E+04 yr 1.000E+00 6.204E-02
```

Meteorological Data

```
MEAN WIND SPEED = 3.300E+00 (m/s) STACK HEIGHT = 0.000E+00 (m)
MIXING LAYER HEIGHT = 7.000E+00 (m) AIR DENSITY = 9.580E+02
(g/cu m)
```

WET DEPOSITION SCAVENGING COEFFICIENT = 0.000E+00 (1/s)
THERE IS 1 SET OF LEAKAGE CONSTANTS (K1,K2)
1.000E+00 0.000E+00
PLUME MEANDER FACTOR = 1.00E+00
PASQUILL CLASS D METEOROLOGY, P-G SIGMA VALUES
BUILDING WIDTH = 8.290E+02 (m) BUILDING HEIGHT = 7.000E+00 (m)
DOWNWIND DISTANCE STACK SIGY SIGZ CHI/Q
HEIGHT (m) (m) (m) (s/m^3)
1.91E+02 0.000E+00 5.545E+01 5.585E+00 4.021E-04

Execution Time

0.00E+00 SECONDS

APPENDIX C

RSAC files associated with Figure 96

Class A stability with building wake at the PCL:

Radiological Safety Analysis Computer Program (RSAC 7.2.0)

Name: INL	**Company:** Idaho National Laboratory	**Serial:** HR688-8449C-M4N6G-E
Computer: INL418751	**Run Date:** 07/17/2013	**Run Time:** 08:29:33

File: Class A_BW_75th percentile_PCL.rsac

Input

```
* 75th percentile Station PCL
#
#
# Radionuclides
2000,1,0
Pu-239,0.0011
2999
# Met Data stability class A
5000,0
5001,3.3,0.,7.,9.58E2,0.,0
5101,10.
5201,1.,0.
5400,3,829.,7.
5421,1.0E-4
5999
# Dose
7000,1,-2,1,0,1,7
7001,3.33E-04,0.,0,0,1.
7999
# Dose Summary
3000,2,7
10000
```

Direct Radionuclide Input

```
PREVIOUS INVENTORY CHANGED TO THE FOLLOWING VALUES
NUCLIDE HALF LIFE CURIE
942390 Pu239 2.411E+04 yr 1.100E-03
```

Meteorological Data

MEAN WIND SPEED = 3.300E+00 (m/s) STACK HEIGHT = 0.000E+00 (m)
MIXING LAYER HEIGHT = 7.000E+00 (m) AIR DENSITY = 9.580E+02 (g/cu m)
WET DEPOSITION SCAVENGING COEFFICIENT = 0.000E+00 (1/s)
THERE IS 1 SET OF LEAKAGE CONSTANTS (K1,K2)
1.000E+00 0.000E+00
CHI/Q VALUES INPUT DIRECTLY
DOWNWIND DISTANCE CHI/Q
1.000E+01 1.000E-04

Inhalation Dose Calculation

USING DOSE CONVERSION FACTORS FROM ICRP-68 FOR ADULT WORKER
RESPIRABLE FRACTION = 1.000E+00
BREATHING RATE = 3.330E-04 (m^3/s)
RELEASE TIME FOR EXPONENTIAL DECAY FUNCTION = 1.000E+00 (s)
INTERNAL EXPOSURE TIME PERIOD = 5.000E+01 (yr)
LUNG ABSORPTION TYPES SELECTED TO GIVE MAXIMUM DOSE
ICRP-68 INHALATION DOSE FOR ADULT WORKER
INHALATION EQUIVALENT DOSE ORDERED BY ORGAN (rem) FOR ADULT WORKER
DOWNWIND DISTANCES (m)

```
ORGAN NO. 1.00E+01
-------- --- --------
ADRENALS 1 2.30E-04
BSURFACE 2 1.36E-01
B_WALL 3 2.30E-04
BRAIN 4 2.30E-04
BREAST 5 2.30E-04
COLON 6 2.44E-04
ESOPHAGU 7 2.30E-04
ET_AIR 8 2.03E-03
KIDNEYS 9 5.56E-04
LIVER 10 2.85E-02
LLI_WALL 11 2.44E-04
LUNGS 12 2.85E-03
MUSCLE 13 2.30E-04
OVARIES 14 1.76E-03
PANCREAS 15 2.30E-04
R_MARROW 16 6.51E-03
SI_WALL 17 2.30E-04
SKIN 18 2.30E-04
SPLEEN 19 2.30E-04
```

ST_WALL 20 2.30E-04
TESTES 21 1.76E-03
THYMUS 22 2.30E-04
THYROID 23 2.30E-04
ULI_WALL 24 2.44E-04
UTERUS 25 2.30E-04
INHALATION EQUIVALENT DOSE ORDERED BY DOSE (rem) FOR ADULT WORKER
DOWNWIND DISTANCES (m)
ORGAN NO. 1.00E+01
-------- --- --------
BSURFACE 2 1.36E-01
LIVER 10 2.85E-02
R_MARROW 16 6.51E-03
LUNGS 12 2.85E-03
ET_AIR 8 2.03E-03
OVARIES 14 1.76E-03
TESTES 21 1.76E-03
KIDNEYS 9 5.56E-04
COLON 6 2.44E-04
LLI_WALL 11 2.44E-04
ULI_WALL 24 2.44E-04
ADRENALS 1 2.30E-04
B_WALL 3 2.30E-04
BRAIN 4 2.30E-04
BREAST 5 2.30E-04
ESOPHAGU 7 2.30E-04
MUSCLE 13 2.30E-04
PANCREAS 15 2.30E-04
SI_WALL 17 2.30E-04
SKIN 18 2.30E-04
SPLEEN 19 2.30E-04
ST_WALL 20 2.30E-04
THYMUS 22 2.30E-04
THYROID 23 2.30E-04
UTERUS 25 2.30E-04
INHALATION EFFECTIVE DOSE ORDERED BY DOSE (rem) FOR ADULT WORKER
DOWNWIND DISTANCES (m)
ORGAN NO. 1.00E+01
-------- --- --------
ADRENALS 1 1.15E-05
BSURFACE 2 6.78E-03
B_WALL 3 2.30E-06
BRAIN 4 1.15E-05
BREAST 5 1.15E-05
COLON 6 2.93E-05
ESOPHAGU 7 1.15E-05

```
ET_AIR 8 1.02E-04
KIDNEYS 9 2.78E-05
LIVER 10 1.42E-03
LLI_WALL 11 1.22E-05
LUNGS 12 3.42E-04
MUSCLE 13 1.15E-05
OVARIES 14 8.81E-05
PANCREAS 15 1.15E-05
R_MARROW 16 7.81E-04
SI_WALL 17 1.15E-05
SKIN 18 2.30E-06
SPLEEN 19 1.15E-05
ST_WALL 20 4.61E-05
TESTES 21 8.81E-05
THYMUS 22 1.15E-05
THYROID 23 1.15E-05
ULI_WALL 24 1.22E-05
UTERUS 25 1.15E-05
E_50 26 4.34E-03
```

Dose Summary

```
ADULT WORKER INHALATION DOSE CALCULATIONS MADE
USING DOSE CONVERSION FACTORS FOR ADULT WORKER
PATHWAY CONTRIBUTION TO THE EFFECTIVE DOSE (rem)
DOWNWIND DISTANCE = 1.00E+01 (m)
NUCLIDE INHALATION INGESTION GROUND SUR AIR IMMERS TOTAL
------------- ---------- ---------- ---------- ---------- ------
----
TOTALS 4.34E-03 - - - 4.34E-03
WARNINGS
--------
NO INGESTION DOSE CALCULATIONS WERE MADE
NO AIR IMMERSION OR CLOUD GAMMA DOSE CALCULATIONS WERE MADE
```

Execution Time

```
4.00E-02 SECONDS
```

Class A stability with building wake at station 169:

Radiological Safety Analysis Computer Program (RSAC 7.2.0)

Name: INL	**Company:** Idaho National Laboratory	**Serial:** HR688-8449C-M4N6G-E
Computer: INL418751	**Run Date:** 07/17/2013	**Run Time:** 08:34:21

File: Class A_BW_75th percentile_Station 169.rsac

Input

```
* 75th percentile Station 169
#
#
# Radionuclides
2000,1,0
Pu-239,0.0011
2999
# Met Data stability class A
5000,0
5001,3.3,0.,7.,9.58E2,0.,0
5101,249.
5201,1.,0.
5400,3,829.,7.
5421,1.2E-5
5999
# Dose
7000,1,-2,1,0,1,7
7001,3.33E-04,0.,0,0,1.
7999
# Dose Summary
3000,2,7
10000
```

Direct Radionuclide Input

```
PREVIOUS INVENTORY CHANGED TO THE FOLLOWING VALUES
NUCLIDE HALF LIFE CURIE
942390 Pu239 2.411E+04 yr 1.100E-03
```

Meteorological Data

```
MEAN WIND SPEED = 3.300E+00 (m/s) STACK HEIGHT = 0.000E+00 (m)
MIXING LAYER HEIGHT = 7.000E+00 (m) AIR DENSITY = 9.580E+02
(g/cu m)
WET DEPOSITION SCAVENGING COEFFICIENT = 0.000E+00 (1/s)
THERE IS 1 SET OF LEAKAGE CONSTANTS (K1,K2)
1.000E+00 0.000E+00
CHI/Q VALUES INPUT DIRECTLY
DOWNWIND DISTANCE CHI/Q
2.490E+02 1.200E-05
```

Inhalation Dose Calculation

```
USING DOSE CONVERSION FACTORS FROM ICRP-68 FOR ADULT WORKER
RESPIRABLE FRACTION = 1.000E+00
BREATHING RATE = 3.330E-04 (m^3/s)
RELEASE TIME FOR EXPONENTIAL DECAY FUNCTION = 1.000E+00 (s)
INTERNAL EXPOSURE TIME PERIOD = 5.000E+01 (yr)
LUNG ABSORPTION TYPES SELECTED TO GIVE MAXIMUM DOSE
ICRP-68 INHALATION DOSE FOR ADULT WORKER
INHALATION EQUIVALENT DOSE ORDERED BY ORGAN (rem) FOR ADULT
WORKER
DOWNWIND DISTANCES (m)
ORGAN NO. 2.49E+02
-------- --- --------
ADRENALS 1 2.76E-05
BSURFACE 2 1.63E-02
B_WALL 3 2.76E-05
BRAIN 4 2.76E-05
BREAST 5 2.76E-05
COLON 6 2.93E-05
ESOPHAGU 7 2.76E-05
ET_AIR 8 2.44E-04
KIDNEYS 9 6.67E-05
LIVER 10 3.42E-03
LLI_WALL 11 2.93E-05
LUNGS 12 3.42E-04
MUSCLE 13 2.76E-05
OVARIES 14 2.11E-04
PANCREAS 15 2.76E-05
R_MARROW 16 7.81E-04
SI_WALL 17 2.76E-05
SKIN 18 2.76E-05
SPLEEN 19 2.76E-05
```

ST_WALL 20 2.76E-05
TESTES 21 2.11E-04
THYMUS 22 2.76E-05
THYROID 23 2.76E-05
ULI_WALL 24 2.93E-05
UTERUS 25 2.76E-05
INHALATION EQUIVALENT DOSE ORDERED BY DOSE (rem) FOR ADULT WORKER
DOWNWIND DISTANCES (m)
ORGAN NO. 2.49E+02
-------- --- --------
BSURFACE 2 1.63E-02
LIVER 10 3.42E-03
R_MARROW 16 7.81E-04
LUNGS 12 3.42E-04
ET_AIR 8 2.44E-04
OVARIES 14 2.11E-04
TESTES 21 2.11E-04
KIDNEYS 9 6.67E-05
COLON 6 2.93E-05
LLI_WALL 11 2.93E-05
ULI_WALL 24 2.93E-05
ADRENALS 1 2.76E-05
B_WALL 3 2.76E-05
BRAIN 4 2.76E-05
BREAST 5 2.76E-05
ESOPHAGU 7 2.76E-05
MUSCLE 13 2.76E-05
PANCREAS 15 2.76E-05
SI_WALL 17 2.76E-05
SKIN 18 2.76E-05
SPLEEN 19 2.76E-05
ST_WALL 20 2.76E-05
THYMUS 22 2.76E-05
THYROID 23 2.76E-05
UTERUS 25 2.76E-05
INHALATION EFFECTIVE DOSE ORDERED BY DOSE (rem) FOR ADULT WORKER
DOWNWIND DISTANCES (m)
ORGAN NO. 2.49E+02
-------- --- --------
ADRENALS 1 1.38E-06
BSURFACE 2 8.13E-04
B_WALL 3 2.76E-07
BRAIN 4 1.38E-06
BREAST 5 1.38E-06
COLON 6 3.51E-06
ESOPHAGU 7 1.38E-06

ET_AIR 8 1.22E-05
KIDNEYS 9 3.33E-06
LIVER 10 1.71E-04
LLI_WALL 11 1.46E-06
LUNGS 12 4.10E-05
MUSCLE 13 1.38E-06
OVARIES 14 1.06E-05
PANCREAS 15 1.38E-06
R_MARROW 16 9.37E-05
SI_WALL 17 1.38E-06
SKIN 18 2.76E-07
SPLEEN 19 1.38E-06
ST_WALL 20 5.53E-06
TESTES 21 1.06E-05
THYMUS 22 1.38E-06
THYROID 23 1.38E-06
ULI_WALL 24 1.46E-06
UTERUS 25 1.38E-06
E_50 26 5.20E-04

Dose Summary

ADULT WORKER INHALATION DOSE CALCULATIONS MADE
USING DOSE CONVERSION FACTORS FOR ADULT WORKER
PATHWAY CONTRIBUTION TO THE EFFECTIVE DOSE (rem)
DOWNWIND DISTANCE = 2.49E+02 (m)
NUCLIDE INHALATION INGESTION GROUND SUR AIR IMMERS TOTAL
------------- ---------- ---------- ---------- ---------- ------
----
TOTALS 5.20E-04 - - - 5.20E-04
WARNINGS

NO INGESTION DOSE CALCULATIONS WERE MADE
NO AIR IMMERSION OR CLOUD GAMMA DOSE CALCULATIONS WERE MADE

Execution Time

4.00E-02 SECONDS

Class A stability with building wake at station 317:

Radiological Safety Analysis Computer Program (RSAC 7.2.0)

Name: INL	**Company:** Idaho National Laboratory	**Serial:** HR688-8449C-M4N6G-E
Computer: INL418751	**Run Date:** 07/17/2013	**Run Time:** 08:35:54

File: Class A_BW_75th percentile_Station 317.rsac

Input

```
* 75th percentile Station 317
#
#
# Radionuclides
2000,1,0
Pu-239,0.0011
2999
# Met Data stability class A
5000,0
5001,3.3,0.,7.,9.58E2,0.,0
5101,249.
5201,1.,0.
5400,3,829.,7.
5421,9.0E-5
5999
# Dose
7000,1,-2,1,0,1,7
7001,3.33E-04,0.,0,0,1.
7999
# Dose Summary
3000,2,7
10000
```

Direct Radionuclide Input

```
PREVIOUS INVENTORY CHANGED TO THE FOLLOWING VALUES
NUCLIDE HALF LIFE CURIE
942390 Pu239 2.411E+04 yr 1.100E-03
```

Meteorological Data

MEAN WIND SPEED = 3.300E+00 (m/s) STACK HEIGHT = 0.000E+00 (m)
MIXING LAYER HEIGHT = 7.000E+00 (m) AIR DENSITY = 9.580E+02 (g/cu m)
WET DEPOSITION SCAVENGING COEFFICIENT = 0.000E+00 (1/s)
THERE IS 1 SET OF LEAKAGE CONSTANTS (K1,K2)
1.000E+00 0.000E+00
CHI/Q VALUES INPUT DIRECTLY
DOWNWIND DISTANCE CHI/Q
2.490E+02 9.000E-05

Inhalation Dose Calculation

USING DOSE CONVERSION FACTORS FROM ICRP-68 FOR ADULT WORKER
RESPIRABLE FRACTION = 1.000E+00
BREATHING RATE = 3.330E-04 (m^3/s)
RELEASE TIME FOR EXPONENTIAL DECAY FUNCTION = 1.000E+00 (s)
INTERNAL EXPOSURE TIME PERIOD = 5.000E+01 (yr)
LUNG ABSORPTION TYPES SELECTED TO GIVE MAXIMUM DOSE
ICRP-68 INHALATION DOSE FOR ADULT WORKER
INHALATION EQUIVALENT DOSE ORDERED BY ORGAN (rem) FOR ADULT WORKER
DOWNWIND DISTANCES (m)

ORGAN	NO.	2.49E+02
--------	---	--------
ADRENALS	1	2.07E-04
BSURFACE	2	1.22E-01
B_WALL	3	2.07E-04
BRAIN	4	2.07E-04
BREAST	5	2.07E-04
COLON	6	2.20E-04
ESOPHAGU	7	2.07E-04
ET_AIR	8	1.83E-03
KIDNEYS	9	5.00E-04
LIVER	10	2.56E-02
LLI_WALL	11	2.20E-04
LUNGS	12	2.56E-03
MUSCLE	13	2.07E-04
OVARIES	14	1.59E-03
PANCREAS	15	2.07E-04
R_MARROW	16	5.85E-03
SI_WALL	17	2.07E-04
SKIN	18	2.07E-04
SPLEEN	19	2.07E-04

ST_WALL 20 2.07E-04
TESTES 21 1.59E-03
THYMUS 22 2.07E-04
THYROID 23 2.07E-04
ULI_WALL 24 2.20E-04
UTERUS 25 2.07E-04
INHALATION EQUIVALENT DOSE ORDERED BY DOSE (rem) FOR ADULT WORKER
DOWNWIND DISTANCES (m)
ORGAN NO. 2.49E+02
-------- --- --------
BSURFACE 2 1.22E-01
LIVER 10 2.56E-02
R_MARROW 16 5.85E-03
LUNGS 12 2.56E-03
ET_AIR 8 1.83E-03
OVARIES 14 1.59E-03
TESTES 21 1.59E-03
KIDNEYS 9 5.00E-04
COLON 6 2.20E-04
LLI_WALL 11 2.20E-04
ULI_WALL 24 2.20E-04
ADRENALS 1 2.07E-04
B_WALL 3 2.07E-04
BRAIN 4 2.07E-04
BREAST 5 2.07E-04
ESOPHAGU 7 2.07E-04
MUSCLE 13 2.07E-04
PANCREAS 15 2.07E-04
SI_WALL 17 2.07E-04
SKIN 18 2.07E-04
SPLEEN 19 2.07E-04
ST_WALL 20 2.07E-04
THYMUS 22 2.07E-04
THYROID 23 2.07E-04
UTERUS 25 2.07E-04
INHALATION EFFECTIVE DOSE ORDERED BY DOSE (rem) FOR ADULT WORKER
DOWNWIND DISTANCES (m)
ORGAN NO. 2.49E+02
-------- --- --------
ADRENALS 1 1.04E-05
BSURFACE 2 6.10E-03
B_WALL 3 2.07E-06
BRAIN 4 1.04E-05
BREAST 5 1.04E-05
COLON 6 2.63E-05
ESOPHAGU 7 1.04E-05

```
ET_AIR 8 9.15E-05
KIDNEYS 9 2.50E-05
LIVER 10 1.28E-03
LLI_WALL 11 1.10E-05
LUNGS 12 3.07E-04
MUSCLE 13 1.04E-05
OVARIES 14 7.93E-05
PANCREAS 15 1.04E-05
R_MARROW 16 7.03E-04
SI_WALL 17 1.04E-05
SKIN 18 2.07E-06
SPLEEN 19 1.04E-05
ST_WALL 20 4.15E-05
TESTES 21 7.93E-05
THYMUS 22 1.04E-05
THYROID 23 1.04E-05
ULI_WALL 24 1.10E-05
UTERUS 25 1.04E-05
E_50 26 3.90E-03
```

Dose Summary

```
ADULT WORKER INHALATION DOSE CALCULATIONS MADE
USING DOSE CONVERSION FACTORS FOR ADULT WORKER
PATHWAY CONTRIBUTION TO THE EFFECTIVE DOSE (rem)
DOWNWIND DISTANCE = 2.49E+02 (m)
NUCLIDE INHALATION INGESTION GROUND SUR AIR IMMERS TOTAL
------------- ---------- ---------- ---------- ---------- ------
----
TOTALS 3.90E-03 - - - 3.90E-03
WARNINGS
--------
NO INGESTION DOSE CALCULATIONS WERE MADE
NO AIR IMMERSION OR CLOUD GAMMA DOSE CALCULATIONS WERE MADE
```

Execution Time

```
4.00E-02 SECONDS
```

Class A stability with building wake at station 326:

Radiological Safety Analysis Computer Program (RSAC 7.2.0)

Name: INL	**Company:** Idaho National Laboratory	**Serial:** HR688-8449C-M4N6G-E
Computer: INL418751	**Run Date:** 07/17/2013	**Run Time:** 08:37:19

File: Class A_BW_75th percentile_Station 326.rsac

Input

```
* 75th percentile Station 326
#
#
# Radionuclides
2000,1,0
Pu-239,0.0011
2999
# Met Data stability class A
5000,0
5001,3.3,0.,7.,9.58E2,0.,0
5101,249.
5201,1.,0.
5400,3,829.,7.
5421,8.3E-6
5999
# Dose
7000,1,-2,1,0,1,7
7001,3.33E-04,0.,0,0,1.
7999
# Dose Summary
3000,2,7
10000
```

Direct Radionuclide Input

```
PREVIOUS INVENTORY CHANGED TO THE FOLLOWING VALUES
NUCLIDE HALF LIFE CURIE
942390 Pu239 2.411E+04 yr 1.100E-03
```

Meteorological Data

MEAN WIND SPEED = 3.300E+00 (m/s) STACK HEIGHT = 0.000E+00 (m)
MIXING LAYER HEIGHT = 7.000E+00 (m) AIR DENSITY = 9.580E+02 (g/cu m)
WET DEPOSITION SCAVENGING COEFFICIENT = 0.000E+00 (1/s)
THERE IS 1 SET OF LEAKAGE CONSTANTS (K1,K2)
1.000E+00 0.000E+00
CHI/Q VALUES INPUT DIRECTLY
DOWNWIND DISTANCE CHI/Q
2.490E+02 8.300E-06

Inhalation Dose Calculation

USING DOSE CONVERSION FACTORS FROM ICRP-68 FOR ADULT WORKER
RESPIRABLE FRACTION = 1.000E+00
BREATHING RATE = 3.330E-04 (m^3/s)
RELEASE TIME FOR EXPONENTIAL DECAY FUNCTION = 1.000E+00 (s)
INTERNAL EXPOSURE TIME PERIOD = 5.000E+01 (yr)
LUNG ABSORPTION TYPES SELECTED TO GIVE MAXIMUM DOSE
ICRP-68 INHALATION DOSE FOR ADULT WORKER
INHALATION EQUIVALENT DOSE ORDERED BY ORGAN (rem) FOR ADULT WORKER
DOWNWIND DISTANCES (m)
ORGAN NO. 2.49E+02
-------- --- --------
ADRENALS 1 1.91E-05
BSURFACE 2 1.12E-02
B_WALL 3 1.91E-05
BRAIN 4 1.91E-05
BREAST 5 1.91E-05
COLON 6 2.02E-05
ESOPHAGU 7 1.91E-05
ET_AIR 8 1.69E-04
KIDNEYS 9 4.61E-05
LIVER 10 2.36E-03
LLI_WALL 11 2.02E-05
LUNGS 12 2.36E-04
MUSCLE 13 1.91E-05
OVARIES 14 1.46E-04
PANCREAS 15 1.91E-05
R_MARROW 16 5.40E-04
SI_WALL 17 1.91E-05
SKIN 18 1.91E-05
SPLEEN 19 1.91E-05

ST_WALL 20 1.91E-05
TESTES 21 1.46E-04
THYMUS 22 1.91E-05
THYROID 23 1.91E-05
ULI_WALL 24 2.02E-05
UTERUS 25 1.91E-05
INHALATION EQUIVALENT DOSE ORDERED BY DOSE (rem) FOR ADULT WORKER
DOWNWIND DISTANCES (m)
ORGAN NO. 2.49E+02
-------- --- --------
BSURFACE 2 1.12E-02
LIVER 10 2.36E-03
R_MARROW 16 5.40E-04
LUNGS 12 2.36E-04
ET_AIR 8 1.69E-04
OVARIES 14 1.46E-04
TESTES 21 1.46E-04
KIDNEYS 9 4.61E-05
COLON 6 2.02E-05
LLI_WALL 11 2.02E-05
ULI_WALL 24 2.02E-05
ADRENALS 1 1.91E-05
B_WALL 3 1.91E-05
BRAIN 4 1.91E-05
BREAST 5 1.91E-05
ESOPHAGU 7 1.91E-05
MUSCLE 13 1.91E-05
PANCREAS 15 1.91E-05
SI_WALL 17 1.91E-05
SKIN 18 1.91E-05
SPLEEN 19 1.91E-05
ST_WALL 20 1.91E-05
THYMUS 22 1.91E-05
THYROID 23 1.91E-05
UTERUS 25 1.91E-05
INHALATION EFFECTIVE DOSE ORDERED BY DOSE (rem) FOR ADULT WORKER
DOWNWIND DISTANCES (m)
ORGAN NO. 2.49E+02
-------- --- --------
ADRENALS 1 9.56E-07
BSURFACE 2 5.62E-04
B_WALL 3 1.91E-07
BRAIN 4 9.56E-07
BREAST 5 9.56E-07
COLON 6 2.43E-06
ESOPHAGU 7 9.56E-07

```
ET_AIR 8 8.44E-06
KIDNEYS 9 2.31E-06
LIVER 10 1.18E-04
LLI_WALL 11 1.01E-06
LUNGS 12 2.83E-05
MUSCLE 13 9.56E-07
OVARIES 14 7.31E-06
PANCREAS 15 9.56E-07
R_MARROW 16 6.48E-05
SI_WALL 17 9.56E-07
SKIN 18 1.91E-07
SPLEEN 19 9.56E-07
ST_WALL 20 3.82E-06
TESTES 21 7.31E-06
THYMUS 22 9.56E-07
THYROID 23 9.56E-07
ULI_WALL 24 1.01E-06
UTERUS 25 9.56E-07
E_50 26 3.60E-04
```

Dose Summary

```
ADULT WORKER INHALATION DOSE CALCULATIONS MADE
USING DOSE CONVERSION FACTORS FOR ADULT WORKER
PATHWAY CONTRIBUTION TO THE EFFECTIVE DOSE (rem)
DOWNWIND DISTANCE = 2.49E+02 (m)
NUCLIDE INHALATION INGESTION GROUND SUR AIR IMMERS TOTAL
------------- ---------- ---------- ---------- ---------- ------
----
TOTALS 3.60E-04 - - - 3.60E-04
WARNINGS
--------
NO INGESTION DOSE CALCULATIONS WERE MADE
NO AIR IMMERSION OR CLOUD GAMMA DOSE CALCULATIONS WERE MADE
```

Execution Time

```
3.00E-02 SECONDS
```

Class A stability with building wake at station 327:

Radiological Safety Analysis Computer Program (RSAC 7.2.0)

Name: INL	**Company:** Idaho National Laboratory	**Serial:** HR688-8449C-M4N6G-E
Computer: INL418751	**Run Date:** 07/17/2013	**Run Time:** 08:38:52

File: Class A_BW_75th percentile_Station 327.rsac

Input

```
* 75th percentile Station 327

#
#
# Radionuclides
2000,1,0
Pu-239,0.0011
2999
# Met Data stability class A
5000,0
5001,3.3,0.,7.,9.58E2,0.,0
5101,249.
5201,1.,0.
5400,3,829.,7.
5421,1.3E-5
5999
# Dose
7000,1,-2,1,0,1,7
7001,3.33E-04,0.,0,0,1.
7999
# Dose Summary
3000,2,7
10000
```

Direct Radionuclide Input

```
PREVIOUS INVENTORY CHANGED TO THE FOLLOWING VALUES
NUCLIDE HALF LIFE CURIE
942390 Pu239 2.411E+04 yr 1.100E-03
```

Meteorological Data

```
MEAN WIND SPEED = 3.300E+00 (m/s) STACK HEIGHT = 0.000E+00 (m)
MIXING LAYER HEIGHT = 7.000E+00 (m) AIR DENSITY = 9.580E+02
(g/cu m)
WET DEPOSITION SCAVENGING COEFFICIENT = 0.000E+00 (1/s)
THERE IS 1 SET OF LEAKAGE CONSTANTS (K1,K2)
1.000E+00 0.000E+00
CHI/Q VALUES INPUT DIRECTLY
DOWNWIND DISTANCE CHI/Q
2.490E+02 1.300E-05
```

Inhalation Dose Calculation

```
USING DOSE CONVERSION FACTORS FROM ICRP-68 FOR ADULT WORKER
RESPIRABLE FRACTION = 1.000E+00
BREATHING RATE = 3.330E-04 (m^3/s)
RELEASE TIME FOR EXPONENTIAL DECAY FUNCTION = 1.000E+00 (s)
INTERNAL EXPOSURE TIME PERIOD = 5.000E+01 (yr)
LUNG ABSORPTION TYPES SELECTED TO GIVE MAXIMUM DOSE
ICRP-68 INHALATION DOSE FOR ADULT WORKER
INHALATION EQUIVALENT DOSE ORDERED BY ORGAN (rem) FOR ADULT
WORKER
DOWNWIND DISTANCES (m)
ORGAN NO. 2.49E+02
-------- --- --------
ADRENALS 1 3.00E-05
BSURFACE 2 1.76E-02
B_WALL 3 3.00E-05
BRAIN 4 3.00E-05
BREAST 5 3.00E-05
COLON 6 3.17E-05
ESOPHAGU 7 3.00E-05
ET_AIR 8 2.64E-04
KIDNEYS 9 7.22E-05
LIVER 10 3.70E-03
LLI_WALL 11 3.17E-05
LUNGS 12 3.70E-04
MUSCLE 13 3.00E-05
OVARIES 14 2.29E-04
PANCREAS 15 3.00E-05
R_MARROW 16 8.46E-04
SI_WALL 17 3.00E-05
SKIN 18 3.00E-05
```

SPLEEN 19 3.00E-05
ST_WALL 20 3.00E-05
TESTES 21 2.29E-04
THYMUS 22 3.00E-05
THYROID 23 3.00E-05
ULI_WALL 24 3.17E-05
UTERUS 25 3.00E-05
INHALATION EQUIVALENT DOSE ORDERED BY DOSE (rem) FOR ADULT WORKER
DOWNWIND DISTANCES (m)
ORGAN NO. 2.49E+02
-------- --- --------
BSURFACE 2 1.76E-02
LIVER 10 3.70E-03
R_MARROW 16 8.46E-04
LUNGS 12 3.70E-04
ET_AIR 8 2.64E-04
OVARIES 14 2.29E-04
TESTES 21 2.29E-04
KIDNEYS 9 7.22E-05
COLON 6 3.17E-05
LLI_WALL 11 3.17E-05
ULI_WALL 24 3.17E-05
ADRENALS 1 3.00E-05
B_WALL 3 3.00E-05
BRAIN 4 3.00E-05
BREAST 5 3.00E-05
ESOPHAGU 7 3.00E-05
MUSCLE 13 3.00E-05
PANCREAS 15 3.00E-05
SI_WALL 17 3.00E-05
SKIN 18 3.00E-05
SPLEEN 19 3.00E-05
ST_WALL 20 3.00E-05
THYMUS 22 3.00E-05
THYROID 23 3.00E-05
UTERUS 25 3.00E-05
INHALATION EFFECTIVE DOSE ORDERED BY DOSE (rem) FOR ADULT WORKER
DOWNWIND DISTANCES (m)
ORGAN NO. 2.49E+02
-------- --- --------
ADRENALS 1 1.50E-06
BSURFACE 2 8.81E-04
B_WALL 3 3.00E-07
BRAIN 4 1.50E-06
BREAST 5 1.50E-06
COLON 6 3.81E-06

```
ESOPHAGU 7 1.50E-06
ET_AIR 8 1.32E-05
KIDNEYS 9 3.61E-06
LIVER 10 1.85E-04
LLI_WALL 11 1.59E-06
LUNGS 12 4.44E-05
MUSCLE 13 1.50E-06
OVARIES 14 1.15E-05
PANCREAS 15 1.50E-06
R_MARROW 16 1.01E-04
SI_WALL 17 1.50E-06
SKIN 18 3.00E-07
SPLEEN 19 1.50E-06
ST_WALL 20 5.99E-06
TESTES 21 1.15E-05
THYMUS 22 1.50E-06
THYROID 23 1.50E-06
ULI_WALL 24 1.59E-06
UTERUS 25 1.50E-06
E_50 26 5.64E-04
```

Dose Summary

```
ADULT WORKER INHALATION DOSE CALCULATIONS MADE
USING DOSE CONVERSION FACTORS FOR ADULT WORKER
PATHWAY CONTRIBUTION TO THE EFFECTIVE DOSE (rem)
DOWNWIND DISTANCE = 2.49E+02 (m)
NUCLIDE INHALATION INGESTION GROUND SUR AIR IMMERS TOTAL
------------- ---------- ---------- ---------- ---------- ------
----
TOTALS 5.64E-04 - - - 5.64E-04
WARNINGS
--------
NO INGESTION DOSE CALCULATIONS WERE MADE
NO AIR IMMERSION OR CLOUD GAMMA DOSE CALCULATIONS WERE MADE
```

Execution Time

```
3.00E-02 SECONDS
```

Class A stability with building wake at station 328:

Radiological Safety Analysis Computer Program (RSAC 7.2.0)

Name: INL	**Company:** Idaho National Laboratory	**Serial:** HR688-8449C-M4N6G-E
Computer: INL418751	**Run Date:** 07/17/2013	**Run Time:** 08:43:54

File: Class A_BW_75th percentile_Station 328.rsac

Input

```
* 75th percentile Station 328
#
#
# Radionuclides
2000,1,0
Pu-239,0.0011
2999
# Met Data stability class A
5000,0
5001,3.3,0.,7.,9.58E2,0.,0
5101,249.
5201,1.,0.
5400,3,829.,7.
5421,2.6E-5
5999
# Dose
7000,1,-2,1,0,1,7
7001,3.33E-04,0.,0,0,1.
7999
# Dose Summary
3000,2,7
10000
```

Direct Radionuclide Input

```
PREVIOUS INVENTORY CHANGED TO THE FOLLOWING VALUES
NUCLIDE HALF LIFE CURIE
942390 Pu239 2.411E+04 yr 1.100E-03
```

Meteorological Data

MEAN WIND SPEED = 3.300E+00 (m/s) STACK HEIGHT = 0.000E+00 (m)
MIXING LAYER HEIGHT = 7.000E+00 (m) AIR DENSITY = 9.580E+02 (g/cu m)
WET DEPOSITION SCAVENGING COEFFICIENT = 0.000E+00 (1/s)
THERE IS 1 SET OF LEAKAGE CONSTANTS (K1,K2)
1.000E+00 0.000E+00
CHI/Q VALUES INPUT DIRECTLY
DOWNWIND DISTANCE CHI/Q
2.490E+02 2.600E-05

Inhalation Dose Calculation

USING DOSE CONVERSION FACTORS FROM ICRP-68 FOR ADULT WORKER
RESPIRABLE FRACTION = 1.000E+00
BREATHING RATE = 3.330E-04 (m^3/s)
RELEASE TIME FOR EXPONENTIAL DECAY FUNCTION = 1.000E+00 (s)
INTERNAL EXPOSURE TIME PERIOD = 5.000E+01 (yr)
LUNG ABSORPTION TYPES SELECTED TO GIVE MAXIMUM DOSE
ICRP-68 INHALATION DOSE FOR ADULT WORKER
INHALATION EQUIVALENT DOSE ORDERED BY ORGAN (rem) FOR ADULT WORKER
DOWNWIND DISTANCES (m)
ORGAN NO. 2.49E+02
-------- --- --------
ADRENALS 1 5.99E-05
BSURFACE 2 3.52E-02
B_WALL 3 5.99E-05
BRAIN 4 5.99E-05
BREAST 5 5.99E-05
COLON 6 6.34E-05
ESOPHAGU 7 5.99E-05
ET_AIR 8 5.29E-04
KIDNEYS 9 1.44E-04
LIVER 10 7.40E-03
LLI_WALL 11 6.34E-05
LUNGS 12 7.40E-04
MUSCLE 13 5.99E-05
OVARIES 14 4.58E-04
PANCREAS 15 5.99E-05
R_MARROW 16 1.69E-03
SI_WALL 17 5.99E-05
SKIN 18 5.99E-05
SPLEEN 19 5.99E-05

ST_WALL 20 5.99E-05
TESTES 21 4.58E-04
THYMUS 22 5.99E-05
THYROID 23 5.99E-05
ULI_WALL 24 6.34E-05
UTERUS 25 5.99E-05
INHALATION EQUIVALENT DOSE ORDERED BY DOSE (rem) FOR ADULT WORKER
DOWNWIND DISTANCES (m)
ORGAN NO. 2.49E+02
-------- --- --------
BSURFACE 2 3.52E-02
LIVER 10 7.40E-03
R_MARROW 16 1.69E-03
LUNGS 12 7.40E-04
ET_AIR 8 5.29E-04
OVARIES 14 4.58E-04
TESTES 21 4.58E-04
KIDNEYS 9 1.44E-04
COLON 6 6.34E-05
LLI_WALL 11 6.34E-05
ULI_WALL 24 6.34E-05
ADRENALS 1 5.99E-05
B_WALL 3 5.99E-05
BRAIN 4 5.99E-05
BREAST 5 5.99E-05
ESOPHAGU 7 5.99E-05
MUSCLE 13 5.99E-05
PANCREAS 15 5.99E-05
SI_WALL 17 5.99E-05
SKIN 18 5.99E-05
SPLEEN 19 5.99E-05
ST_WALL 20 5.99E-05
THYMUS 22 5.99E-05
THYROID 23 5.99E-05
UTERUS 25 5.99E-05
INHALATION EFFECTIVE DOSE ORDERED BY DOSE (rem) FOR ADULT WORKER
DOWNWIND DISTANCES (m)
ORGAN NO. 2.49E+02
-------- --- --------
ADRENALS 1 3.00E-06
BSURFACE 2 1.76E-03
B_WALL 3 5.99E-07
BRAIN 4 3.00E-06
BREAST 5 3.00E-06
COLON 6 7.61E-06
ESOPHAGU 7 3.00E-06

```
ET_AIR 8 2.64E-05
KIDNEYS 9 7.22E-06
LIVER 10 3.70E-04
LLI_WALL 11 3.17E-06
LUNGS 12 8.88E-05
MUSCLE 13 3.00E-06
OVARIES 14 2.29E-05
PANCREAS 15 3.00E-06
R_MARROW 16 2.03E-04
SI_WALL 17 3.00E-06
SKIN 18 5.99E-07
SPLEEN 19 3.00E-06
ST_WALL 20 1.20E-05
TESTES 21 2.29E-05
THYMUS 22 3.00E-06
THYROID 23 3.00E-06
ULI_WALL 24 3.17E-06
UTERUS 25 3.00E-06
E_50 26 1.13E-03
```

Dose Summary

```
ADULT WORKER INHALATION DOSE CALCULATIONS MADE
USING DOSE CONVERSION FACTORS FOR ADULT WORKER
PATHWAY CONTRIBUTION TO THE EFFECTIVE DOSE (rem)
DOWNWIND DISTANCE = 2.49E+02 (m)
NUCLIDE INHALATION INGESTION GROUND SUR AIR IMMERS TOTAL
------------- ---------- ---------- ---------- ---------- ------
----
TOTALS 1.13E-03 - - - 1.13E-03
WARNINGS
--------
NO INGESTION DOSE CALCULATIONS WERE MADE
NO AIR IMMERSION OR CLOUD GAMMA DOSE CALCULATIONS WERE MADE
```

Execution Time

```
3.00E-02 SECONDS
```

Class A stability with building wake at station 329:

Radiological Safety Analysis Computer Program (RSAC 7.2.0)

Name: INL	**Company:** Idaho National Laboratory	**Serial:** HR688-8449C-M4N6G-E
Computer: INL418751	**Run Date:** 07/17/2013	**Run Time:** 08:47:27

File: Class A_BW_75th percentile_Station 329.rsac

Input

```
* 75th percentile Station 329
#
#
# Radionuclides
2000,1,0
Pu-239,0.0011
2999
# Met Data stability class A
5000,0
5001,3.3,0.,7.,9.58E2,0.,0
5101,249.
5201,1.,0.
5400,3,829.,7.
5421,9.0E-5
5999
# Dose
7000,1,-2,1,0,1,7
7001,3.33E-04,0.,0,0,1.
7999
# Dose Summary
3000,2,7
10000
```

Direct Radionuclide Input

```
PREVIOUS INVENTORY CHANGED TO THE FOLLOWING VALUES
NUCLIDE HALF LIFE CURIE
942390 Pu239 2.411E+04 yr 1.100E-03
```

Meteorological Data

```
MEAN WIND SPEED = 3.300E+00 (m/s) STACK HEIGHT = 0.000E+00 (m)
MIXING LAYER HEIGHT = 7.000E+00 (m) AIR DENSITY = 9.580E+02
(g/cu m)
WET DEPOSITION SCAVENGING COEFFICIENT = 0.000E+00 (1/s)
THERE IS 1 SET OF LEAKAGE CONSTANTS (K1,K2)
1.000E+00 0.000E+00
CHI/Q VALUES INPUT DIRECTLY
DOWNWIND DISTANCE CHI/Q
2.490E+02 9.000E-05
```

Inhalation Dose Calculation

```
USING DOSE CONVERSION FACTORS FROM ICRP-68 FOR ADULT WORKER
RESPIRABLE FRACTION = 1.000E+00
BREATHING RATE = 3.330E-04 (m^3/s)
RELEASE TIME FOR EXPONENTIAL DECAY FUNCTION = 1.000E+00 (s)
INTERNAL EXPOSURE TIME PERIOD = 5.000E+01 (yr)
LUNG ABSORPTION TYPES SELECTED TO GIVE MAXIMUM DOSE
ICRP-68 INHALATION DOSE FOR ADULT WORKER
INHALATION EQUIVALENT DOSE ORDERED BY ORGAN (rem) FOR ADULT
WORKER
DOWNWIND DISTANCES (m)
ORGAN NO. 2.49E+02
-------- --- --------
ADRENALS 1 2.07E-04
BSURFACE 2 1.22E-01
B_WALL 3 2.07E-04
BRAIN 4 2.07E-04
BREAST 5 2.07E-04
COLON 6 2.20E-04
ESOPHAGU 7 2.07E-04
ET_AIR 8 1.83E-03
KIDNEYS 9 5.00E-04
LIVER 10 2.56E-02
LLI_WALL 11 2.20E-04
LUNGS 12 2.56E-03
MUSCLE 13 2.07E-04
OVARIES 14 1.59E-03
PANCREAS 15 2.07E-04
R_MARROW 16 5.85E-03
SI_WALL 17 2.07E-04
SKIN 18 2.07E-04
SPLEEN 19 2.07E-04
```

ST_WALL 20 2.07E-04
TESTES 21 1.59E-03
THYMUS 22 2.07E-04
THYROID 23 2.07E-04
ULI_WALL 24 2.20E-04
UTERUS 25 2.07E-04
INHALATION EQUIVALENT DOSE ORDERED BY DOSE (rem) FOR ADULT WORKER
DOWNWIND DISTANCES (m)
ORGAN NO. 2.49E+02
-------- --- --------
BSURFACE 2 1.22E-01
LIVER 10 2.56E-02
R_MARROW 16 5.85E-03
LUNGS 12 2.56E-03
ET_AIR 8 1.83E-03
OVARIES 14 1.59E-03
TESTES 21 1.59E-03
KIDNEYS 9 5.00E-04
COLON 6 2.20E-04
LLI_WALL 11 2.20E-04
ULI_WALL 24 2.20E-04
ADRENALS 1 2.07E-04
B_WALL 3 2.07E-04
BRAIN 4 2.07E-04
BREAST 5 2.07E-04
ESOPHAGU 7 2.07E-04
MUSCLE 13 2.07E-04
PANCREAS 15 2.07E-04
SI_WALL 17 2.07E-04
SKIN 18 2.07E-04
SPLEEN 19 2.07E-04
ST_WALL 20 2.07E-04
THYMUS 22 2.07E-04
THYROID 23 2.07E-04
UTERUS 25 2.07E-04
INHALATION EFFECTIVE DOSE ORDERED BY DOSE (rem) FOR ADULT WORKER
DOWNWIND DISTANCES (m)
ORGAN NO. 2.49E+02
-------- --- --------
ADRENALS 1 1.04E-05
BSURFACE 2 6.10E-03
B_WALL 3 2.07E-06
BRAIN 4 1.04E-05
BREAST 5 1.04E-05
COLON 6 2.63E-05
ESOPHAGU 7 1.04E-05

```
ET_AIR 8 9.15E-05
KIDNEYS 9 2.50E-05
LIVER 10 1.28E-03
LLI_WALL 11 1.10E-05
LUNGS 12 3.07E-04
MUSCLE 13 1.04E-05
OVARIES 14 7.93E-05
PANCREAS 15 1.04E-05
R_MARROW 16 7.03E-04
SI_WALL 17 1.04E-05
SKIN 18 2.07E-06
SPLEEN 19 1.04E-05
ST_WALL 20 4.15E-05
TESTES 21 7.93E-05
THYMUS 22 1.04E-05
THYROID 23 1.04E-05
ULI_WALL 24 1.10E-05
UTERUS 25 1.04E-05
E_50 26 3.90E-03
```

Dose Summary

```
ADULT WORKER INHALATION DOSE CALCULATIONS MADE
USING DOSE CONVERSION FACTORS FOR ADULT WORKER
PATHWAY CONTRIBUTION TO THE EFFECTIVE DOSE (rem)
DOWNWIND DISTANCE = 2.49E+02 (m)
NUCLIDE INHALATION INGESTION GROUND SUR AIR IMMERS TOTAL
------------- ---------- ---------- ---------- ---------- ------
----
TOTALS 3.90E-03 - - - 3.90E-03
WARNINGS
--------
NO INGESTION DOSE CALCULATIONS WERE MADE
NO AIR IMMERSION OR CLOUD GAMMA DOSE CALCULATIONS WERE MADE
```

Execution Time

```
3.00E-02 SECONDS
```

Class A stability with building wake at station 330:

Radiological Safety Analysis Computer Program (RSAC 7.2.0)

Name: INL	**Company:** Idaho National Laboratory	**Serial:** HR688-8449C-M4N6G-E
Computer: INL418751	**Run Date:** 07/17/2013	**Run Time:** 08:48:26

File: Class A_BW_75th percentile_Station 330.rsac

Input

```
* 75th percentile Station 330
#
#
# Radionuclides
2000,1,0
Pu-239,0.0011
2999
# Met Data stability class A
5000,0
5001,3.3,0.,7.,9.58E2,0.,0
5101,249.
5201,1.,0.
5400,3,829.,7.
5421,4.3E-5
5999
# Dose
7000,1,-2,1,0,1,7
7001,3.33E-04,0.,0,0,1.
7999
# Dose Summary
3000,2,7
10000
```

Direct Radionuclide Input

```
PREVIOUS INVENTORY CHANGED TO THE FOLLOWING VALUES
NUCLIDE HALF LIFE CURIE
942390 Pu239 2.411E+04 yr 1.100E-03
```

Meteorological Data

```
MEAN WIND SPEED = 3.300E+00 (m/s) STACK HEIGHT = 0.000E+00 (m)
MIXING LAYER HEIGHT = 7.000E+00 (m) AIR DENSITY = 9.580E+02
(g/cu m)
WET DEPOSITION SCAVENGING COEFFICIENT = 0.000E+00 (1/s)
THERE IS 1 SET OF LEAKAGE CONSTANTS (K1,K2)
1.000E+00 0.000E+00
CHI/Q VALUES INPUT DIRECTLY
DOWNWIND DISTANCE CHI/Q
2.490E+02 4.300E-05
```

Inhalation Dose Calculation

```
USING DOSE CONVERSION FACTORS FROM ICRP-68 FOR ADULT WORKER
RESPIRABLE FRACTION = 1.000E+00
BREATHING RATE = 3.330E-04 (m^3/s)
RELEASE TIME FOR EXPONENTIAL DECAY FUNCTION = 1.000E+00 (s)
INTERNAL EXPOSURE TIME PERIOD = 5.000E+01 (yr)
LUNG ABSORPTION TYPES SELECTED TO GIVE MAXIMUM DOSE
ICRP-68 INHALATION DOSE FOR ADULT WORKER
INHALATION EQUIVALENT DOSE ORDERED BY ORGAN (rem) FOR ADULT
WORKER
DOWNWIND DISTANCES (m)
ORGAN NO. 2.49E+02
-------- --- --------
ADRENALS 1 9.91E-05
BSURFACE 2 5.83E-02
B_WALL 3 9.91E-05
BRAIN 4 9.91E-05
BREAST 5 9.91E-05
COLON 6 1.05E-04
ESOPHAGU 7 9.91E-05
ET_AIR 8 8.74E-04
KIDNEYS 9 2.39E-04
LIVER 10 1.22E-02
LLI_WALL 11 1.05E-04
LUNGS 12 1.22E-03
MUSCLE 13 9.91E-05
OVARIES 14 7.58E-04
PANCREAS 15 9.91E-05
R_MARROW 16 2.80E-03
SI_WALL 17 9.91E-05
SKIN 18 9.91E-05
SPLEEN 19 9.91E-05
```

ST_WALL 20 9.91E-05
TESTES 21 7.58E-04
THYMUS 22 9.91E-05
THYROID 23 9.91E-05
ULI_WALL 24 1.05E-04
UTERUS 25 9.91E-05
INHALATION EQUIVALENT DOSE ORDERED BY DOSE (rem) FOR ADULT WORKER
DOWNWIND DISTANCES (m)
ORGAN NO. 2.49E+02
-------- --- --------
BSURFACE 2 5.83E-02
LIVER 10 1.22E-02
R_MARROW 16 2.80E-03
LUNGS 12 1.22E-03
ET_AIR 8 8.74E-04
OVARIES 14 7.58E-04
TESTES 21 7.58E-04
KIDNEYS 9 2.39E-04
COLON 6 1.05E-04
LLI_WALL 11 1.05E-04
ULI_WALL 24 1.05E-04
ADRENALS 1 9.91E-05
B_WALL 3 9.91E-05
BRAIN 4 9.91E-05
BREAST 5 9.91E-05
ESOPHAGU 7 9.91E-05
MUSCLE 13 9.91E-05
PANCREAS 15 9.91E-05
SI_WALL 17 9.91E-05
SKIN 18 9.91E-05
SPLEEN 19 9.91E-05
ST_WALL 20 9.91E-05
THYMUS 22 9.91E-05
THYROID 23 9.91E-05
UTERUS 25 9.91E-05
INHALATION EFFECTIVE DOSE ORDERED BY DOSE (rem) FOR ADULT WORKER
DOWNWIND DISTANCES (m)
ORGAN NO. 2.49E+02
-------- --- --------
ADRENALS 1 4.95E-06
BSURFACE 2 2.91E-03
B_WALL 3 9.91E-07
BRAIN 4 4.95E-06
BREAST 5 4.95E-06
COLON 6 1.26E-05
ESOPHAGU 7 4.95E-06

```
ET_AIR 8 4.37E-05
KIDNEYS 9 1.19E-05
LIVER 10 6.12E-04
LLI_WALL 11 5.25E-06
LUNGS 12 1.47E-04
MUSCLE 13 4.95E-06
OVARIES 14 3.79E-05
PANCREAS 15 4.95E-06
R_MARROW 16 3.36E-04
SI_WALL 17 4.95E-06
SKIN 18 9.91E-07
SPLEEN 19 4.95E-06
ST_WALL 20 1.98E-05
TESTES 21 3.79E-05
THYMUS 22 4.95E-06
THYROID 23 4.95E-06
ULI_WALL 24 5.25E-06
UTERUS 25 4.95E-06
E_50 26 1.86E-03
```

Dose Summary

```
ADULT WORKER INHALATION DOSE CALCULATIONS MADE
USING DOSE CONVERSION FACTORS FOR ADULT WORKER
PATHWAY CONTRIBUTION TO THE EFFECTIVE DOSE (rem)
DOWNWIND DISTANCE = 2.49E+02 (m)
NUCLIDE INHALATION INGESTION GROUND SUR AIR IMMERS TOTAL
------------- ---------- ---------- ---------- ---------- ------
----
TOTALS 1.86E-03 - - - 1.86E-03
WARNINGS
--------
NO INGESTION DOSE CALCULATIONS WERE MADE
NO AIR IMMERSION OR CLOUD GAMMA DOSE CALCULATIONS WERE MADE
```

Execution Time

```
3.00E-02 SECONDS
```

Class A stability with building wake at station 331:

Radiological Safety Analysis Computer Program (RSAC 7.2.0)

Name: INL	**Company:** Idaho National Laboratory	**Serial:** HR688-8449C-M4N6G-E
Computer: INL418751	**Run Date:** 07/17/2013	**Run Time:** 08:49:53

File: Class A_BW_75th percentile_Station 331.rsac

Input

```
* 75th percentile Station 331
#
#
# Radionuclides
2000,1,0
Pu-239,0.0011
2999
# Met Data stability class A
5000,0
5001,3.3,0.,7.,9.58E2,0.,0
5101,249.
5201,1.,0.
5400,3,829.,7.
5421,2.1E-5
5999
# Dose
7000,1,-2,1,0,1,7
7001,3.33E-04,0.,0,0,1.
7999
# Dose Summary
3000,2,7
10000
```

Direct Radionuclide Input

```
PREVIOUS INVENTORY CHANGED TO THE FOLLOWING VALUES
NUCLIDE HALF LIFE CURIE
942390 Pu239 2.411E+04 yr 1.100E-03
```

Meteorological Data

```
MEAN WIND SPEED = 3.300E+00 (m/s) STACK HEIGHT = 0.000E+00 (m)
MIXING LAYER HEIGHT = 7.000E+00 (m) AIR DENSITY = 9.580E+02
(g/cu m)
WET DEPOSITION SCAVENGING COEFFICIENT = 0.000E+00 (1/s)
THERE IS 1 SET OF LEAKAGE CONSTANTS (K1,K2)
1.000E+00 0.000E+00
CHI/Q VALUES INPUT DIRECTLY
DOWNWIND DISTANCE CHI/Q
2.490E+02 2.100E-05
```

Inhalation Dose Calculation

```
USING DOSE CONVERSION FACTORS FROM ICRP-68 FOR ADULT WORKER
RESPIRABLE FRACTION = 1.000E+00
BREATHING RATE = 3.330E-04 (m^3/s)
RELEASE TIME FOR EXPONENTIAL DECAY FUNCTION = 1.000E+00 (s)
INTERNAL EXPOSURE TIME PERIOD = 5.000E+01 (yr)
LUNG ABSORPTION TYPES SELECTED TO GIVE MAXIMUM DOSE
ICRP-68 INHALATION DOSE FOR ADULT WORKER
INHALATION EQUIVALENT DOSE ORDERED BY ORGAN (rem) FOR ADULT
WORKER
DOWNWIND DISTANCES (m)
ORGAN NO. 2.49E+02
-------- --- --------
ADRENALS 1 4.84E-05
BSURFACE 2 2.85E-02
B_WALL 3 4.84E-05
BRAIN 4 4.84E-05
BREAST 5 4.84E-05
COLON 6 5.12E-05
ESOPHAGU 7 4.84E-05
ET_AIR 8 4.27E-04
KIDNEYS 9 1.17E-04
LIVER 10 5.98E-03
LLI_WALL 11 5.12E-05
LUNGS 12 5.98E-04
MUSCLE 13 4.84E-05
OVARIES 14 3.70E-04
PANCREAS 15 4.84E-05
R_MARROW 16 1.37E-03
SI_WALL 17 4.84E-05
SKIN 18 4.84E-05
SPLEEN 19 4.84E-05
```

ST_WALL 20 4.84E-05
TESTES 21 3.70E-04
THYMUS 22 4.84E-05
THYROID 23 4.84E-05
ULI_WALL 24 5.12E-05
UTERUS 25 4.84E-05
INHALATION EQUIVALENT DOSE ORDERED BY DOSE (rem) FOR ADULT WORKER
DOWNWIND DISTANCES (m)
ORGAN NO. 2.49E+02
-------- --- --------
BSURFACE 2 2.85E-02
LIVER 10 5.98E-03
R_MARROW 16 1.37E-03
LUNGS 12 5.98E-04
ET_AIR 8 4.27E-04
OVARIES 14 3.70E-04
TESTES 21 3.70E-04
KIDNEYS 9 1.17E-04
COLON 6 5.12E-05
LLI_WALL 11 5.12E-05
ULI_WALL 24 5.12E-05
ADRENALS 1 4.84E-05
B_WALL 3 4.84E-05
BRAIN 4 4.84E-05
BREAST 5 4.84E-05
ESOPHAGU 7 4.84E-05
MUSCLE 13 4.84E-05
PANCREAS 15 4.84E-05
SI_WALL 17 4.84E-05
SKIN 18 4.84E-05
SPLEEN 19 4.84E-05
ST_WALL 20 4.84E-05
THYMUS 22 4.84E-05
THYROID 23 4.84E-05
UTERUS 25 4.84E-05
INHALATION EFFECTIVE DOSE ORDERED BY DOSE (rem) FOR ADULT WORKER
DOWNWIND DISTANCES (m)
ORGAN NO. 2.49E+02
-------- --- --------
ADRENALS 1 2.42E-06
BSURFACE 2 1.42E-03
B_WALL 3 4.84E-07
BRAIN 4 2.42E-06
BREAST 5 2.42E-06
COLON 6 6.15E-06
ESOPHAGU 7 2.42E-06

```
ET_AIR 8 2.13E-05
KIDNEYS 9 5.83E-06
LIVER 10 2.99E-04
LLI_WALL 11 2.56E-06
LUNGS 12 7.17E-05
MUSCLE 13 2.42E-06
OVARIES 14 1.85E-05
PANCREAS 15 2.42E-06
R_MARROW 16 1.64E-04
SI_WALL 17 2.42E-06
SKIN 18 4.84E-07
SPLEEN 19 2.42E-06
ST_WALL 20 9.68E-06
TESTES 21 1.85E-05
THYMUS 22 2.42E-06
THYROID 23 2.42E-06
ULI_WALL 24 2.56E-06
UTERUS 25 2.42E-06
E_50 26 9.11E-04
```

Dose Summary

```
ADULT WORKER INHALATION DOSE CALCULATIONS MADE
USING DOSE CONVERSION FACTORS FOR ADULT WORKER
PATHWAY CONTRIBUTION TO THE EFFECTIVE DOSE (rem)
DOWNWIND DISTANCE = 2.49E+02 (m)
NUCLIDE INHALATION INGESTION GROUND SUR AIR IMMERS TOTAL
------------- ---------- ---------- ---------- ---------- ------
----
TOTALS 9.11E-04 - - - 9.11E-04
WARNINGS
--------
NO INGESTION DOSE CALCULATIONS WERE MADE
NO AIR IMMERSION OR CLOUD GAMMA DOSE CALCULATIONS WERE MADE
```

Execution Time

```
4.00E-02 SECONDS
```